Improving clinical outcomes for patients with locally advanced non-small cell lung cancer treated with photon and proton radiotherapy

Swee- Ling Wong

MA MBBS MRCP FRCR

University College London

Thesis submitted for Degree of MD (*Res)*

I, Swee- Ling Wong, confirm that the work presented in this thesis is my own. Where information has been derived from other sources, I confirm that this has been indicated in the thesis.

Abstract

Objectives

To identify mechanisms improving clinical outcomes for patients with unresectable locally advanced non-small-cell lung cancer (LA-NSCLC) treated with photon and proton radiotherapy.

Strategies explored include 1. Investigating using routine healthcare datasets to estimate survival outcomes for patients with LA-NSCLC treated with definitive radiotherapy, in order to assess the effectiveness of current strategies; 2. Assessing the physical advantages of protons by conducting a retrospective planning study comparing volumetric modulated arc therapy (VMAT) and pencil beam scanning (PBS) proton plans of superior sulcus tumours (SSTs), a rare subset of LA-NSCLC; 3. Exploring potential biological advantages of protons by examining major cell death pathways following XRT, high and low linear energy transfer (LET) proton irradiation of NSCLC cells.

Methods

Workflow 1:

LA-NSCLC patients receiving definitive radiotherapy were identified. For each, key time points (date of diagnosis, recurrence, death or last clinical encounter) were used to calculate overall survival (OS) and progression free survival (PFS) from manual-data (hospital notes) and compared to estimated OS and PFS from routine-data (electronic databases). Dataset correlations were then tested to establish if routine-data were a reliable proxy measure for manual-data.

Workflow 2:

Patients with SSTs treated with 4D radiotherapy were identified. Tumour motion was assessed and excluded if >5 mm. Comparative VMAT and PBS plans were generated retrospectively. Robustness analysis was assessed for both plans involving: 1. 5 mm geometric uncertainty scenarios, with an additional 3.5% range uncertainty for proton plans; 2. verification plans at breathing extremes. Comparative dosimetric and robustness analyses were carried out.

Workflow 3:

Human NSCLC cell lines were irradiated with single doses of 2-15 Gy photon radiotherapy, high- or low-linear energy transfer (LET) protons (12 keV/µm and 1 keV/µm, respectively) and analysed 24-144 hours post-irradiation. DNA damage foci and cell death mechanisms were investigated.

Results

Workflow 1:

In forty-three patients, routine data underestimated PFS by 0.09 months (p=0.86; 95% CI -0.86-1.03) and OS by 1.02 months (p=0.00; 95% CI 0.34-1.69) but there was good correlation with a Pearson correlation coefficient of 0.94 (p=0.00, 95% CI 0.90-0.97) for PFS and 0.97 (p= 0.00, 95% CI 0.95-0.98) for OS.

Workflow 2:

In ten patients, both modalities achieved similar target coverage with mean clinical target volume D95 of 98.1% + 0.4 (97.5-98.8) and 98.4% $\pm$ 0.2 (98.1-98.9) for PBS and VMAT plans, respectively. The same four PBS and VMAT plans failed robustness. Proton plans significantly reduced mean lung dose (by 21.9%), lung V5, V10, V20 (by 47.9%, 36.4%, 12.1%, respectively), mean heart dose (by 21.4%) and vertebra dose (by 29.2%) ($p<0.05$).

Workflow 3:

XRT predominantly induced mitotic catastrophe, autophagy and senescence. Senescence, established via the p53/p21 pathway, was the major cell death pathway by which protons more effectively reduce clonogenic potential compared to XRT in NSCLC cell lines. High LET protons at a dose of 10 Gy(RBE) resulted in the lowest cell survival. The mechanisms driving the LET- and dose-dependent senescence was unclear but did not appear to be related to differential DNA repair machineries.

Conclusions

Proton radiotherapy could be pivotal in improving outcomes in select cases of LA-NSCLC. These studies demonstrate that 1. survival-outcomes are reliably estimated by routine data and such a methodology could enable rapid outcomes analysis to keep pace with trial development; 2. robust PBS plans are achievable in carefully selected patients and

considerable dose reductions to the lung, heart and thoracic vertebra are possible without compromising target coverage; 3. Identification of LET- and dose-dependent proton-induced cellular senescence may guide radiotherapy optimisation and drug-radiotherapy combinations, maximising tumour cell kill.

This work contributes to important preliminary research required to understand the physical and biological strengths and weaknesses prior to trials.

Impact Statement

In the UK, survival from lung cancer is poor, reported to having been amongst the lowest in Europe with a 5-year survival of approximately 10% compared to up to 20% in other countries [1], [2]. Non-small cell lung cancer (NSCLC) is the most common subtype and approximately 70% of patients present with locally advanced or metastatic disease [3]. For patients with locally advanced NSCLC, survival has improved with modern radiotherapy techniques and 2-year survival rates of 55.6% can be expected when combined with chemotherapy, and up to 66.3% with further consolidation immunotherapy [4].

The incorporation of algorithm-driven mechanisms into healthcare systems and proton radiotherapy for lung cancer treatment are two major broad themes that will dominate research efforts in the immediate future. Proton radiotherapy is expected to play a pivotal role in improving outcomes for patients with locally advanced NSCLC as this promises both physical and biological advantages over state-of-the-art photon radiotherapy. Unfortunately, clinical evidence supporting an advantage of proton therapy is currently lacking. The UK is poised to set up lung proton clinical trials with the first high energy proton centres opened/opening in The Christie (Manchester, 2019) and University College London Hospital (London, 2021), featuring the latest technology, pencil beam scanning (PBS) protons.

Using routine data to estimate survival outcomes and its potential application into AI algorithms enables rapid large scale analysis of lung cancer strategies. Not only does this have important health economic implications for radiotherapy centres, due to the outcomes-based commissioning framework, but this same methodology can be tailored to auto-analyse outcomes for other stages of NSCLC and other tumour types. This would have a huge impact on healthcare systems and will support the pace of evolving research.

Patients with superior sulcus tumours (SSTs) seem likely candidates to benefit from scanning protons and present a unique opportunity to develop PBS techniques in locally advanced NSCLCs because 1) their invasion of local structures limits motion, circumventing the challenging issues of interplay 2) their apical location results in smaller volumes of aerated tissue surrounding them, reducing heterogeneity along proton paths. Demonstrating the feasibility of PBS proton therapy in SSTs will form the basis for prospective clinical trials investigating if dosimetric advantages translate in to superior outcomes. These principles can be applied to other locally advanced NSCLCs with limited movement.

Key biological differences, particularly in the context of high and low LET proton irradiation, are thought to be tissue-, cell line- and endpoint-specific [5]–[9]. It is biologically important and relevant to distinguish cellular responses to high and low LET protons due to non-uniformity within a clinical proton beam; and the consequence of predominant cell death mechanisms that include varying immunogenicity and clonogenic potential. Understanding how they differ can guide radiotherapy optimisation and enable advantage to be taken of the biological benefits by identifying optimal drug-radiotherapy combinations to maximise tumour cell kill.

State-of-the-art proton therapy is anticipated to show significant advantages over photon therapy in select cases of lung cancer treatment. This work forms part of the crucial preliminary research required to understand the physical and biological strengths and weaknesses prior to trials that will identify new indications over state of the art photon therapy.

Table of Contents

Publications, presentations and awards (see Appendix 6)

Full papers published from this project

- **A methodology to extract outcomes from routine healthcare data for patients with locally advanced non-small cell lung cancer. Wong, SL.**, Ricketts, K., Royle, G., Williams, M. and Mendes, R. *BMC Health Services Research.* 2018. **18**:278. (**From Chapter 2)**
- **Retrospective planning study of patients with superior sulcus tumours comparing pencil beam scanning protons to volumetric modulated arc therapy. Wong, SL.,** Alshaikhi, J., Grimes, H., Amos, RA., Poynter, A., Rompokos, V., Gulliford, S., Royle, G., Liao, Z., Sharma, RA., Mendes, R. *Clin Oncol*, 2020. DOI 10.1016/j.clon.2020.07.016 (**From Chapter 4)**

Full papers pending submission

- **Study of photon and proton-induced cell death in non-small cell lung cancer cell lines. Wong, SL.,** Carter, R., Westhorpe, A., Royle, G., Parsons, J., Sharma, RA. (**From Chapter 5)**
- **Critical research gaps and recommendations to inform research prioritisation for improved outcomes in lung cancer using proton radiotherapy.** *Cobben, D., ***Wong, SL**, Aznar, M., Dempsey, C., Faivre-Finn, C., Hiley, C., Lines, D., Mohindra, P., Taylor, M., Rompokos, V., Teoh, S., Salem, A. (**Joint 1st authors*). (**From Chapter 4)**

Posters and Presentations

- **Use of routine healthcare data for the estimation of disease outcomes in locally advanced non-small cell lung cancer (LA NSCLC). Wong, SL.,** Ricketts, K., Royle, G., Williams, M., Mendes, R. *British Thoracic Oncology Group Conference 2016.* 27th – 29th 2016. **(From Chapter 2)Planning study comparing the use of photon radiation therapy compared to proton therapy for superior sulcus tumours**. **Wong, SL**., Alshaikhi, J., Lalli, N., Bhudia, P., D' Souza, D., Amos, R., Royle, G., Mendes, R. *British Thoracic Oncology Group Conference 2016.* 27th – 29th 2016; ***Cancer Research UK Lung Cancer Centre of Excellence Conference 2016***. 13th -15th December 2015. (**From Chapter 4)**
- **Planning study comparing the use of photon radiation therapy to proton therapy for superior sulcus tumours (SSTs). Wong, SL**, J. Alshaikhi, N. Lalli, R. Amos, G. Royle, R. Mendes. *PPRIG Proton Therapy Physics Workshop*. 1st – 2nd October 2015. ***Oral presentation of preliminary results. (*From Chapter 4)**

Awards

- **Poster Prize British Thoracic Oncology Group 2016:** Use of routine healthcare data for the estimation of disease outcomes in locally advanced non-small cell lung cancer (LA NSCLC). **Wong, SL.** et al. *1 of 10 prize winners (out of a total of 195 posters) awarded £100 by the BTOG 2016 Poster Committee. (***From chapter 2)**

Dedication

To my parents, who taught me that education is a privilege, to my husband who has supported me throughout this journey, and to Maia and Sammy, both of whom I carried along the way and have shown me life's most valuable lesson.

Acknowledgements

I wish to express my deepest gratitude to Professor Gary Royle for his wisdom, educational and pastoral support throughout, as well as Dr Ruheena Mendes for encouraging me to do research and Professor Ricky Sharma for the valuable laboratory research opportunities.

List of figures

Fig 14. A. Quantification of cells undergoing mitotic catastrophe following XRT irradiation. **B.** Quantification of cells undergoing autophagy following XRT irradiation. **C**. Quantification of cells undergoing senescence following XRT irradiation. **D.** Comparative cell death pathways induced by XRT in A549, H1975, H1792 and H2122 cell lines at peak time points (Apoptosis: at 72h following 10 Gy; necrosis: at 144 h following 15 Gy; Autophagy: at 96 h following 10 Gy; Senescence: at 144 h following 10 Gy; Mitotic catastrophe: at 96 h following 10 Gy). **E.** In the cell lines studied, XRT-induced cell death was predominantly via MC (observed maximally at 96 h), autophagy (observed maximally at 96 h) and senescence (observed maximally at 144 h). **(i).** Comparative quantification of cells undergoing mitotic catastrophe following XRT irradiation at peak time point of 96 h. **(ii).** Comparative quantification of cells undergoing autophagy following XRT irradiation at peak time point of 96 h. **(iii)**. Comparative quantification of cells undergoing senescence following XRT irradiation at peak time point of 144 h.

Fig 15. Increased radiosensitivity of non- small cell lung cancer cell lines to PBT compared to XRT irradiation is not due to differences in mitotic catastrophe or autophagy. **A.** Clonogenic survival following increasing doses of high (HLET) and low LET (LLET) PBT compared to XRT for A549 and H2122. **B.** Comparative cell death pathways induced by XRT, LLET protons and HLET protons in (i) A549 and (ii) H2122 cell lines at peak time points (Autophagy: at 96 h following 10 Gy (RBE); Senescence: at 144 h following 10 Gy (RBE); Mitotic catastrophe: at 96 h following 10 Gy (RBE)).**C.** Quantification of cells undergoing mitotic catastrophe following irradiation: A549 cells at **(i)** 72h and **(ii)** 96 h; and in H2122 cells at **(iii)** 72 h and **(iv)** 96 h. **D.** Quantification of cells undergoing autophagy following irradiation: A549 cells at **(i)** 72 h and **(ii)** 96 h; and in H2122 cells at **(iii)** 72 h and **(iv)** 96 h.

Fig 16. Senescence is the major cell death pathway by which PBT more effectively inhibits clonogenic survival compared to XRT in NSCLC cell lines. **A.** SA- β- Gal staining of H2122 cells 6 days following irradiation with **(i)** 5 Gy (RBE) and **(ii)** 10 Gy (RBE). **B.** Quantification of mean number of SA- β- Gal positive cells in A549 cells following irradiation at **(i)** 72 h and **(ii)** 144 h; and in H2122 cells at **(iii)** 72 h and **(iv)** 144 h. **C.** Western blot showing senescence induction following 10 Gy (RBE) **(i)** Western blot of irradiated A549 cells and; **(ii)** Western blot of irradiated H2122 cells at 24 h and 96 h.

Fig 17. Difference in radiation- induced cellular senescence is not related to activation of differential repair machineries. **A.** Representative micrographs of ϒH2AX, 53BP1 and RAD51 foci in A549 cells exposed to 5 Gy XRT at indicated time points. **B.** Average number of DNA foci per cell in A549 cells following 5 Gy (RBE) XRT and high LET (HLET) and low LET (LLET) proton irradiation at 0.5 h, 4 h and 24 h**. C.** Average number of DNA foci per cells in H2122 cells following 5 Gy (RBE) at 0.5 h, 4 h and 24 h.

Fig 18. Western blot showing changes in STING expression following 10 Gy (RBE) irradiation of (A) A549 cells and (B) H2122 cells at 24 h and 96 h.

List of tables

Chapter 1

Introduction

Lung cancer is a global health challenge and leading cause of cancer-related mortality world-wide (18.4% of total cancer deaths) (Globocan 2018). Although paradigm-shifting systemic treatments have recently been discovered [4], [10], improved long-term survival continues to be hindered by major hurdles existing at both ends of the management pathway: lack of established screening programmes that enable detection of early stage cancer and late presentation that make current curative treatment options difficult or impossible.

Efforts to establish lung cancer screening programmes include the Dutch-Belgian NELSON study [11] and the US-based National Lung Screening Trial [12], [13]. Both have demonstrated reduced mortality from lung cancer in high-risk individuals [11]–[13] of up to 20% using low-dose CT compared to screening with chest radiography [12], [13]. In the UK, the SUMMIT Study (NCT03934866) [14] is an ongoing trial and the largest lung screening programme in the UK. However, until routine screening becomes standard practice, the majority of patients are likely to continue presenting late with locally advanced or metastatic disease, the rates of which can be as high as 70% [3].

Non-small cell lung cancer (NSCLC) is the most common lung cancer subtype and there is an unmet need to improve the outcomes for patients with locally advanced NSCLC. An important first step is to assess the effectiveness of the current standard of care. Historically, such a process would have relied on analysing patients' notes (known as manual data), which is both time-consuming and inefficient. The value of easy and rapid analysis of survival outcome measures is widely recognised and means that they can be undertaken frequently and on a large scale. This is particularly useful when the treatment landscape is rapidly evolving [10], [15].

Information from routinely collected electronic datasets (known as routine data) can be used to estimate survival by identifying clinical codes that act as surrogates for landmark events. The methodology of synthesising and interpreting these sets of clinical codes are unique to cancer type and disease stage, requiring knowledge of the tumour-specific management pathway. This has not been done before for in lung cancer and this task is undertaken as one work stream of this thesis. Not only is this an inexpensive solution but this process can be built into an automated algorithm, an important application of artificial intelligence that has huge potential to improve oncologic care.

Up till recently, photon radiotherapy, with or without chemotherapy, was the standard of care for patients with locally advanced NSCLC that is surgically unresectable. Modern radiotherapy techniques and immunotherapy has improved survival for these patients and 2-year survival rates of up to 66.3% can be achieved with chemoradiotherapy and consolidation immunotherapy [4]. However, despite these advances in precision photon radiotherapy,

image-guidance and motion mitigation strategies, outcomes for patients with locally advanced can still be improved.

Radiotherapy is often challenging in patients with locally advanced disease. The difficulties are both physical and biological: disease can be bulky requiring large volumes to be irradiated; and geometrically heterogeneous resulting in differential motion within different parts of the tumour. In addition to this, innate or acquired radioresistance results in loss of locoregional tumour control, which is strongly correlated with NSCLC survival [1], [2].

Global interest lies in developing proton radiotherapy in lung cancer as this promises both physical and biological advantages over state-of-the-art photon radiotherapy. Due to its Bragg peak, proton therapy results in a relatively low entrance dose and minimal exit dose, achieving superior conformality at the tumour site with reduced dose to surrounding tissues [18]–[20]. This means it is possible for safe dose escalation to the tumour, which can improve local control by overcoming radioresistance, whilst sparing normal tissues. Most clinical experience with proton therapy has come from using older technology passively scattered protons [21]–[26]. Over the past decade, proton technology has significantly advanced with the introduction of pencil beam scanning protons (PBS) that enable superior precision and modulated proton therapy, as well as image guidance systems.

However, it has yet to be determined which patients will benefit most from these advanced proton technologies. A better understanding of both proton physical capabilities and proton-induced biological differences at the cellular and intra-cellular level will help identify patient groups, optimal planning and delivery strategies as well as combination treatments to maximise enhance cell kill.

Because locally advanced NSCLC encompasses a range of complex anatomical varieties, one approach is to conduct planning studies that focus on subtypes based on geometry. Planning studies allow the physical limitations and advantages of proton therapy to be examined. Patients with superior sulcus tumours, a select cohort of locally advanced NSCLC, seem likely candidates to benefit from scanning protons due to their characteristic apical location, proximity to critical structures (like the spinal cord and brachial plexus) and their limited motion [27]–[29]. A retrospective planning study comparing robust pencil beam scanning proton therapy to state-of-the-art photon volumetric modulated arc-therapy (VMAT) for this select cohort is another work stream of this thesis.

The biological advantages of proton therapy is not well known. It has been established that proton therapy has a higher radiobiologic effect (RBE) resulting in increased cell kill [30] and preclinical studies have demonstrated that protons result in more complex DNA lesions [31]–[33], different cellular responses to DNA damage and immunogenicity [34]. However, although

non- uniformity within clinical proton beams is known, with high linear energy transfer (LET) occurring at the end and lateral edges of the beam (resulting with different biological consequences) [35]–[37], most in-vitro studies have only compared high LET irradiation from heavy ion particles [38] or low LET protons [39], [40] to photon therapy, which may not be biologically relevant. The final work stream of this thesis examines major death pathways in NSCLC cells to identify key differences in their cellular response to DNA damage following photon therapy compared to high and low LET proton irradiation.

This thesis aims to identify methods to improve radiotherapy outcomes in locally advanced NSCLC by 1. assessing current outcomes, using novel data-mining and algorithm-generating applications 2. review current lung radiotherapy practice 3. explore the role of proton radiotherapy in the treatment of locally advanced NSCLC, by examining gaps in lung proton radiotherapy research and identify its physical advantages, as well as 4. elucidate cell death mechanisms by which high and low LET proton therapy kills NSCLC cells.

Chapter 2

Current outcomes in patients with locally advanced non-small cell lung cancer: Using routine data to estimate outcomes

2.1 Background

Assessing outcomes is important for analysing the effectiveness of current practice. National cancer strategies have been implemented to incentivize centres to formally assess radiotherapy outcomes with the introduction of an outcomes-based commissioning framework [41]. As a result, there is a recognised need to be able to assess, qualify and quantify the quality of radiotherapy practice which is valuable for research and strategic planning of service provision. However, data collection is laborious and challenging as data quality is inconsistent. Furthermore, with advancing radiotherapy technologies emerging and systemic therapies rapidly evolving, there is critical need for frequent and efficient large scale outcomes analysis to assess the effectiveness of such treatments.

Progression free survival (PFS) and overall survival (OS) are key outcome measures for lung cancer that are important assessment tools of the effectiveness of an institution's lung cancer strategy. PFS has become an increasingly important outcome measure in clinical trials, used as a surrogate for OS that is less influenced by subsequent therapies, and important for evaluating treatment response. Measuring PFS is in itself a challenge due to an inconsistency of definition and use in the literature and measurement accuracy [42], [43]. To reliably determine these outcomes measures, the quality, completeness and consistency of data recording is important as well as the ability to efficiently interpret these. Manually collected prospective data taken from patients' notes, as collected in trials, is considered the gold standard in most accurately identifying clinically significant dates for patients' investigation and management pathways. However, data quality can be inconsistent and collecting it is labour-intensive, making assessment of large numbers time-consuming. Routine datasets are nationally collected patient data, including hospital episodes statistic (HES), radiotherapy database (RTDS), systemic anti-cancer therapy (SACT) and personal demographics service (PDS).

Information from routinely collected electronic datasets is inexpensive and its use in population- based studies to investigate disease incidence, mortality and public health issues has long been established. There has been growing interest in using routine data to assess clinical outcomes [44], particularly in cancer management, in the hope that regular feedback will facilitate improved outcomes [45]–[49]. Whilst dates of diagnosis and recurrence may not be directly captured in the data it is possible to identify information to serve as surrogates for these relevant time points and Ricketts et al recently demonstrated that routine data could be used to estimate OS and PFS in patients with head and neck cancers treated with radical radiotherapy [50], [51].

This project aims to develop and optimise a methodology to extract OS and PFS from routinely collected electronic healthcare data for patients treated with primary radical radiotherapy for LA NSCLC that will enable information to be evaluated effectively and efficiently.

2.1.1 Aims

This chapter will focus on assessing current survival outcomes for patients with stage IIIA/B NSCLC treated with radical radiotherapy with or without chemotherapy, using routine data.

2.1.2 Objectives

- Assess current survival outcomes in patients treated with definitive radiotherapy for LA NSCLC using a methodology developed to perform large scale data analysis by extracting information from routine data to analyse survival estimates
    - Work with our hospital informatics team to collect data
    - Learn to interpret coded data from routine data sets and correlate them to relevant time points in patients' diagnostic and management pathways
    - Develop a mechanism for back-dating codes that act as proxy measures for key events to improve accuracy of survival estimates

2.2 Methods

All patients with LA NSCLC, taken to be any patient with stage IIIA/B disease (appendix 1), treated with primary radical radiotherapy in a 2 year period (August 2013 to August 2015) in University College London Hospital, a regional referral centre, were identified for this initial pilot study of 43 patients.

For each patient, routine data was obtained via the hospital informatics team. Key time points were identified and extracted from the integrated routine data to form a timeline that reflected the Gold standard manual data (table 1). OS and PFS, based on manual data, was then compared to estimated OS and PFS, based on paired routine data (figure 1).

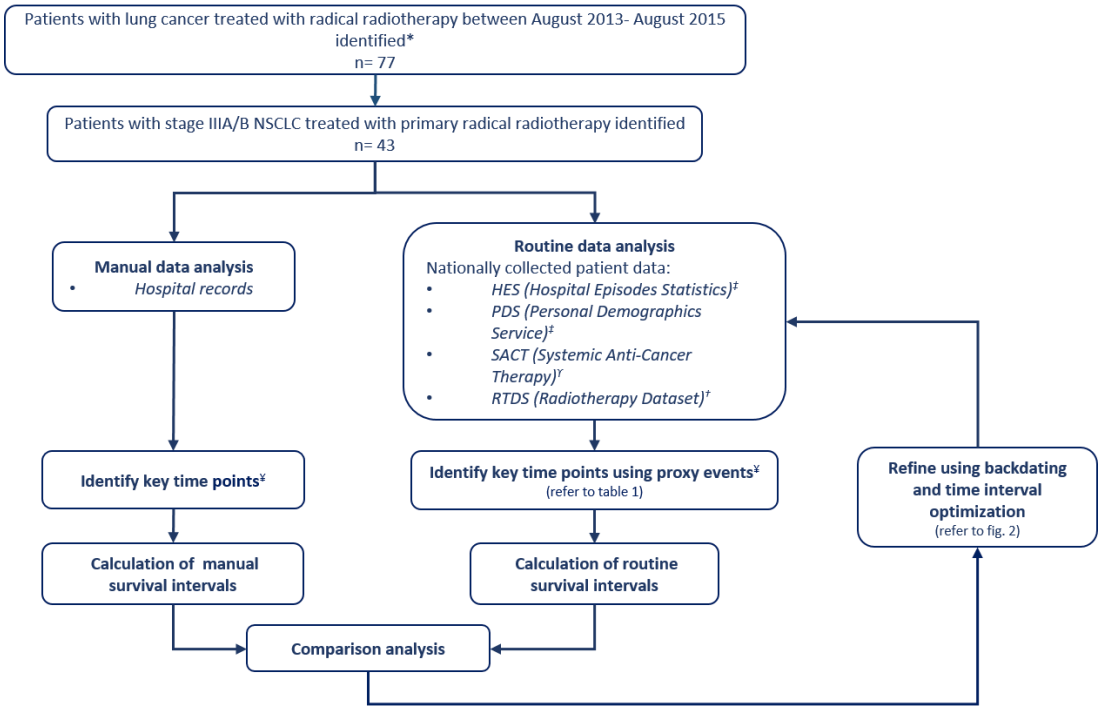

Figure 1. Flow chart showing the process of manual and routine data analysis for patients with LA NSCLC. * Patients were identified from RTDS data by searching lung cancer ICD10 codes. ‡ Data obtained via the Hospital Informatics team. ϒ Data obtained from the hospital prescribing Chemocare system. †Data obtained via the radiotherapy department. Relevant time points were identified (¥ date of diagnosis, recurrence, death or last clinical encounter) and used to calculate PFS and OS intervals for the data sets which were then compared to assess agreement. Backdating and time interval optimisation was then used to refine the process and improve correlation.

2.2.1 Manual Dataset

The manual data was extracted from hospital notes which included clinic letters, multidisciplinary team (MDT) meetings, histopathology and radiology reports, and chemotherapy and radiotherapy treatment records. The relevant time points required to calculate PFS and OS were the date of diagnosis, recurrence, and death or last known appointment.

a. **Manual diagnosis date:** The diagnostic biopsy date was chosen to most accurately represent the date of diagnosis as this is when histological confirmation of disease is obtained. If the biopsy date was not available (eg. if the biopsy was performed in a different hospital) then other dates were used following a hierarchy, as defined by the UK National Lung Cancer Audit, of date of: i) imaging in the form of CT (computed tomography) and PET CT (positron emissions tomography CT) ii) admission to hospital due to this malignancy iii) patient's evaluation at an out-patient clinic relating to this malignancy and iv) referral [52] (table 1).

b. Manual recurrence date: The recurrence date was taken to be the date of recognized progression, recurrence, metastases, death, or last known clinical encounter (if no progression occurred). Progression, recurrence or metastatic disease was determined by dates of any investigative procedure, including radiological scans or biopsies, which first positively identified disease recurrence (table 1).

Time Points	Definitions for Manual Data	Definitions for Routine Data
Diagnosis date	In order of preference [52]: ❖ Date of first histological or cytological confirmation of malignancy. - date when specimen taken - date of receipt by pathologist - date of pathology report ❖ Date of imaging from a CT, PET scan or other form of clinical diagnosis ❖ Date of admission to hospital because of this malignancy. ❖ When evaluated at an oncology out-patient clinic only: date of first consultation at out-patient clinic because of this malignancy ❖ Date of referral	HES ❖ Date of biopsy (taken as the optimal date of diagnosis) within pre-specified time window of X weeks of treatment initiation If not available, then the earliest within a pre-specified time window of X weeks of treatment initiation: HES ❖ First relevant ICD10 code (appendix 2) ❖ OPCS identifying relevant time points and proxy measures for investigation (appendix 4a) and management (appendix 4b) RTDS ❖ Date of request on booking form consent date for secondary treatment. (This date must correspond to treatment that is also documented in the RTDS with "Category: Radical") SACT ❖ Start date
Recurrence date	Any of the following that first positively identifies recurrent, progressive or metastatic disease: ❖ Date of radiological scan identifying recurrence, progressive, or metastatic disease ❖ Date of biopsy procedure confirming recurrence	The earliest within a pre-specified time window of X weeks of *secondary treatment initiation: HES ❖ ICD10 codes for secondary malignancies (appendix 3) ❖ OPCS and ICD10 codes identifying relevant time points

	❖ Date of clinic if a clinical diagnosis of recurrence, progressive, or metastatic disease is made and no scans or biopsies undertaken	and proxy measures for recurrent, progressive or metastatic disease investigation (appendix 5a). RTDS ❖ Date of request on booking form consent date. (This date must correspond to treatment that is also documented in the RTDS with "Category: Palliative" If there are no secondary treatment codes (appendix 5b) but there are ICD10 codes for secondary malignancies (appendix 3), these can be used to identify recurrence dates. If there are no ICD10 codes for secondary malignancies or investigative procedures then the start date of secondary treatment can be used: HES ❖ OPCS identifying secondary management for recurrent, progressive or metastatic disease (Appendix 5b) RTDS ❖ Start date SACT ❖ Start date
Death date	❖ Date of recorded death from medical notes or clinical letters	❖ Date of recorded death on PDS
Endpoint if no recurrence or death	❖ Last known clinical encounter with any specialty (in the hospital or community) based on clinical letters or letters of correspondence from the patient or their next of kin	❖ Date of last HES, SACT, RTDS entry.

Table 1. Definitions of key time points used to calculate PFS and OS for manual data and the ICD-10 (international classification of diseases) and OPCS (Office of population censuses and surveys classification of surgical operations and procedures) codes used for diagnosis and recurrence flag events from the routine data. ***** Secondary treatment is defined as any treatment being initiated 10 weeks following completion of primary treatment, identified using relevant codes (appendix 5b).

2.2.2 Routine Dataset

Routine data was collected from HES, SACT, RTDS, and PDS (table 2).

Routine Dataset	Information available
PDS (Personal Demographics Service) *National electronic database and component part of the NHS Spine (the national databases of information regarding patients' health and care)*	• Name • Address • Date of birth • NHS Number • Date of death
HES (Hospital Episodes Statistics) *Patient care data of all patients treated by the NHS in England (including private patients treated in NHS hospitals and patients resident outside England receiving treatment funded by the NHS)*	• Dates of all hospital encounters including admissions and discharge dates, outpatient appointments, and A&E attendances. • Diagnoses • Operations • Age group • Gender • Ethnicity • Area of patient's residence
SACT (Systemic Anti-Cancer Therapy) *Clinical management information on patients undergoing chemotherapy in (or funded by) the NHS in England.*	• Demographics- including commissioner and provider initiating treatment • Clinical status-diagnosis, performance status, treatment intent • Programme and regimen- drug details, cycle and regime number, supportive medications , treatment dates • Outcome- regimen modification eg. dose reductions, cycle delays, early termination of treatment, and outcome summary.
RTDS (Radiotherapy Dataset) *Clinical management information on patients undergoing radiotherapy treatment collected locally by radiotherapy centres and submitted to the National Clinical Analysis and Specialised Applications Team.*	• Demographics- commissioner and provider initiating treatment • Clinical status- diagnosis, treatment intent, history of previous radiotherapy (diagnosis relating to that treatment, treatment intent, dose, fractionation, site treated, dates of referral and of treatment). • Dose prescription- dose and fractionation regime, treatment site • Outcome- actual dose delivered, treatment dates

Table 2. Routine datasets. This shows the national datasets available for analysis, their intended function and the patient-specific information that can be collected from the different databases.

Surrogates were identified as suitable proxy measures for dates of diagnosis and recurrence events.

a. **Routine diagnosis date:** This was taken to be the corresponding date of biopsy OPCS codes (appendix 4a) (available for all patients investigated within our centre), so long as it fell within a pre-specified time window of x weeks of lung cancer treatment initiation (appendix 4b) (see section “Interval definitions for back-dating”). If biopsy codes were not found on routine data , proxy time points were used as surrogates as long as they occurred within this pre-specified time window from start of primary treatment: the earliest of (i) the first relevant ICD10 codes denoting lung malignancy (appendix 2) or (ii) other investigative OPCS codes (appendix 4a).

b. **Routine recurrence date:** The date of progression, recurrence or metastases was identified using (i) ICD 10 codes for secondary malignancies (appendix 3) or investigative procedures (appendix 5a) which occurred within a pre-specified time window prior to secondary treatment (appendix 5b) initiation (ii) ICD10 codes identifying secondary malignancies if no secondary treatment codes appeared (iii) the start date of secondary treatment if no ICD10 codes for secondary malignancies or investigative procedures were seen on routine data.

Secondary treatment was defined as any treatment event occurring more than 10 weeks after the end of primary treatment (last day of radiotherapy or chemotherapy, whichever occurred last) and further identified by OPCS codes in appendix 5b.

2.2.3 Survival Intervals

PFS was taken to be the time interval between the diagnosis date and the date of progression, recurrence or metastases. If no progression occurred the date of last known clinical encounter or death was used.

OS was taken to be the time interval between the diagnosis date to the date of death from any cause or date of last known clinical encounter (if the patient was still alive at the time of analysis).

Key code tables were generated to aid interpretation of the routine data (appendices 2-5b), enabling the identification of codes signifying the relevant time points. The datasets were analysed separately in this manner and then merged to create a timeline.

2.2.4 Code identification and classification

Codes were identified and sorted according to diagnostic ICD 10 codes consistent with lung malignancy (appendix 2 and 3) and OPCS codes consistent with diagnostic investigations (including biopsies and CT or CT PET imaging) (appendices 4a and 5a) and management strategies (appendices 4b and 5b), separated into radiotherapy, chemotherapy and interventional treatment.

a. ICD-10 codes indicating primary site lung malignancies (appendix 2)

All codes relating to “malignant neoplasm of bronchus or lung” [C34], “malignant neoplasm of heart, mediastinum and pleura” [C38], and “Secondary and unspecified malignant neoplasm of intrathoracic lymph nodes” [C77.1] were identified as the majority of patients with LA NSCLC have mediastinal lymph node involvement. The additional code, “Abnormal findings on diagnostic imaging of lung” [R91] was included given the first suspicion of lung malignancy arises from abnormalities seen on chest x-rays or CTs, acknowledging this does not confirm diagnosis.

b. OPCS codes identified for primary diagnostic event (appendix 4a)

Codes identified as surrogates for the diagnosis of LA NSCLC included biopsies of the lung, pleura and mediastinal lymph nodes and procedures whereby specimens are obtained for cytological confirmation of malignancy. Imaging with body and head CT and PET CT are important for staging of disease and glomerular filtration rate testing is standardly performed for any patient being considered for chemotherapy.

c. OPCS codes identifying primary management (appendix 4b)

Primary management codes included those denoting treatment with radical radiotherapy (identified as intensity modulated radiotherapy [X67.1] and complex conformal radiotherapy [X67.7]) and chemotherapy. Interventional codes included endovascular stent placement [L76.9] and insertion of stent into vena cava [L79.3] (which means the patient experienced superior vena cava obstruction secondary to a locally advanced tumour in the lung apex) and required treatment with stent insertion.

d. ICD-10 codes indicating secondary site malignancies or complications from recurrent/ progressive/ metastatic disease (appendix 3)

The codes identified for the diagnosis of recurrent, progressive or metastatic disease mostly included those with “Secondary & unspecified malignant neoplasm of-“ as this implies that malignant disease has metastasized to this site; and codes that identified complications from metastases, such as cerebral oedema [G93.6], which can result from cerebral metastases. Additionally, there were codes that overlapped with those identifying primary presentation as recurrent and metastatic disease can present with similar complications depending on the location of disease.

e. OPCS codes identified for recurrent, progressive or metastatic disease diagnostic event (appendix 5a)

Codes identified as surrogates for the diagnosis of recurrent, progressive or metastatic disease overlapped codes for primary presentation, as biopsies are used to confirm recurrence and imaging is used to re-stage disease. Additional imaging OPCS codes included those denoting MRI spines ([U211 AND Z06.1], [U21.1 AND Z06.2], [U21.1 AND Z99.2], [U21.1 AND Z06.3]) and bone scans [U14.1], as these are not routinely done at initial staging but are performed to investigate metastases to the spine and bones, respectively.

f. OPCS codes identifying secondary management for recurrent, progressive or metastatic disease (appendix 5b)

Radiotherapy OPCS codes for “simple radiotherapy” ([X67.5], [Y91.2]) were used as they indicate that treatment is non- curative (as opposed to “complex radiotherapy” [X67.7], which indicates treatment is radical with the intention of cure). The only exception to this rule is that “Preparation for intensity modulated radiation therapy” [X67.1] (considered complex radiotherapy that is usually delivered in the radical setting) is also used to code for SABR (stereotactic ablative radiotherapy), which can be used to treat oligometastatic (single or few systemic metastases that are amenable to surgery or ablative therapy) disease.

For chemotherapy OPCS codes, only “Delivery of exclusively oral chemotherapy for neoplasm” [X73.1] is exclusive to patients being treated for recurrent or metastatic disease because there are no oral chemotherapy drugs currently used in the radical setting. The SACT data can be used in conjunction with the OPCS codes as it details the specific chemotherapy drugs delivered to patients and this information can be used to help discriminate curative or non-curative (palliative) treatment as some drug regimens are used exclusively as palliative treatment.

Interventional codes for endovascular stent placement and insertion of stent into vena cava were also included here as superior vena cava obstruction can be a complication of locally recurrent or metastatic disease requiring treatment with stent insertion.

2.2.5 Interval definitions for back-dating

The process of interval back-dating was used to optimize the correlation of manual and routine intervals when using proxy time points from the routine data and filter out diagnostic events that yielded negative results (Figure 2). For the date of diagnosis, a back-dating window of 6 weeks (1.5 months) was chosen as the interval during which a diagnostic event might occur prior to the initiation of primary treatment (denoted by a relevant investigative OPCS code), or ICD10 code indicating primary diagnosis (whichever occurred earliest). If a biopsy OPCS code was available, this was taken to be the date of diagnosis, so long as it occurred within 6 weeks prior to the start of primary treatment, with no further back-dating to other investigate codes. The same backdating interval was used to identify the diagnostic events for secondary malignancy presentation prior to initiation of secondary treatment.

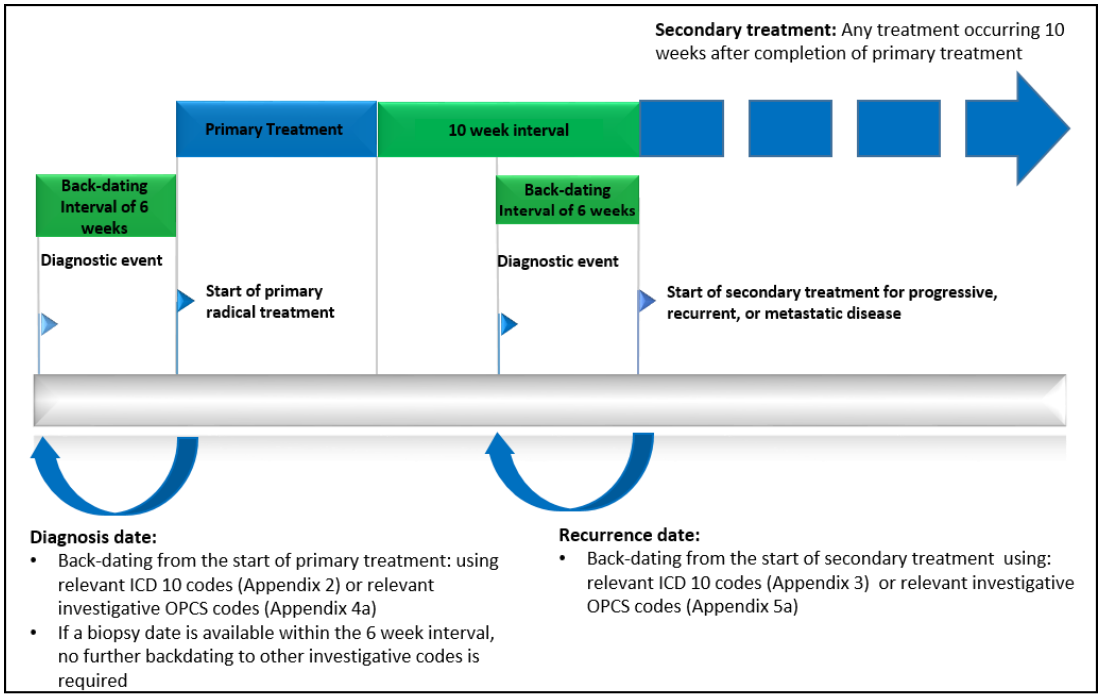

Figure 2. Schematic showing back-dating intervals used for optimization of key time points extracted from routine data. The date of biopsy is taken to be the date of diagnosis, so long as this date is within a 6 week period of an OPCS code indicating the start of primary treatment. If there is no biopsy date, then any diagnostic event or relevant ICD 10 code (whichever occurs first) occurring within a 6 week period prior to an OPCS code indicating the start of primary treatment is taken to be the date of diagnosis of primary disease. For example, an OPCS code for investigative imaging occurring within 6 weeks prior to treatment, implies there was already clinical suspicion of malignancy at the time of that scan. For the date of recurrence, progressive or metastatic disease, any diagnostic event or ICD10 code (whichever occurs first) occurring within a 6 week period prior to an OPCS code indicating the

start of secondary treatment is taken to be the date of recurrence. Any treatment event occurring after 10 weeks after completion of primary treatment was interpreted as secondary treatment. If no secondary treatment has been given then a secondary malignancy ICD 10 code (appendix 3) can be used to identify recurrent disease.

Correlation of these datasets were then tested on the key clinical outcome indicators of OS and PFS to establish if routine data could be used as a reliable proxy measure for manual data.

2.3 Results

One hundred and sixty patients were identified as receiving radical radiotherapy, 43 of whom were patients with stage IIIA/B NSCLC.

The manual data showed a median age of 67 years (range 46- 89years) and all patients had stage IIIA/B disease. Using the manual data, the median PFS was 10.78 months (range 1.58- 37.49 months) and median OS was 16.36 months (range 2.69- 37.49 months).

Based on routine data, using proxy measures, the estimated median PFS was 10.68 months (range 1.61- 31.93 months) and estimated median OS was 15.38 months (range 2.14- 33.71 months).

Overall, the routine data underestimated the PFS and OS of the manual data but there was good correlation with a Pearson correlation coefficient of 0.94 for PFS and 0.97 for OS.

2.3.1 Patients' characteristics

We identified 43 consecutive patients for this pilot study, 27 of whom were men and 16 women. Patient demographics are displayed in Table 3. The median age was 67 years (range 46-89years) and all patients had stage IIIA/B disease. The majority of patients were PS (performance status) 0-1 but for 6/43 patients the PS was not recorded and 3/43 patients had a PS of 2. 20/43 patients had the optimal cCRT (concurrent chemoradiotherapy) [53], 9/43 patients had sCRT (sequential chemoradiotherapy), 13/43 patients had radical radiotherapy alone, and 1 patient unconventionally received gefitinib followed by radical radiotherapy (table 3).

22 patients had adenocarcinomas (18 of whom had no sensitizing mutations and 3 with unknown EGFR/ALK status), 19 had squamous cell carcinomas, in 1 patient it was not possible to further differentiate the tumour beyond determining that it was a NSCLC.1 patient

had no definitive invasive malignancy demonstrated on biopsy but was treated due to high clinical suspicion.

Patient	Age range	PS	Stage	Histology	Treatment
1	45-49y	PS1	IIIA	Squamous cell carcinoma	cCRT (CVx4; 64Gy in 32#)
2	65-69y	PS0	IIIA	Squamous cell carcinoma	sCRT (GCarb x4; 64Gy in 32#)
3	70-74y	PS1	IIIA	Squamous cell carcinoma	cCRT (CV x1-stopped due to AE; 64Gy in 32#)
4	70-74y	PS1	IIIA	Squamous cell carcinoma	sCRT (GCis x4; 55 Gy in 20#)
5	80-84y	PS1	IIIA	Adenocarcinoma. EGFR WT	sCRT (pemcarbo x2- stopped due to AE; 64Gy in 32#)
6	55-59y	PS1	IIIA	Adenocarcinoma EGFR WT	cCRT (CV x4, 64Gy in 32#)
7	70-74y	PS1	IIIB	Squamous cell carcinoma	sCRT (GCarbo x3- stopped due to AE; 55Gy in 20#)
8	65-69y	PS0	IIIA	Squamous cell carcinoma	cCRT (CVx3; 55gy in 20#)
9	65-69y	NR	IIIA	Squamous cell carcinoma	RT alone: 55gy in 20#
10	55-59y	NR	IIIA	Squamous cell carcinoma	RT alone: 64Gy in 32#
11	65-69y	NR	IIIB	Squamous cell carcinoma	sCRT (GCisx2 switched to GCarbo x 2 due to AE; 64Gy in 32#
12	65-69y	NR	IIIA	Adenocarcinoma. EGFR and ALK WT	cCRT (CV x4, 64Gy in 32#)
13	75-79y	PS1	IIIA	Adenocarcinoma. EGFR mutation	Gefitinib x6 followed by 55 in 20#
14	65-69y	PS0	IIIA	Adenocarcinoma. EGFR and ALK WT	cCRT (CVx1 switched to CarboV x3 due to AE; 64Gy in 32#)
15	65-69y	PS1	IIIA	High grade dysplasia at least; no definitive invasive malignancy	cCRT (CV x4; 64Gy in 32#)
16	55-59y	PS1	IIIA	Squamous cell carcinoma	cCRT (CV x2; 64Gy in 32#)
17	70-74y	NR	IIIB	Adenocarcinoma. EGFR and ALK WT	RT alone: 64Gy in 32#
18	75-79y	PS0	IIIB	Adenocarcinoma. EGFR and ALK WT	cCRT (CisN; 64Gyin 32#)
19	80-84y	PS2	IIIB	Squamous cell carcinoma	RT alone: 64Gy in 32#

20	50-54y	PS1	IIIA	Adenocarcinoma. EGFR and ALK WT	cCRT (CV x4; 64Gy in 32#)
21	50-54y	PS0	IIIA	Adenocarcinoma. EGFR and ALK WT	cCRT (CV x3; 64Gy in 32#)
22	55-59y	PS1	IIIB	Adenocarcinoma. EGFR and ALK WT	RT alone: 64Gy in 32#
23	70-74y	PS1	IIIA	Squamous cell carcinoma	RT alone: 55Gy in 20#
24	75-79y	PS1	IIIA	Adenocarcinoma. EGFR and ALK WT	sCRT (CVx4; 64Gy in 32#)
25	80-84y	PS1	IIIA	PD carcinoma(no comment on EGFR/ALK)	RT alone: 55Gy in 20#
26	60-64y	PS0	IIIA	Adenocarcinoma. EGFR and ALK WT	sCRT (CV x2 switched to CarboV x2 due to AE; 64Gy in 32#)
27	80-84y	PS0	IIIA	Squamous cell carcinoma	cCRT (CV x4; 64Gy in 32#)
28	45-49y	PS1	IIIB	Squamous cell carcinoma	cCRT (CV x4; 64Gy in 32#)
29	65-69y	PS1	IIIA	Squamous cell carcinoma	cCRT (CarboVx3; 64Gy in 32#)
30	45-49y	PS1	IIIA	Adenocarcinoma-insufficient material for ALK/EGFR testing	sCRT (cispem x4; 64Gy in 32#)
31	65-69y	PS0	IIIA	Adenocarcinoma. EGFR and ALK WT	cCRT (CV x4; 64Gy in 32#)
32	60-64y	PS1	IIIA	Adenocarcinoma. EGFR and ALK WT	sCRT (cispemx2 switched to CV x2 due to AE; 64Gy in 32#)
33	60-64y	PS1	IIIB	Squamous cell carcinoma	cCRT (CV x4; 64Gy in 32#)
34	70-74y	PS1	IIIB	Squamous cell carcinoma	RT alone: 64Gy in 32#
35	60-64y	PS1	IIIB	Adenocarcinoma. EGFR and ALK WT, KRAS mutation	cCRT (CV x4; 64Gy in 32#)
36	45-49y	PS1	IIIA	NSCLC-not possible to further differentiate tumour type	cCRT (CV x4; 64Gy in 32#)
37	70-74y	PS2	IIIA	Squamous cell carcinoma	RT alone: 55Gy in 20#
38	65-69y	PS1	IIIB	Adenocarcinoma. EGFR and ALK WT	cCRT (CV x4; 64Gy in 32#)
39	55-59y	PS1	IIIB	Adenocarcinoma. EGFR and ALK WT	cCRT (CV x6; 64Gy in 32#)
40	80-84y	PS1	IIIA	Adenocarcinoma	RT alone: 55Gy in 20#
41	75-79y	NR	IIIB	Adenocarcinoma. EGFR and ALK WT	RT alone: 64Gy in 32#; declined chemo
42	60-64y	PS2	IIIA	Adenocarcinoma. EGFR and ALK WT	RT alone: 55Gy in 20#
43	85-89y	PS1	IIIA	Squamous cell carcinoma	RT alone: 55Gy in 20#

Table 3. Patients' characteristics. NR (Not recorded). PS (Performance status)* (index 4 [54]), EGFR (epidermal growth factor receptor), EGFR mutation (epidermal growth factor receptor with a sensitizing mutation to targeted therapy), ALK (anaplastic lymphoma kinase), Kras (K-rat sarcoma), WT (wild type) meaning no sensitizing mutations

are found. cCRT (concurrent chemoradiotherapy), sCRT (sequential chemoradiotherapy). RT (radiotherapy). 4 cycles of chemotherapy are usually given. CV (cisplatin and vinorelbine), CarboV (carboplatin and vinorelbine), GCis (gemcitabine and cisplatin), GCarb (gemcitabine and carboplatin), Pemcarbo (pemetrexed and carboplatin), CisN (cisplatin and navelbine). AE (adverse event).

2.3.2 Survival and Recurrence

Using the manual data, the median PFS was 10.78 months (range 1.58- 37.49 months) and median OS was 16.36 months (range 2.69- 37.49 months). Based on the routine data, using proxy measures, the median PFS was estimated at 10.68 months (range 1.61- 31.93 months) and median OS was estimated at 15.38 months (range 2.14- 33.71 months) (figure 3a and 3b).

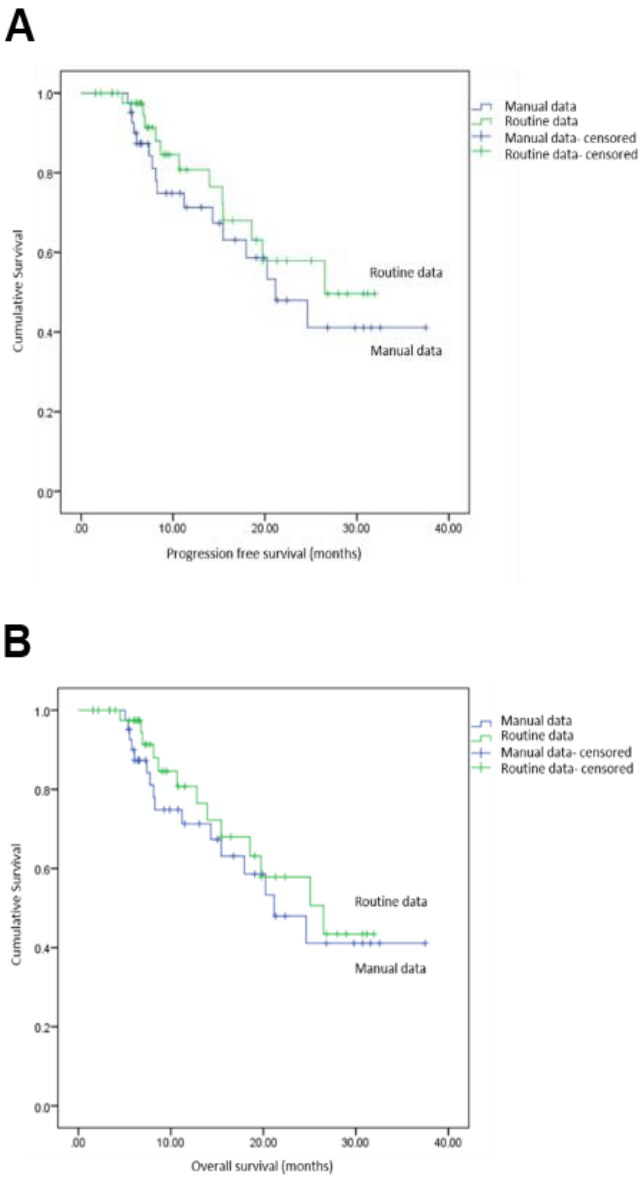

Figure 3. A. Kaplan Meier Curve for PFS (in months). Survival curves for the routine (green line) and manual (blue line) data are shown. 27/43 events censored from the manual data and 31/43 events censored from the routine data.

Wilcoxon signed-ranks test statistic 1.10, p(0.29). **B. Kaplan Meier Curve for OS** (in months). Survival curves for the routine (green line) and manual (blue line) data are shown. 27/43 events censored from the manual data and 30/43 events censored from the routine data. Wilcoxon signed-ranks test statistic 0.080, p(0.78).

The routine methodology failed to detect 4 recurrences and 3 deaths resulting in increased censoring of events and a separation of the curves that was not statistically significant for either endpoint.

2.3.3 Data correlation

Overall the routine data underestimated the PFS (manual (mean=13.88 months, SD= 9.31); routine (mean= 13.79 months, SD=8.95) and OS (manual (mean=16.49 months, SD= 9.33); routine (mean= 15.48 months, SD=9.17) of the manual data. A paired sample t-test for the mean PFS showed a difference of 0.09 months (p=0.86; 95% confidence interval -0.86- 1.03) and 1.02 months (p=0.00; 95% confidence interval 0.34- 1.69) for the difference in the mean OS. However, there was good overall correlation of 0.94 (p=0.00, 95% confidence interval 0.90- 0.97) for PFS (figure 4a) and 0.97 (p= 0.00, 95% confidence interval 0.95- 0.98) for OS (figure 4b).

The routine methodology correctly identified 32/43 routine diagnosis dates to within 2 weeks accuracy of the manual diagnosis dates, and of those, 21/43 dates matched exactly. 5/43 routine diagnosis dates were earlier than the manual dates (ranging from 1-6 days earlier). 5/43 routine diagnosis dates were outside of 2 weeks but within 4 weeks of the manual data; and for 6/43 patients, there was a >28 day difference in routine and manual diagnosis dates, with the routine dates occurring later than the manual. 3 patients had a difference in diagnosis dates of >100 days. Whilst the paired sample t test showed that routine data tend to suggest later diagnosis dates compared to that identified by manual data (t=-2.45; p=0.02) and the overall correlation was 0.98 (p=0.00, 95% confidence interval 0.96- 0.99) (figure 4c).

The sensitivity and specificity of using routine data instead of manual data to determine recurrences was 0.75 and 1, respectively. 12/16 recurrences were correctly detected when assessing the routine data alone. 4/16 routine recurrence dates were within 2 weeks of the manual diagnosis dates, and of those, 3/16 dates matched exactly. 6/16 routine diagnosis dates were outside of 4 weeks but less than 100 days of the manual data. For 2/16 patients, there was a >100 day difference in routine and manual diagnosis dates (figure 4c).

The sensitivity and specificity of using routine data instead of manual data to determine death event was 0.81 and 1, respectively. 13/16 death events were correctly detected on the routine

data and of those, 12/13 dates of death matched exactly and for the remaining other patient, the routine date fell within 1 week of the manual death date. For 27 patients who were still alive at the time of assessment and for whom the last clinical encounter was used as the end-interval, the manual and routine dates matched exactly for 24/27 patients (figure 4b).

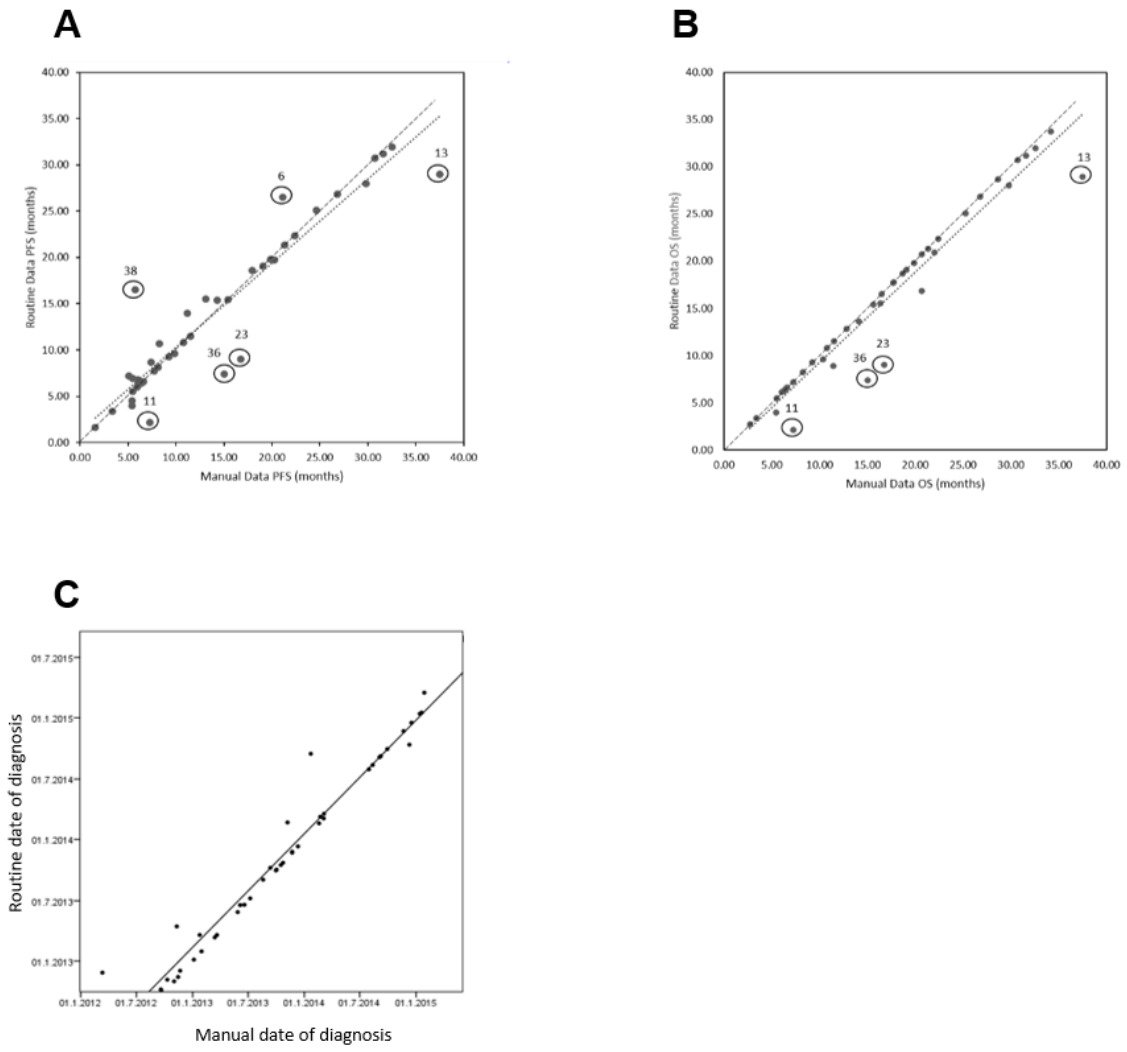

Figure 4. A. Correlation between manual and routine derived PFS intervals. Correlation coefficient of 0.94, p<0.0001. Solid line represents the line of best fit for the data points. Dashed line represents the correlation line if the manual and routine data were equal. Outliers are circled and identified with their patient number corresponding to table 3. **B. Correlation between manual and routine derived OS intervals.** Correlation coefficient of 0.97, p<0.0001. Solid line represents the line of best fit for the data points. Dashed line represents the correlation line if the manual and routine data were equal. Outliers are circled and identified with their patient number corresponding to table 3. **C. Correlation between manual and routine dates of diagnosis.** Correlation coefficient of 0.98, p<0.0001. Solid line represents the line of best fit for the data points.

For patients 13 and 11, diagnosis and chemotherapy (as part of sCRT) were initiated in other hospitals and followed-up continued there, resulting in missing clinical episodes on routine

data but detection on manual data (as clinical correspondence letters were available). The result was later routine diagnosis dates and shorter overall routine PFS and OS. Patient 36 similarly continued follow-up in another hospital. For patients 23 and 6 a late routine diagnosis date resulted from positive diagnostic investigations falling outside the 6 week back-dating interval from treatment and alternative surrogates being used, resulting in a shorter PFS and OS. For patient 38, the routine PFS was shorter as recurrence was not detected on routine data due to individualised treatment which was not listed as a standard treatment code.

Excluding patients with missing data (patients 11, 13, 36- referred from other hospitals), correlation in PFS and OS increased to 0.96 and 0.99, respectively (figure 5).

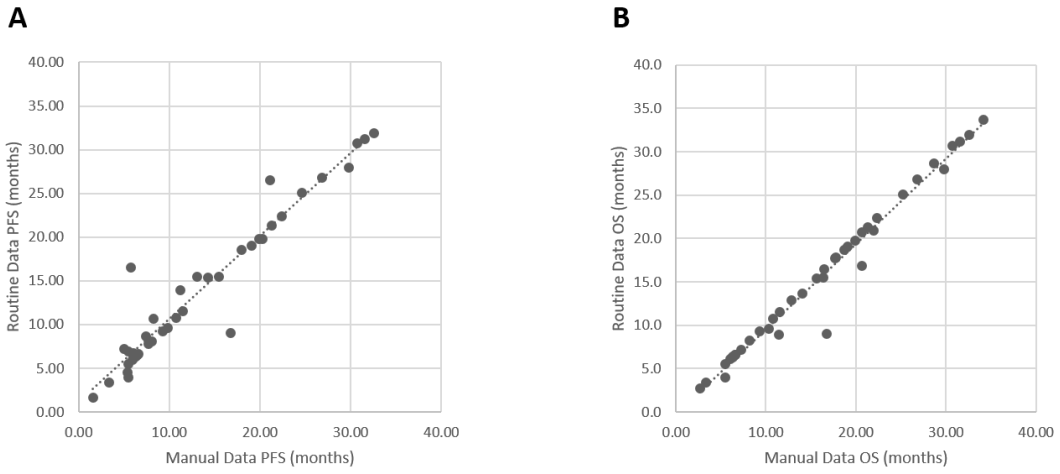

Figure 5. Improved correlation between manual and routine derived survival-outcomes when using single-centre data. A. Correlation for PFS intervals. Improved correlation coefficient of 0.96 (from 0.94). Dashed line represents the line of best fit for the data points. **B. Correlation for OS intervals.** Improved correlation coefficient of 0.99 (from 0.97).

2.4 Discussion

In this pilot study, we analyzed the PFS and OS for 43 patients with LA NSCLC treated in our regional referral centre in north London over a 2 year period. The results suggest that routine data can potentially be used to reliably estimate survival outcomes for patients with LA NSCLC treated with primary radical radiotherapy. This method relies on identifying relevant ICD-10 and OPCS codes that are used as surrogates for diagnosis and recurrence dates followed by a refining process that involves back-dating interval optimization to improve correlation.

There are some crucial considerations in defining the key time points both for the manual data and routine data interpretation: 1. Manual diagnosis dates: These followed a hierarchy with imaging following the preferred diagnostic biopsy date due to certain limitations: Whilst imaging can give a strong indication of malignancy, patients with lung cancer often have background lung disease that makes them prone to recurrent chest infections. Radiological changes seen during active chest infections make identifying malignancy less reliable. This is in contrast to identifying recurrence and/or metastatic disease when malignancy is already known, and diagnosis is often done radiologically without repeat biopsies, unless diagnosis is uncertain. 2. Manual and routine recurrence interval dates: Taken to be the date of progression, recurrence, metastases, death, or last known clinical encounter (if no progression occurred) for practical reasons- so that events would be reached. 3. Identifying secondary treatment in routine data: Any therapy starting after a 10 week interval from the last day of radiotherapy or chemotherapy (whichever was completed last) was chosen as an indicator of secondary treatment because it is standard practice for patients to have reassessment imaging at 8- 12 weeks following completion of treatment. At this point, progressive or metastatic disease can be observed so a 10 week interval was selected as a compromise- too short an interval might pick up delayed primary treatment events, and too long an interval might miss the start of secondary treatment.

OS and PFS values derived from our routine data methodology correlated well with that derived from the gold standard manual data with the Wilcoxon signed-rank test results suggesting no statistically significant difference between the survival curves when assessed by manual versus routine data. Based on the manual data, the median PFS and OS was 10.78 months and 16.36 months, respectively. Using the proxy measures from the routine data, the estimated median PFS and OS was 10.68 months and 15.38 months, respectively. The paired sample t-tests showed the difference in the mean PFS to be small and non-significant but the difference in the mean OS to be larger and significant. However, these results correlated well overall with the manual data, giving a statistically significant correlation coefficient of 0.94 for PFS and 0.97 for OS. The high sensitivity and specificity of our method indicate that analyzing

routine data does not tend to falsely identify recurrence or death events so survival estimates are less likely to be underestimated.

All discrepancies between the manual and routine data sets could be attributed to 1.Missing or inaccurately entered OPCS or ICD10 codes due to a) patients having diagnosis and/or recurrence detected with treatment initiation in other hospitals b) codes appearing on patients' admission dates rather than the dates of the procedures themselves or c. treatment of recurrence being non-standard (eg. oligometastatic disease being treated surgically) and 2. Delays in initiation of treatment beyond the NHS England target of 31 days due to, for example, patients becoming unwell, resulting in alternative surrogates having to be used for dates of diagnosis or recurrence. The reasons for deaths escaping detection on routine data were mostly unclear although 1 patient died abroad, a situation that is perhaps less reliably updated on to the system. However, there is a time lag between the occurrence of death and its record being updated on the system, and it is possible that this affected the ability to detect death events on routine data. These all led to late diagnosis dates, late or absent recurrence dates, and/or absent death dates and subsequently inaccurately calculated PFS and OS. Although this resulted in an increased censoring of events and a separation of the survival curves, the differences were not statistically significant (figure 3a and b).

Our back-dating strategy, used to optimize correlation between manual and routine primary diagnosis and recurrence event dates, utilized time intervals tailored to reflect clinical practice and the clinical target times set out by NHS England (2013). This framework recommends that the maximum time from diagnosis to first definitive treatment is 1 month (or 31 days); and that for all subsequent treatments for new cases or primary and recurrent cancer, the maximum time interval is 1 month (or 31 days). Therefore, ICD10 codes consistent with a primary diagnosis or recurrent, progressive or metastatic disease, are likely to be preceded by diagnostic investigation codes within a period of up to 31 days. A longer interval of 6 weeks was chosen to avoid potentially missing relevant investigative and diagnostics flag for patients who may have started treatment beyond the 31 day target. This meant we still captured patients who may have had delays in starting treatment due to 1. patients' choice 2. becoming unwell 3.radiotherapy re-planning requirements resulting from significant changes in anatomy or 4.an inability to start in the preferred time period due to patient load exceeding treatment capacity at that time.

Our findings are similar to Ricketts et al [50] who used routine data to estimate survival outcomes in patients with head and neck cancer treated radically in a single-institution. Their methodology also showed good correlation between the datasets for OS, with a correlation coefficient of 0.97 ($p<0.0001$) and 0.82 ($p<0.0001$) for PFS. Similarly, they noted that

recurrence rates were underestimated with routine data but only 21 of 40 recurrences were correctly identified compared to our 12 out of 16 recurrences. They attributed the missed recurrences to incorrect diagnosis ICD10 codes, miscoding of treatment, and very early recurrences that was not captured within their optimization window. This reinforces the known limitations of routine data when data integrity is compromised - although Ricketts et al minimized some of these issues by only including patients diagnosed and followed up in a single center, data inaccuracies still resulted in reduced correlation.

There is no ideal solution to missing data but strategies have been developed to address this, which is especially important when handling large datasets. One pragmatic approach is complete-case analysis (CCA), whereby cases with missing data are eliminated. For this study, the missing data is not dependent on the survival outcomes (known as missing not at random- MNAR) and tend to be missing at random (MAR). Where data is MAR, CCA can be used although can introduce bias [55].

An alternative approach would be to use multiple imputation (MI), which can be adapted for survival data [56], and works by replacing the missing data with plausible values. These values are derived from imputation models that contain all variables in the analysis model, including outcomes, those that predict missing data (for example, when using multicentre data and treatment initiation or follow-up occur elsewhere, interim illness resulting in delays to start of treatment) and proxy data. In order to account for uncertainty of these imputed datasets, multiple completed dataset versions are generated, analysed separately and then combined [57]–[59].

The completeness of recorded information is a fundamental limitation of both manual and routine data. Manual data not only most reliably determines outcome measures but contains important details such as histological subtype, mutation status, lung function, detailed smoking status (ex-smoker, recent ex-smoker, and quantification by pack-years), response to treatment demonstrated on CT (stable disease, partial response, progressive disease), and grading of side effects from treatment. At present such information can only be identified in manual data as these are not coded in routine data. However, clinical outcome measures can be inferred or used as proxy indicators. For example, it would be reasonable to assume that ICD10 codes for oesophagitis or neutropenia in a patient receiving chemotherapy and radiotherapy might be experiencing these side effects as a direct result from their treatment. The caveat is that there may be confounding factors or comorbidities causing these problems, the severity of these side effects are not coded, and the absence of these ICD10 codes does not mean they were not experienced. Adverse effects from treatment have an important impact on patients' ability to complete treatment and their quality of life.

Additional limitations include potentially confusing routine information for patients who have other synchronous or metachronous malignancies (eg. head and neck and bladder cancers) where recurrences and treatment may occur. For these patients with dual pathology, where “Secondary & unspecified malignant neoplasm of-” or “Secondary malignancy of-” codes appear in the HES data, referring to the RTDS and SACT data can help distinguish if treatment is being initiated for disease relating to the lung cancer or to the other malignancy as 1) the RTDS data will state the site being treated and the relevant ICD-10 diagnosis code relating to that treatment (eg. Pelvic metastases from a lung cancer primary will have “pelvis” documented as the treatment site and an ICD10 code denoting a lung cancer primary) 2) the SACT data would inform us as to what chemotherapy is being delivered (which, in itself, might be indicative of the primary, if the regime is exclusive to lung cancer) and the primary diagnosis relating to that chemotherapy regime.

Interestingly, although it is well recognized that PS impacts OS [1], [52], [60], is used to help determine the most appropriate management course [61], and is required to be recorded in manual and routine databases, this appears to be poorly recorded in both. This perhaps reflects a view that the usefulness of a PS score is limited by the degree of subjectivity and inter-observer variability in assessment [60], [62].

There has been a recognized need to improve the quality of routine data in order to broaden its clinical application. An example of one such database developed for quality improvement is the Cancer Outcomes and Service Dataset (COSD) that has recently been introduced as the new national standard for reporting cancer in the NHS in England, having replaced the National Cancer Dataset. This system will enable the clinical details and outcomes from multidisciplinary team meetings (where all patients diagnosed with and being considered for cancer treatment are discussed) to be entered in to COSD. This has begun to be in use in our hospital and one of the changes this will have on outcomes analysis will be to ascertain a more accurate diagnosis date.

In addition, national cancer strategies [41], [63] have placed increasing emphasis on recording of clinical outcome measures to help monitor if national targets are being met which will drive the enrichment of the available clinical databases, and focus more attention on developing methods to analyse routine datasets. This will not only promote the clinical usefulness of routine data for survival outcomes but potentially for treatment toxicity and patient-screening for entry into trials.

Future work includes integrating new national datasets and testing our method on a larger cohort to see if accuracy can be improved. Whilst the identified event flags used as proxy measures and the chosen back-dating intervals reflect our local practice, we have deliberately ensured they are not specific to it such that this method is transferable to other centres. As the management of NSCLC in the UK is standardized by NICE guidelines any nuances in practice across the country are unlikely to limit the application of this technique although adjustments for optimization may be required. Once this technique has been sufficiently refined, a computational algorithm will be developed to automate this process such that large scale routine data can be processed more efficiently.

2.5 Conclusions

This is a novel approach to use routine datasets to determine outcome indicators in patients with LA NSCLC that will be a surrogate to analysing manual data. The ability to enable efficient and large scale analysis of current lung cancer strategies has a huge potential impact on the healthcare system.

- *Published in BMC Health Services Research- Appendix 6*

Chapter 3

Photon radiotherapy in lung cancer

3.1 Background

Current standard practice is to use photon radiotherapy to treat locally advanced NSCLC that is limited to the thorax and surgically unresectable. For those fit enough, optimal concurrent chemoradiotherapy gives a 4.5% absolute OS benefit at 5 years compared to sequential chemoradiotherapy [53].

The major challenges with lung radiotherapy is tumour motion, changes in anatomy and tumour location over the course of treatment and tissue inhomogeneity. Four- dimensional computed tomography imaging, motion mitigation techniques and adaptive strategies using image- guidance systems, as well as improved delivery systems in the form of volumetric modulated arc therapy (VMAT), have all worked to minimise the impact of these uncertainties, improve treatment accuracy and reduce side effects [64]. Although these advances have enabled a larger population of patients with locally advanced disease to receive curative-intent doses, this has not translated into improved survival rates. This is because disease volume is often bulky, requiring large volumes to be irradiated.

The physical characteristics of photon irradiation are such that dose is deposited from entrance, builds up to a maximum before exponentially declining as it exits the patient [65]. The consequences of these features are both positive and negative. It is advantageous that photons are more forgiving of the uncertainties previously mentioned. On the other hand, large low-dose bath volumes result from multiple beams required to achieve precision therapy, making it more difficult to deliver curative doses to the tumour without compromising normal tissue tolerances. The detrimental consequences of this low-dose bath exposure to normal tissue has been highlighted by dose-escalation studies. Patients receiving higher radiation dose to the tumour showed poorer survival due to increased dose to the lungs and heart, as well as increased overall treatment time, all of which negatively impact survival and negate benefit [66].

Accumulating evidence has emphasised the importance of sparing dose to the heart, lungs and thoracic vertebrae. Radiation- induced cardiac toxicity is an independent risk factor for reduced survival [67], [68] and studies are currently attempting to identify specific substructures that are critically important, such as the base of the heart, with appropriate dose limits to guide radiotherapy planning and reduced the risk of cardiac-related mortality [68], [69]. Similarly, post-radiotherapy lymphopenia has emerged as a poor prognosticator with increasing attention being paid to limiting dose to lymphopenia related organs in the thorax, which includes the thoracic vertebra, heart and lungs [66], [70]–[75]. These organs contain

pools of circulating lymphocytes, which are critical to the body's tumour surveillance [66], [70], [71] and are extremely radiosensitive. Significant correlation between lung V5-10 and lymphocyte nadir [76]; and integral heart doses and decline in post-treatment lymphocyte counts[72] have been shown. Unsurprisingly, limiting dose to the thoracic vertebra, where 35% of haematopoietic bone marrow is located, has also been shown to reduce the risk of lymphopenia [74], [75].

The findings of the PACIFIC trial has thrust immunotherapy into the forefront of NSCLC treatment and prompted even greater emphasis on limiting radiation-related toxicity. Patients with stage III NSCLC who received PD-L1 inhibitor, durvalumab, following radical chemoradiotherapy showed an improved progression free survival of 11.2 months compared to placebo [10]. However, patients needed to have resolved grade 2 or above toxicity prior to initiating durvalumab. Furthermore, minimizing dose to organs that harbour circulating lymphocytes (ie. Heart, lungs and thoracic vertebra) may improve response to immunotherapy and improve patients' survival.

3.1.1 Aims

This chapter will review the role of advanced photon radiotherapy techniques in lung cancer management, its strengths and limitations, and potential applications to proton radiotherapy.

3.1.2 Objectives

- A literature review that will examine current standard of care when using photon irradiation for LA NSCLC
    - I drew up the VMAT lung planning protocol for patients with NSCLC for UCLH to aid service development- *appendix 7 (This planning protocol was the first UCLH VMAT lung planning protocol. It involved working with medical physicists and planning radiographers and was sanctioned for implementation in 2017.)*

3.2 Challenges in current practice

3.2.1 Motion management

Lung tumour motion is well documented. The amplitude is greatest in the superior-inferior direction and dependent on location, with lower lobe tumours moving more that upper lobe tumours where the maximum amplitude is up to 30 mm compared to 10 mm, respectively [77]–[79]. Additionally, larger tumours tend to demonstrate less motion than smaller tumours; and hilar and mediastinal nodes commonly move more than 5 mm with respiration and are known to move distinctly from the primary creating additional uncertainty [80]. This motion results in artefacts and image degradation leading to errors in tumour localization. Motion mitigation strategies are therefore imperative to minimise uncertainties required for high precision treatment.

No motion management strategy completely eliminates breathing-related uncertainty and the simplest method is to add margins to the target volume to encompass this. However, when disease volume is already bulky, adding unnecessarily large margins can result in target volumes that cannot be encompassed by a radical dose or unacceptable side effects. Patient immobilisation to minimise external motion is commonly achieved with a combination of vacuum bags and lung boards [81]. Strategies to manage internal motion can be divided into 1. Imaging organ motion by 4D CT or 4D MRI 2. Motion surrogates such as respiratory bellows or Varian real-time patient position management system or 3. Motion compensation using gating, deep inspiratory breath hold and abdominal compression and real-time motion tracking. I will focus on compensation strategies as the first two methods simply assess and verify patient-specific tumour motion rather than reduce motion.

Limiting diaphragmatic movement allows smaller internal target volumes to be applied. Abdominal compression (AC) involves use of a belt or plate that applies sustained pressure to the patient's upper abdomen [82]. Whilst this is effective in many cases, it is not easily tolerated in patients with poor respiratory function or obese patients; restricting abdominal movement can cause a reduction in lung volume, which could inadvertently result in larger doses of normal lung volume being irradiated [80]; respiratory motion can actually increase in some patients [83]; and it can cause erratic breathing and intra-fraction variation [83], [84].

Alternatives include voluntary breath hold (deep inspiratory breath hold- DIBH), Activated Breathing Control (ABC) system and gated radiotherapy, where radiation is delivered only when the tumour is in the target field and turns off when outside it [85]. However, these strategies limit acquisition and intervention times, which lengthens overall treatment time and

this is not always tolerated by patients. Furthermore, there is evidence suggesting that treatment time (greater than 34minutes) [86] has a greater impact on intra-fractional uncertainties than degree of immobilisation [87] or extent of tumour motion [88].

Intra-treatment real-time dynamic tumour tracking is the optimal form of motion management but currently requires invasive procedures in order to implant radio-opaque fiducials which have risks of pneumothorax and marker migration. A potential solution to this problem is using markerless tracking techniques which incorporate motion modelling, a process of using surrogate data as input, such as respiratory waveform, and producing a motion estimate as an output [89]. Markerless tracking techniques are not currently available clinically but there have been studies investigating the use of MV electronic portal imaging devices (EPID) [90]–[92], which are limited by treatment field size and poor contrast; or use of enhanced KV imaging systems [93], [94] [95], which enable larger views, better image quality and have demonstrated mean tracking errors as low as 2 mm using a 4DCT based templated matching method on cone beam CT projection images [93]. However all these methods require the tumour to be visible on KV images at all times, which can be problematic for locally advanced disease where proximity and/ or attachment to central structures are more likely or when radiological path length varies due to gantry rotation.

Using the 18F-FDG-PET signal is one example for PET-guided tumour tracking. Most studies investigating the feasibility of PET for dynamic lung tumour tracking have focused on the ^{18}F-FDG tracer as this is routinely used for tumour staging, making data more readily available for analysis [96]. Although ^{18}F-FDG PET imaging has not yet been incorporated into commercial radiotherapy systems, the introduction of the PET-Linac is imminent. However, two important considerations are: 1. slow imaging time (typically 3-5minutes per bed position, time-averaged over numerous respiratory cycles, each of which are approximately 4-5 seconds) and image-based reconstruction that present a significant computational burden and hurdle for real-time PET [96]; 2. the reliability of the 18F-FDG-PET signal. Abravan et al showed no significant change in FDG signal over the course of treatment in patients with stage III-IV NSCLC treated with radiotherapy (30Gy in 10fractions) and erlotinib [97]. In contrast, Masaccesi et al found differential changes in the maximum standardized uptake value (SUV_{max}) of the primary tumour and lymph nodes that was dose-dependent [98]. MRI-guided tumour tracking solutions [99]–[102] may be a suitable alternative in the future.

Proper immobilisation and optimizing motion management strategies are critical and translatable to all forms of precision radiotherapy.

3.2.2 Adaptation

Anatomical changes in the tumour and patient can occur between the planning scan and treatment and over the course of treatment. Advanced image-guidance systems like kilovoltage (KV) cone-beam computed tomography (CBCT) and megavoltage (MV) CBCT and tomotherapy have made radiotherapy treatment more robust by enabling verification of tumour location and assessment of changes in anatomy [103]. Adaptive radiotherapy is the process using such image-guidance to deliver accurate treatment in response to changes in anatomy. Such measures are crucial for high precision radiotherapy techniques where steep dose-gradients means potentially under-dosing the tumour or over-doing organs at risk if there is target misalignment.

It has been reported that tumour shrinkage can be greater than 40% in up to 50% of tumours [104], [105] and approximately one third of those having chemoradiotherapy show significant regression by the end of treatment [106]. In their study of 210 patients receiving definitive lung radiotherapy, Kwint et al demonstrated that intra-thoracic anatomical changes (ITAC) are time-dependent and treatment-dependent. More than 50% of ITACs occur in the first 1-2 weeks of treatment and are seen more commonly in those receiving concurrent (77% of ITAC) or sequential chemoradiotherapy (74% of ITAC). One or more of the following anatomical changes may be seen in the same patient during their treatment course: tumour regression or progression, tumour baseline shift, pleural effusions, atelectasis developing or resolving and infiltrative changes [105]. Interesting, despite the high incidence of anatomical changes, a significantly smaller proportion of patients (9%) require an adapted plan [105].

The incidence and variability of anatomical changes makes it important to repeat CBCTs over the course of treatment. Corrections can be done offline (between fractions) or online (immediately prior to a fraction) using linac-integrated CBCT for online isocentre corrections. Offline review help rectify systemic errors but random errors need online review and decision-trees [107]. Most commonly, the criteria to initiate adaptive planning is qualitative eg. anatomical changes are assessed by visual examination alone [108] but semi-quantitative traffic light systems have been proposed [105]. Robust image verification protocols and decision support systems are necessary to guide radiographers and clinicians on how to prioritise changes. As yet, there is no global consensus on how best to identify which patients might need adaptive planning, which anatomical landmarks plans should be made robust to eg. bony anatomy, carina, trachea, mediastinal contour, frequency of imaging or thresholds that should trigger adaptation. Currently, such protocols are department-specific.

Online adaptive replanning that can address systemic and random anatomical changes is the next step in adaptive radiotherapy evolution. The introduction of MR-linacs has meant high soft-tissues contrast images can be exploited and used for replanning [109]. However a critical limitation for any linac is the scanning and treatment planning turn-around time. For online adaptive replanning to be feasible, this needs to be minutes rather than days. Software to enable such rapid processing is under research. Examples include using deformation of treatment plans onto the "image of the day" as an online correction mechanism [110], [111]; or the segment aperture morphing (SAM) approach whereby beams are adjusted by applying "the spatial relationship between the planning target contour and the apertures to the new target contour" [112].

With new technologies on the horizon, the hope is that dosimetric gains from advanced adaptive replanning will translate into improved clinical outcomes. However, it is critical that the strengths and limitations are comprehensively evaluated prior to clinical implementation. A further hope is that we learn from evolving photon-based adaptive radiotherapy mechanisms and identify which strategies can be applied appropriately to new proton technology where image-guidance has only just been introduced.

3.3 Clinical developments in photon radiotherapy -Combination treatment with immunotherapy

The latest in personalised combination therapy is immunotherapy [10], [15]. Targeting the anti-programmed death protein-1 (PD-1) and programmed death ligand-1 (PD-L1) has been at the forefront of immune- oncology in light of the recent PACIFIC trial. This phase 3 randomised trial established immunotherapy in the radical setting for patients with stage III NSCLC treated with durvalumab following definitive chemoradiotherapy by demonstrating a 11.2 month progression free survival benefit [10] and a 24 month overall survival advantage of 10.7% (66.3% versus 55.6%) in the durvalumab group compared to the placebo group [4].

Despite these practice-changing findings, a large group of patients show primary or acquired resistance to PD-L1 inhibitors [113]. Recent research efforts have focused on improving response to immunotherapy by investigating combination treatment with chemotherapy, other immunotherapeutics or radiotherapy.

The rationale behind combining chemotherapy and immunotherapy is that there will be improved antigen presentation to T cells and a reduction in the tumour's immunosuppressive microenvironment [114]. Evidence supporting a synergy between these treatment modalities

have come from studies in patients with metastatic NSCLC and show response rates of up to approximately 60% at best. These include pembrolizumab-based trials (Cohort G of the phase II KEYNOTE-021 trial [115]; the phase III KEYNOTE-189 trial [116]); and atezolizumab-based trials (IMpower 150 [117] and IMpower 132 [118]).

Combination immunotherapeutics, such as nivolumab and ipilimumab, have also been investigated but have only shown marginal benefit of 1.7 month PFS advantage compared to chemotherapy in patients with tumour mutational burden (ie. increased number of nonsynonymous mutations that result in unique tumour neoantigens, triggering tumour recognition and killing by adaptive immune cells) [119].

Recent data has shown that radiotherapy induces immunogenic cell death and immunomodulation [120], prompting reassessment of how conventional radiotherapy can boost anticancer immunity. Radiotherapy can enhance immunotherapy by two major mechanisms. Firstly, via the increased production of pro- inflammatory cytokines resulting from increased expression of calreticulin that encourage phagocytosis by dendritic cells (known as immunogenic cell death) [121] and 2. Stimulation of cyclin guanosine monophosphate- adenosine monophosphate synthase (cGAS)-stimulator of interferon genes (STING) pathway and production of type I interferons, that is triggered by DNA-damaged cytosolic DNA [122], [123]. So far, trials investigating concurrent immunotherapy and radiotherapy for patients with locally advanced NSCLC have not demonstrated any benefit [124]–[126]. However, the optimal sequencing of treatment (ie. concurrent or following radiotherapy), radiation dosing and fractionation are unknown but might be quite different to classic radiotherapy paradigms.

Further steps to improve the radio-immunotherapeutic response has led investigators to explore use of proton therapy with immunotherapy. Proton radiotherapy has the advantage of having higher tumour immunogenicity and lower normal tissue immunosuppressive effects, compared to photon radiotherapy [34], which could translate into improved tumour control and enhanced patient survival. There are currently three ongoing proton trials investigating combination treatment with protons and immunotherapy [127]–[129] to address this and is discussed further in chapter 4.

3.4 Limitations

The greatest advantage of photon therapy is that its use has been well established such that physical and biological strengths and weakness are mostly known [130]. In lung cancer treatment, its depth-dose characteristics make photon radiotherapy more forgiving to tumour motion and tissue heterogeneity, thereby reducing uncertainties in dose distribution. However,

this same characteristic behaves as a limitation when it comes to dose-escalation and sparing critical organs.

Even with the most accurate technology to image tumour location, robustly manage motion and deliver treatment with high precision, doses required to overcome radioresistance will inevitably compromise toxicity to critical organs. Such toxicities often have significant impact on patients' quality of life, especially when treated with concurrent chemotherapy.

Critical organs include the heart, normal lung tissue, oesophagus, thoracic vertebra, spinal cord and the brachial plexus. Although it is well known that sparing these organs from high dose irradiation is important, more recently, there has been accumulating evidence that even low dose to the heart, lungs and thoracic vertebra impact not only toxicity but survival [67], [68], [72], [75], [131]. For this reason, I will focus on these organs.

3.4.1 Cardiac toxicity

Cardiovascular disease following radiotherapy to malignancies of the thorax is well-documented [66], [67], [131], [132]. Cardiac toxicity from radiation therapy can encompass pericardial effusions, arrhythmia, acute coronary syndrome, valvular disease, congestive cardiac failure and death [67], [133]. Previous studies have suggested that at high dose levels, cardiac toxicity risk shows a linear response occurring within 1-2 years [134], [135]; whereas at moderate dose levels a linear-quadratic function is demonstrated [136]. More recently, low dose has been shown to negatively impact survival [66], [68]; and an increase in 1 Gy to the mean heart dose (MHD), to be associated with an increase risk of ischaemic heart disease by 7.4% [134]. Complications tend to have a long latency but increase in a radiation dose-dependent fashion [136], [137]. Studies investigating which cardiac substructures might be particularly important have highlighted the left anterior descending (LAD) artery and left ventricle (LV), linked to coronary stenosis [133], [138], and the base of the heart [69].

Advanced photon radiotherapy techniques, such as image-guided radiotherapy [139], intensity modulated radiotherapy [140] and stereotactic body radiotherapy [141] combined with motion management techniques like deep inspiration breath hold can reduce the mean heart dose by about 50% when treating left- sided breast cancer [142], [143]. However, with no clear threshold dose studies the most sensible approach would be to keep dose as low as possible; and to determine quantifiable predictive and prognostic markers (eg. blood markers, such as troponin, BNP, NT-pro-BNP, CRP; and imaging using cardiac MR scans) to identify

patients most at risk of cardiac toxicity so that appropriate therapeutic intervention can be undertaken [68], [132], [144].

Proton therapy may spare dose to the heart and reduce cardiac damage for patients needing chest radiotherapy. When comparing photon to proton studies, Sun et al's study of VMAT compared to IMRT, helical therapy and IMPT for synchronous bilateral whole breast irradiation using IMPT plans improved target coverage and cardiac sparing (V5, V10 and V20) compared to VMAT, IMRT and helical therapy [131]. There is little evidence proving that reduced dose to the heart translates into diminished toxicity. The ongoing PRONTOX trial is a randomised controlled trial comparing photon and proton therapy to treat stage II-III NSCLC with concomitant chemotherapy to answer this question, assessing if better sparing of normal tissues translates into a reduction of radiation–induced side effects [145]. The PARTICLE-D proton trial [127] is specifically investigate cardiac sparing in patients with unresectable NSCLC receiving definitive accelerated fractionated proton radiotherapy with concurrent durvalumab [127].

Whilst it is known that photon irradiation causes biological damage to the heart by endothelial dysfunction, resulting in accelerated atherosclerosis [146]; and microvascular damage leading to chronic myocardial ischaemia and fibrosis [147], significantly less is known about the radiobiological responses of cardiovascular tissues to proton radiotherapy. There are limited studies analysing the effects of protons compared to photons on cardiovascular tissue. Ricciotti et al used RNA sequencing to analyse changes gene expression in mice thoracic aorta cells following proton and photon irradiation as a cardiovascular-model. They reported that proton irradiation upregulated fewer dose-responsive genes than photon radiation but the upregulation of these genes (including those related to DNA repair, apoptosis, cell growth and inflammation) was greater. Photon radiation appeared to upregulate more genes and those of a broader range of functions, including angiogenesis signalling. This divergence in genomic response pathways suggesting photon-induced cardiovascular- risk- models may not be applicable to that associated with proton irradiation [148].

3.4.2 Haematological toxicity- thoracic bone marrow, lungs and heart

Shifts in treatment paradigms encompassing immunotherapies has led to increased emphasis on minimising irradiation of circulating lymphocytes (CL), which play a crucial role in tumour surveillance [66], [70], [71]. Lymphopenia- related organs include the functional bone marrow of the thoracic vertebra, the heart and the lungs. By limiting irradiation of the thoracic vertebrae, where 35% of haematopoietic bone marrow (HMB) is located and CL are produced

[71], [74]; and the heart and lungs, which harbour pools of circulating lymphocytes (CL) haematological, toxicity can be minimised.

Studies have shown that a reduction in pre-treatment CL and decreased lymphocyte infiltration in pathologically resected NSCLC specimens are associated with a reduction in disease-free survival and overall survival [71]. Significant correlation between lung V5-10 and lymphocyte nadir [76]; and integral heart doses and decline in post-treatment lymphocyte counts [72] have been shown. Unsurprisingly, limiting dose to the thoracic vertebrae has also been shown to reduce the risk of lymphopenia. The downstream effect of being able to minimizing dose to CLs is that patients may respond better to immunotherapy and show improved survival.

Despite being well- established that haematopoeitic bone marrow (HBM) is extremely sensitive to irradiation [149], [150], there are no standardised protocols for delineating it and no consensus on suitable radiation dose parameter limits. Identifying HBM requires functional imaging techniques, such as MRI, [^{18}F]fluorodeoxyglucose (FDG)-PET, or ^{99m}Tc-sulfur colloid single-photon emission computed tomography [150]–[152]. However, most studies have contoured entire bone, which is arguably a more reliable and reproducible surrogate, accepting that dose to HBM may be over-estimated. Of the studies that have attempted to outline HBM, different studies have taken different approaches as there is no evidenced-based SUV threshold definition. More recently emerging studies focusing on radiation dose to thoracic bone marrow (BM) have suggested that it is the dose to thoracic vertebral volume that correlates with HT, with the mean thoracic vertebral dose (MTVB) and volumes of thoracic vertebrae receiving various cut-off values correlating with greater than or equal to grade 3 HT [73]–[75], [153].

Sparing dose to these lymphopenia-related organs that are located in the central thorax when treating stage III NSCLC is almost always impossible when using photon therapy given mediastinal involvement is common. Proton therapy may be able to achieve what photons cannot. Evidence has demonstrated an advantage of passively scatted protons in reducing the median BM volume receiving 10 Gy (CGE) by 30% compared to 3D conformal radiotherapy (3DCRT) and by 27% for volumes receiving 10 Gy (CGE) compared to intensity modulated radiotherapy (IMRT) [154]. Similarly Warren et al retrospectively compared 3DCRT with volumetric modulated arc therapy (VMAT) and PBS using for patients receiving CRT for oesophageal cancer and showed that PBS significantly reduced bone V10 and mean BM dose [155]. Based on previous studies, we can hypothesize that if the V5, V10 , V20 (percentage volume of lung receiving 5, 10 and 20Gy, respectively) and mean thoracic vertebral dose to thoracic BM are kept under approximately 65%, 55%, 45%, and 23Gy, respectively, then these

translate into a potential 2-fold increased risk of grade 3 (or higher) HT being avoided [73]–[75].

3.5 Conclusions

There have been significant advances in photon radiotherapy over the past one to two decades. The emergence of immunotherapy in lung cancer has revived interests in the therapeutic gains of photon radiotherapy but has also highlighted its limitations. At present, the lack of clinical evidence for proton therapy, means that photon radiotherapy remains the mainstay treatment for patients with unresectable locally advanced non-small cell lung cancer.

Chapter 4

Proton radiotherapy in lung cancer

4.1 Background

Proton irradiation was first recognised as a valid therapeutic in 1946 [156] and the first patient was treated in 1954 [157]. Since then proton technology has evolved significantly and photon technology appears to have reached its limit, dosimetrically. Despite its long history and advancing technology, there is no high quality clinical evidence supporting proton therapy as advantageous and globally, approximately less than 1% of patients are treated with protons [65]. In this chapter, I will examine the merits of proton therapy, particularly in lung cancer, why current clinical evidence does not reflect its theoretical advantages and how advancing technology may address some of its historical limitations.

Proton beam therapy (PBT) has a number of advantages over state-of-the art photon treatment. It is a form of charged particle therapy whose unique depth-dose characteristics result in a relatively low entrance dose and minimal exit dose. This achieves superior conformality of the high-dose region at the tumour site, enabling dose escalation and improved local control; whilst sparing dose to adjacent critical organs and limiting the low-dose bath, thereby minimizing toxicity [18]–[20]. Pencil beam scanning (PBS) is the latest technology whereby narrow proton beams are scanned across the tumour volume by scanning magnets. This offers even higher precision than passively scattered protons (PSP) [158], as well as reduced neutron-scattered dose [159], and enables intensity-modulated proton therapy (IMPT) to be delivered.

However, protons are more vulnerable to uncertainties so treating lung tumours present a combination of challenges- tumour motion and tissue heterogeneity. Together, these compound range uncertainties due to variation in radiological path lengths [18], [79], [104]. Subsequent motion-related target dose degradation [160] and potential overdose to critical organs, make robust planning and treatment delivery difficult.

Pre-clinical planning studies have demonstrated dosimetric advantages of PBT for both early stage and locally advanced NSCLC. For early stage disease, studies have demonstrated median relative differences in lung dose of up to 10%, with reduction in volumes of lower-dose regions of irradiation in the lungs and a reduction in mean lung dose of up to 3.2 Gy compared to stereotactic body radiotherapy [161]–[163]. The clinical experience of PBT for early stage disease has been encouraging, demonstrating local control rates of up to 90% with minimal toxicity [23], [164]–[167]. For locally advanced disease, significant dose sparing to normal lung, spinal cord, heart and oesophagus is possible when treating stage III NSCLC with PBS compared to passive scattering proton therapy or IMRT [158], [168] and the ongoing PRONTOX trial aims to assess if this translates into reduced radiation-induced toxicity [145]. These findings are consistent with Nichols (2011) [169] who demonstrated the particular

advantage of protons in enabling larger target volumes that encompass high risk lymph node regions.

Recent research efforts have particularly focused on patients with LA NSCLC with aim of improving local control and survival and improving toxicity to normal tissue. A number of single arm clinical trials have been encouraging for patients with stage III disease treated with PSP and concurrent chemotherapy [21], [22], [24]–[26], [170]–[172]. Chang's (2011) [25] prospective clinical Phase 2 study investigating chemoradiation with PBT for patients with stage III NSCLC demonstrated local recurrence of 20.5% and overall survival (OS) of 86% at 1 year with a median survival of 29.4 month and no grade 4 or 5 adverse side effects. Oshiro (2012) [172] reported OS of 21.3 months and local control at 2 years of 64.1% when PBT is used alone for stage III disease. When combining PBT with chemotherapy, the median survival was 26.7 months [171].

Unfortunately, to date, there is no clinical evidence supporting an advantage of proton radiotherapy over state-of-the-art photon radiotherapy for patients with LA NSCLC. Few large scale randomised trials have been conducted and the recent study in patients with stage II-IV NSCLC reported no reduction in local failure after passively scattered protons [173]. However, heterogeneity of disease stages treated, outdated proton technology and lack of image-guidance used in these trials have meant that there is sustained interest in developing lung proton radiotherapy.

It is clear that lung proton radiotherapy is largely considered to be in its infancy. We have yet to explore the full advantages of advanced proton techniques that incorporate recently developed image- guidance systems and we have yet to identify key niche cohorts.

4.1.1 Aims

This chapter will focus on reviewing current understanding and experience of proton therapy in the treatment of lung cancer and its potential role in LA NSCLC.

4.1.2 Objectives

- A gap analysis will review current evidence for proton therapy in lung cancer and identify research gaps to guide future work
    - Review on published clinical trials
    - Identify ongoing clinical trials

- Assess how the global lung proton community prioritise these research gaps using a survey

- A planning study comparing volumetric modulated arc therapy (VMAT) and pencil beam scanning (PBS) proton radiotherapy plans of superior sulcus tumours will examine robust planning strategies in this rare subset of stage III NSCLC.
    - Demonstrate the feasibility of delivering PBS protons to patients with superior sulcus tumours
    - Be proficient in independent PBS proton planning and have a better understanding of the benefits and limitations of proton therapy compared to photon therapy in lung cancer
    - Be able to quantify dosimetric advantages of using PBS protons in degree of tumour coverage and sparing of normal tissue by assessing radiotherapy plans compared to VMAT photon radiotherapy plans.
    - Learn to be proficient in PBS proton planning
    - Learn to be proficient in photon VMAT planning
    - Quantify dosimetric differences of PBS proton radiotherapy planning compared to VMAT planning in tumour coverage and normal tissue sparing
    - Quantify the impact of dosimetric uncertainties due to motion in proton plans compared to photon plans

4.2 Gap analysis

This work was undertaken as a co-ordinated effort with the Advanced Radiotherapy Technologies Network (ART-NET) group. It is a systematic literature review analysing publish and ongoing studies in lung proton radiotherapy. My contributions are as follows:

1. Analysis of published work- I worked within a core team of four to identify and analyse relevant published work using the PRISMA approach.
2. Analysis of ongoing trials- I searched, identified and analysed trials registered in *ClinicalTrials.gov*
3. Survey design- I contributed to the format and questions posed in the survey
4. For the manuscript submitted to the International Journal of Radiation Oncology Biology Physics, I am the joint first author, having played a central role in structuring the manuscript and being the lead author of the following sections:
    a. Results subsections: “Ongoing trials”, “Gaps in ongoing trials”, “Survey results”
    b. “Ongoing trials table”
    c. Discussion subsections: “Clinical priorities” and “Physics”

The full contents of the gap analysis has not been included here as some themes are beyond the scope of my thesis. Only the sections that are relevant to my thesis and that I have authored are included in this chapter. For the full manuscript please refer to Appendix 8.

4.2.1 Introduction

Many questions remain regarding the clinical benefit of proton radiotherapy in lung cancer and challenges to safe and robust optimization and delivery are yet to be fully resolved. As it stands, there is huge scope for future clinical trials. With the opening of new high-energy proton radiotherapy centres in the UK, the global research capacity is growing, but the number of proton centres are still limited so research efforts need to be prioritized.

This gap analysis is aimed at identifying thoracic proton radiotherapy research gaps via a systematic literature review, a review of the ongoing trials and an analysis of the results from a survey sent to international radiotherapy healthcare professionals. In identifying gaps we hope to help direct future research priorities.

4.2.2 Methods

i) Literature review method

"We used the Preferred Reporting Items for Systematic Reviews and Meta-Analyses (PRISMA) guidelines[174] to identify original research from 01/01/2008 to 01/01/2019. Search terms included “proton therapy/ particle therapy/ passive scatter/ PSPT/ pencil beam/ PBS/ pencil scan AND lung cancer/ lung carcinoma/ lung tumour/ NSCLC”. Articles were accepted if they met this inclusion criterion; prospective research with assessment of survival, toxicity and/or disease recurrence parameters. Retrospective studies, case reports, non-proton studies, letters and review articles were excluded. Of 1779 abstracts, we identified 22 papers which met these criteria.” - *authored by David Cobben and Clare Dempsey*

An initial 32 active and recruiting trials were identified using the search terms “Lung cancer” and “protons” in *ClinicalTrials.gov*. Of those, only 9 trials focused on proton therapy in lung cancer. Trial details were extracted from *ClinicalTrials.gov* or the trial protocol (if available via personal communication with chief investigators).

ii) Survey method

“Open and close-ended questions addressing the following topics were formulated based of feedback from a multi-disciplinary team (oncologists, physicists and radiographers). In summary, we aimed to cover the following:

What are the key gaps/ research needed?

What are the appropriate clinical endpoints, populations and trial design?

What are the research challenges and barriers?

The survey was constructed using Google forms (Google LLC, Mountain View, Ca, USA) and circulated online. The target was international lung cancer proton experts (defined as healthcare professionals with direct experience in treating patients with thoracic proton radiotherapy and/or setting up proton radiotherapy services; expert group) and lung cancer healthcare professionals (no prior direct proton experience; non-expert group). "**-** *authored by Ahmed Salem*

4.2.3 Results

It is felt that research priorities should lie in clinical studies that compare protons and photons, particularly in patients with stage III NSCLC, investigating fractionation regimes and combination therapies; but also the physical and radiobiological aspects of proton therapy.

i. a) Published trials (2008 - 2019)

"The 22 studies that met the inclusion criteria recruited over an average of 3 years (table 4). In the majority of the studies, passive scattering was used as the beam delivery method. One used pencil scanning beams. The majority were single arm prospective studies. Only 4 studies were randomised controlled trials (RCT), comparing proton and photon radiotherapy. Patient accrual varied greatly; the lowest enrolment was 9 with the largest study recruiting 212 patients.

These trials included stage I-IV NSCLC, with the exception of 2 small trials investigating SCLC and one was open to all thoracic malignancies. In around two-third of the studies, patients were treated with concurrent chemo-radiotherapy with or without induction therapy. The fractionation schemes employed were highly variable between studies, both the dose and fractionation regimen.

The endpoints for the majority of trials were overall survival (OS), progression-free (PFS) and disease-free survival (DFS) and dose-limiting toxicity (DLT). Only half of the trials reported the dose to the organs at risk (OAR), notably the lung, heart and oesophagus. Acute toxicity was reported in lung (pneumonitis), oesophagus (oesophagitis) and skin (dermatitis). Very few papers reported on long term toxicity, mainly restricted to pneumonitis. "- *authored by David Cobben and Clare Dempsey*

Study	Inclusion	Technique	RCT vs Single arm	No	Stage	Endpoints	OAR Dose	Acute	Late	Comparing studies
1 [17]	2009-2013	PSPT	Single	14	III	OS, PFS	NA	L O	L	NA
2 [18]	2006-2010	PSPT	Single	134	II to III	OS, DFS	L O D	L O D		NA
3 162]	2011-2013	NA	Single	9	III	DLT		O D	O	NA
4 [163]	2010-2013	NA	Single	15	III	OS, PFS	NA	O D	L D	NA
5 [167]	2009-2013	PSPT vs IMRT	RCT	212	I-IV	LRF	NA	NA		No difference
6 [168]	2006-2008	NA	Single	62	I-IV,	DLT	NA	L O D	L	NA
7 [169]	NA	IMRT vs IMPT SIB	RCT	15	II to IIIb	OS, DFS, LRF	L H	L O D		NA
8 [170]	2012-2014	PSPT vs IMRT	RCT	19	I to IIb	lack of accrual	NA	NA		closed
9 [156]	NA	NA	Single	115	IA to IIb	OS	NA	NA		NA
10 [171]	2009-2012	PSPT	Single	56	I	OS, PFS	L	O D	L	NA
11 [19]	2003-2007	PSPT	2 plans	80	I	OS, CSS, LC	NA	L D		NA
12 [20]	2009-2011	PSPT	Single	64	III	OS, PFS	NA	L O D	L O	NA
13 [172]	2009-2014	PSPT	RCT	149	II-IV	RP, LF	L H O	L		Reduced heart dose
14 [173]	2006-2011	PSPT	Single	35	IA-IIB	OS, RFS	NA	L O H		NA
15 [174]	2008-2010	PSPT	Single	19	IIB -IIIB	OS, PFS	L H O	O D	L O D	NA
16 [175]	2011-2016	PSPT	Single	30	limited stage	OS, RFS	L H O SC	L O D		NA
17 [21]	2006-2009	PSPT	Single	44	III	OS	L H O	L O D		NA
18 [176]	2001-2008	NA	Single	55	I	OS, PFS	NA	L		NA
19 [177]	NA	PSPT	Single	18	I-II	DLT, LC, LN, DM	L H O	L O D BT		NA
20 [178]	2009-2012	PSPT	Single	6	limited stage	OS, PFS, DLT	L O D	L O D		NA
21 [22]	2006-2009	PSPT	Single	44	III	LC, RC, OS	L H O	L O D SC		NA
22 [179]	2010-2012	NA	Single	25	T1-4, N0-3	DLT	L H O	L O D BP SC K Li		NA

Table 4. Summary of prospective lung proton clinical trials. Not applicable (NA). Passively scattered proton therapy (PSPT).Intensity modulated proton therapy (IMPT). Intensity modulated radiotherapy (IMRT). Overall survival (OS). Progression free survival (PFS). Relapse free survival (RFS). Dose limiting toxicity (DLT). Local control (LC). Regional control (RC). Distant metastases (DM). Lymph nodes (LN). locoregional failure (LRF). Disease free survival (DFS). Cancer specific survival (CSS). Radiation pneumonitis (RP). Lung (L). Heart (H). Oesophagus (O). Dermatitis (D). Spinal cord (SC). Brachial plexus (BP). Kidney (K). Liver (Li). Bronchial tree (BT).

i. b) Gaps in previous trials

“Dosimetric analyses were uncommonly reported (n=11). Only one trial reported better heart sparing with proton radiotherapy, compared to photons. None of the studies reported on patient reported outcome measures or performed a comparative health economical evaluation. “- *authored by David Cobben and Clare Dempsey*

ii. a) Ongoing trials- *authored by Swee-Ling Wong*

To date, no clear clinical advantage of proton therapy over state-of-the-art photon therapy has been demonstrated. For instance a randomised trial comparing passive scattering proton radiotherapy with state-of-the-art photon (intensity modulated) radiotherapy both delivered concurrently with chemotherapy in stage II-III NSCLC failed to detect benefit of a decreasing of grade ≥3 radiation pneumonitis and local tumour recurrence [1]. This negative result could be explained by the use of outdated proton technology (beam delivery and lack of image guidance), an imbalance in trial arms as well as the learning curve effect associated with proton radiotherapy delivery over the course of the trial, since improvements in both trial endpoints were reported in proton-treated patients recruited after trial midpoint. In addition, the biological effects of proton radiotherapy on organs at risk, particularly in the Bragg peak, are likely to differ from computational models on the planning systems [2]. For these reasons, there is sustained worldwide interest in image-guided proton radiotherapy in NSCLC and clinical trials are ongoing (table 5).

Trial ID	Inclusion	Technique	RCT vs Single arm	Patient no.	Stage	Fractionation	Endpoints	OAR Dose	Acute	Late
NCT00875901	2019 onwards	NS	Single arm	23	I	Peripheral: 12 CGyE/# for 4#, 2-3 treatments/week over 2 w; Central: 6CGyE/# for 10#, 5#/week over 2-3w	MTD	L O D H SC, BP	L O D H	L O H D
NCT01770418	2019 onwards	PS/IMPT	Single arm	61	II/III	Dose 1: 60 Gy (RBE) at 2.5 Gy (RBE) per fraction x 24 fractions; Dose 2: 60Gy (RBE) at 3Gy (RBE)/# x 20#; Dose 3: 60.01Gy (RBE) at 3.53Gy (RBE)/#x 17#; Dose 4: 60Gy (RBE) at 4Gy (RBE)/# x 15#	MTD, OS 12 months	L O H	L O D	L O
NCT02731001	2019 onwards	Passive scattering	RCT 1:1	98	II/III	PBT: 66 Gy (RBE) in 6#/w; IMRT: 66Gy in 6#/w	Early & late toxicity	L O H	L O D H	L O H D GI
NCT01629498	2019 onwards	IMPT	RCT	60	II/III	Phase I starting dose: 60Gy (RBE) in 30# over 6w; Starting SIB Dose: 72 - 84Gy (RBE); Phase II: 66-72Gy (RBE) in 30#	MTD	NS	L O H	NS
NCT03818776	2019 onwards	NS	Non-randomised	27	II/III	Arm 1: 60 CGyE in 20# (3+3 participants, 3-6 total); Arm 2: 69 CGyE in 23# (3+3 participants, 3-6 total)	Safety	Heart	L H	NS
NCT03132532	2019 onwards	NS	RCT	120	II-III	60Gy V 66Gy V 72Gy in 2Gy/# daily	PFS	NS	NS	NS
NCT03087760	2019 onwards	NS	Single arm	41	Previously treated NSCLC	Not stated	PFS	NS	NS	NS
NCT01993810	2019 onwards	NS	Randomised	330	II/III	70Gy(RBE) in 2Gy/# over 5w	OS, Toxicity	NS	H	NS
NCT01165658	2019 onwards	NS	Single arm	30	NS	1 of 3 dose regimes ranging from 45Gy in 3Gy/#s - 60Gy in 4Gy/#	MTD	NS	L O D H	NS

Table 5. Summary of ongoing lung proton clinical trials. Not specified (NS). Randomised controlled trial (RCT). Overall survival (OS). Progression free survival (PFS). Maximum tolerated dose (MTD). Lung (L). Heart (H). Oesophagus (O). Dermatitis (D). Spinal cord (SC). Brachial plexus (BP). Gastrointestinal (GI).

Nine ongoing trials are investigating proton therapy in lung cancer and collectively address some of the gaps identified in previous trials. Four are randomised, 3 of which compare protons to photons and the fourth comparing different doses of proton irradiation. All studies focus on patients with NSCLC except one, which includes various thoracic malignancies. Of

the 8 studies in patients with NSCLC, 6 focus on patients with stage II-III disease, 1 investigates hypofractionated proton therapy in those with stage I NSCLC and the remaining trial examines PBT as salvage treatment for thoracic recurrence. The majority of the trials are single arm studies investigating variable optimal overall doses and fractionation regimes [127], [175], [176]. Five trials combine proton therapy with concurrent chemotherapy and 3 trials incorporate concurrent [127] and consolidation immunotherapy [128], [177].

Most of the trials do not fully disclose planning and delivery techniques but four describe image-guided, motion management and adaptive strategies. These include combinations of 4DCT imaging and fiducial markers; breath-holding, gating, or compression techniques; and repeat 4DCTs, daily orthogonal xray imaging and weekly CTs [175], [178]–[180]. Despite IMPT demonstrating dosimetric superiority over passively scattered proton techniques, only 2 of the ongoing studies are utilising IMPT. Two trials employ passively scattered protons and the remaining trials have not declared the technique planned for use.

All trials aim to report on toxicity and/or survival outcomes. Four of the studies state their intent to report on dose to the OARs, all focusing primarily on dose to the heart, and the PRONTOX trial [179] is investigating if the dosimetric benefits of PBT result in reduced radiation-induced toxicity. Only 2 trials will further assess toxicity utilising objective cardiac and pulmonary functional measures [127], [177] and three will utilise patient- reported quality of life assessments [177]–[179]. Prior to initiating consolidation durvalumab, it is necessary for $\geq$2 grade adverse events to be resolved. Therefore, investigating if PBT can significantly reduce toxicity and improve patient functionality is especially important given the increasing prominence of immunotherapy in lung cancer treatment.

ii. b) Gaps in ongoing trials- *authored by Swee-Ling Wong*

A critical gap is the need for more randomised clinical trials with quality assurance measures to ensure uniformity of research outputs and enable comparability. In need are trials comparing state of the art image-guided proton therapy to the latest in photon technology, particularly in patients with locally advanced disease, dosimetric analyses and toxicity reporting, combination treatment with immunotherapy, investigating the safety of hypofractionated and dose-optimised regimes in locally advanced disease and the need for health economic evaluation.

iii. a) Survey Results - *authored by Swee-Ling Wong*

Nineteen international lung cancer healthcare community members, based in various cancer centres in the United Kingdom, United States of America and Netherlands, responded to our survey to identify key research gaps. There were 10 members (8 clinicians, 1 physicist and 1 radiographer) in the “non-expert” group and nine members (all radiation oncologists) in the “expert” group, 4 of whom have treated more than 50 patients.

The majority of participants agreed that that the highest research priorities are to: 1. Identify patients most likely to benefit from proton therapy by developing and validating predictive biomarkers and/or dosimetric models and 2. establish comparative photon and proton clinical trials in a Phase II design, with or without randomisation and that late toxicity was a key outcome of interest.

It was felt that proton radiotherapy trials were most warranted for patients with stage III NSCLC suitable for concurrent chemoradiotherapy or trimodality treatment. One hundred percent of responders identified the heart as the critical organ most likely to benefit from dose-sparing capabilities of proton therapy, and predicted additional advantages to be reduced immune, lung and oesophageal toxicity. Other areas where it was agreed that current evidence is poorly established include outcome data on acute toxicity and overall survival, investigating combination therapies, optimizing fractionation and investigating the role and safety of proton hypofractionation.

Differences in opinions between the “expert” and “non-expert” groups arose in whether or not further research efforts should prioritise focusing on the role of protons in the re-irradiation setting, the impact of respiratory motion on dose, 4D robust optimisation, range verification, and relatively biological effectiveness of proton irradiation. The “non- expert” group felt that these were all areas that warranted more interrogation (the majority giving priority scores of 4) whereas the “expert” group considered these lower priority (the majority giving priority scores of 2- 3). The need for health economic data was another point of contention with significant disparity in opinions regarding its relevance- 7 of 10 “non-expert” responders assigning priority scores of 4-5 compared to only 2 of 9 “expert” responders assigning high priority scores of 4-5.

iii) b) Gaps identified in survey

“Interestingly, research gaps identified by the expert and non-expert group were different. Non-experts placed more importance on the development and validation of robust motion mitigation approaches, comparative clinical trials and health economic analyses. Non-experts thought that future trials are warranted the most in the re-irradiation setting in NSCLC and in stage III NSCLC patients treated with concurrent chemoradiotherapy. Experts on the other hand placed more emphasis on the development and validation biomarkers to predict patient benefit from proton radiotherapy and combination therapy trials. Experts thought that stage III NSCLC patients treated with concurrent chemoradiotherapy represented the highest priority target population for a future trial. This was followed by stage III NSCLC patients treated with sequential chemoradiotherapy and limited-stage small-cell lung cancer.

Window of opportunity radiobiology studies and research addressing the relative biological effectiveness (RBE) of proton RT were classified as moderate priorities. Biomarker analyses, to improve patient selection in future phase III trials, were reported as important. “*-authored by Ahmed Salem.*

4.2.4 Discussion- *authored by Swee-Ling Wong*

In this gap analysis we identified thoracic proton radiotherapy research gaps via a systematic literature review, a review of the ongoing trials and an analysis of the results from a survey sent to international radiotherapy healthcare professionals. Based on gaps identified, the following will be discussed in this section: clinical trial design and quality, utilising advanced proton technology, patients with locally advanced disease and identification of further niche cohorts most likely to benefit from proton therapy, combination treatment with immunotherapy, investigating the safety of hypofractionated and dose-optimised regimes.

4.2.4.1 Clinical priorities- recommendations for future research - *authored by Swee-Ling Wong*

i) Clinical trial design and quality

There is a pressing need for more randomised clinical trials comparing state-of-the art proton technology to the latest photon technology in order to justifying complex PBT treatment. We will first discuss trial design. Whilst large randomised controlled trials are the gold standard, these are not always possible or the most practical approach. This is because the standard of care is ever changing and different between countries-access to targeted drug therapy is an example. This makes defining a “standard” treatment arm challenging. Furthermore,

developing personalised oncological treatment, which encompasses risk-adapted radiation treatment as well as mutation-driven targeted drug therapy, requires more contemporary trial designs to be considered so that results can be generated efficiently and cost-effectively. Examples include Bayesian adaptive randomisation [181], [182] that adjusts patient allocation ratios to the more favourable treatment according to real-time assessment; and umbrella studies testing multiple targeted therapies, such as the Lung-MAP study (NCT03851445) [183]. It is likely that future trials will employ such designs so that complex questions regarding different fractionation regimes, and multimodality therapeutics and their sequencing can be answered.

Furthermore, patient recruitment may be difficult due to limited numbers of centres offering proton therapy thus imposing travel implications, patients may refuse entering randomisation, and insurance policies may affect the ability to randomise patients. Co-ordinated multi-centre and international participation will facilitate sufficient patient recruitment.

Uniformity and transparency of research outputs thus far have been lacking. This is critical to enable valid comparability across trials. Standardisation of radiotherapy planning (including OAR-contouring by using internationally accepted atlas), treatment delivery, quality assurance and consistency of dose, fractionation, and outcome–reporting will address this. Equally important is the clear reporting of chemotherapy and immunotherapy regimes prescribed and achieved; and criteria used to determine patient eligibility for immunotherapeutic agents.

ii) Patient cohorts in which to focus clinical trials

Patients with stage III LA-NSCLC, in whom there is an unmet need to improve outcomes, are a high priority gap, as well as identifying niche groups who will benefit from proton therapy.

Emerging clinical evidence from large prospective trials in patients with LA-NSCLC have been disappointing with no improvement in local or regional failure [173], [184]. However, the advantages of proton therapy may have been obscured by the heterogeneity of inclusion groups [185]. Identifying patients most likely to benefit may be aided by predictive biomarkers and/or model-based approaches, as highlighted by our survey. This would be particularly helpful given the spectrum of anatomical geometry encompassed by the American Joint Committee of Cancer (AJCC) definition of stage III disease. Future trial designs could then consider grouping patients according to various geometric permutations.

Patients with thoracic recurrences requiring re-treatment are another select cohort who may benefit. Surprisingly, our survey revealed a divided opinion regarding thoracic re-irradiation trials- 9 of 10 non-experts, compared to only 4 of 9 experts, gave a priority scale of 4-5. The ongoing NCT03087760 Phase II study [128], which combines PBT with pembrolizumab for in- or near-field recurrent thoracic disease, will provide the basis for future trials needed to further investigate achievable doses, characterise treatment toxicity and assess survival outcomes in this context.

iii) Study of radiotherapy regimes in patients with LA-NSCLC

Optimal fractionation regimes and the safety of proton hypofractionation in patients with LA-NSCLC remain unclear. Two ongoing trials are assessing hypofractionation [175], [178] although only one investigates this in locally advanced disease [175]; and the ongoing Phase I/II trial (NCT01629498) [180] is assessing dose escalation. So far, proton dose- escalation trials [170], [186] have not shown an advantage but these studies have been small. Photon studies have shown that a dose increase of 1 Gy-BED is associated with an approximate 4% relative increase in survival [187]; but that increased dose to the lungs and heart and increased overall treatment time negatively impact survival and negate benefit [66]. For this reason, future trials investigating various fractionation regimes and dose-escalation should be mindful of maintaining or reducing overall treatment time, as well as sparing dose to the heart and lungs.

iv) Immunotherapy

Recent landmark trials have brought immunotherapy to the forefront of lung cancer treatment [10], [15] and the potential for proton radiotherapy to enhance the immunogenic response is a key research gap. Three ongoing trials investigate various sequencing of immunotherapy in combination with proton therapy: as concurrent definitive radio-immunotherapy [127], [128], adjuvantly following concurrent chemoradiotherapy [129] and as consolidation treatment following proton irradiation for thoracic recurrence [128]. More randomised trials are necessary to elucidate optimal sequencing of therapy and immunotherapeutic agent.

4.2.4.2 Physics recommendations for future research - *authored by Swee-Ling Wong*

Shifts towards the most advanced PBS technique for lung cancer have been hindered by concerns regarding the impact of respiratory motion on dose and inadequate image guidance.

We will discuss research gaps in motion management, on-board imaging and adaptation approaches, and robust optimisation.

i) State of the art proton technology

Pencil beam scanning protons that enable IMPT delivery is the latest in proton technology. Although the dosimetric advantage of IMPT over IMRT is well documented, only one prospective clinical study utilises IMPT for patients with stage II-III NSCLC [186] and there are no randomised controlled trials comparing IMPT to state-of-the-art photon technology, VMAT. Such trials should be explored in combination with robust motion management strategies and improved image-guidance in proton systems that are now available.

ii) Motion management

Motion management strategies employed in some of the ongoing lung proton trials include breath-holding, abdominal compression and gating. Although these are established techniques to overcome target motion, logistically they may prove difficult in centres with a single proton accelerator and multiple treatment rooms. New strategies under development are, prolonged inspiratory breath-hold using pre-oxygenation and hypocapnia which can enable multiple prolonged breath-holds of up to 6 minutes at a time [188], [189]; and high frequency jet-ventilation whereby rapid, low tidal volume gas is exchanged during simulation and treatment, to virtually stop breathing [190]. Methods such as these, or combination motion mitigation approaches, as well as rescanning and increasing the spot size [191] may need to be considered.

iii) On-board imaging -*Marianne Aznar is a co-author of this paragraph*

“Until recently, one of the gaps has been the lack of 3D image guidance (e.g. Cone Beam CT) on proton systems. This has limited the comparison between photon and proton arms in comparative studies, as well as inclusion in proton arms- only tumours visible on 2D imaging could be included in studies. The availability of 3D on-board image guidance on newer proton delivery systems, such as those used in some of the ongoing trials, will address this, and will enable a more detailed investigation of anatomical changes over a treatment course, and of the need for adaptation and motion management. It will also allow a better estimate of the doses delivered to organs at risk, and a more reliable assessment of the robustness requirements. On board 4D imaging for proton therapy remains to be developed, but will be valuable to assess changes in respiration patterns. Repeat 3D/4D after treatment delivery would also offer possibilities to assess intra-fraction changes (such as baseline drifts during a single fraction), which have not been investigated in the setting of proton therapy to date. “

iv) Robustness

Robustness encompasses a multitude of factors from 4D robust optimization and analysis of dose degradation due to respiratory motion, to motion management and image-verification required throughout the course of treatment. All components of this pathway have been identified as requiring further research.

For true “robustness” a quantitative assessment of all uncertainties must be carried: this will depend on the clinical application (e.g fractionation), choice of image-guidance (e.g. bone versus soft tissue registration) as well as patient specific parameters (e.g weight loss, tumour shrinkage). While a vast body of literature covers these uncertainties in photon therapy, they need to be re-investigated in the context of proton therapy. Interestingly, the “expert” group felt that preparatory steps, such as 4D robust optimization and plan evaluation; and analysing degradation of proton dose due to respiratory motion, were not such high research priorities (4 of 9 giving a priority score of $\geq$4 and 1 of 9 giving a priority score of $\geq$4, respectively), compared to the “non-expert” group (6 of 10 giving a priority score of $\geq$4 and 7 of 10 giving a priority score of $\geq$4). However, this may be because the “expert” group consisted entirely of physicians without input from physicists or radiographers/ radiation therapists; and/or reflect the “expert” group’s experience that have highlighted to them where “robustness” challenges have been more pressing.

Studies thus far have lacked transparency in their methods or criteria for robustness analysis and/or varied in their assessment methods- if plans are made robust to the tumour, bony anatomy or surrogates. Various margin recipes (eg. in passive scattering techniques) and robust optimisation strategies have been developed but a lack of standardisation makes a direct comparison between approaches challenging. While reporting standards are being developed, a way to facilitate this comparison may be to systematically report GTV, CTV and irradiated volumes (i.e. at the 95% of dose prescription) in addition to robustness parameters.

4.2.4.3 Radiobiology recommendations for future research

i) DNA damage and repair from proton radiotherapy

The gap analysis identified that a global assessment of the quality of DNA damage induced by low and high LET protons needs to be assessed.

I will later address this gap in the context of my experiment comparing the cellular responses of NSCLC cell lines following photon and low and high LET proton irradiation (Chapter 5 of this thesis).

ii) Proton radiotherapy immunological interactions

"The immunological impact of proton irradiation has been reported in a limited number of publications. Preclinical evidence suggests that proton radiotherapy has higher tumour immunogenic and lower normal tissue immunosuppressive effects, compared to photon radiotherapy [34]. Tumour immunogenicity is associated with long-tern tumour control. Overall, these effects could enhance tumour response and patient survival, particularly if proton radiotherapy is sequenced prior to- or in combination with- immunotherapy. Proton-immunotherapy combination trials, which represented a high research priority among our survey respondents, are as such urgently needed.

Gameiro *et al.* have demonstrated similar effects on the levels of HLA and calreticulin upregulation, molecules involved in antigen presentation and immune recognition, and T cell mediated cytotoxicity from both photons and proton irradiation [34]. Others have demonstrated greater micronuclei formation following proton irradiation, compared to photons [192], [193]. This is pertinent in light of recent papers that show that cytosolic DNA sensing of radiation induced micronuclei is responsible for cGAS-STING signalling and a type 1 immune response [194]. Several studies have also looked at the impact of proton irradiation induced bystander effect as a result of cytokine release. However recent advances in techniques to assess the complexity of the tumour microenvironment such as mass cytometry mean there is opportunity for more comprehensive study of the immunological effects of proton irradiation in realistic tumour models and in patient samples. "- *authored by Crispin Hiley.*

iii) Relative biological effectiveness (RBE)

It is acknowledged that the widely accepted use of a generic RBE of 1.1 for proton radiotherapy is an inaccurate oversimplification. However, RBE is a function of multiple factors including cell type, dose, dose fractionation used, LET and clinical end point meaning there is too much uncertainty to propose RBE values that accurately take into account all these factors [195]. As a consequence unexpected toxicity can arise due to underestimated radiobiological effects as well as proton range uncertainties. Critically, proton RBE is dependent on depth of penetration resulting in inhomogeneous biological dose distribution through the tumour- eg. higher in the centre of target compared to peripheral regions uncertainties [196].

RBE-based proton planning is considered a moderated research priority based on our survey feedback.

iv) Proton radiotherapy and hypoxia

Hypoxia is a known cause of radioresistance which negatively impacts survival in lung cancer. The physical properties of proton therapy may allow safe dose escalation to hypoxic regions of the tumour and the reduced oxygen enhancement ratio of high LET protons may improve effective cell kill[197]. Hypoxia- adapted treatment planning, known as kill painting, is under investigation [198].

v) Future radiobiology research

“Investment in preclinical proton radiotherapy infrastructure is lagging behind worldwide. Challenges of accessing charged particle facilities for preclinical research need to be overcome. Equally important is the integration of robust translational endpoints in lung cancer proton radiotherapy trials. The aim should be to direct research aimed at improving patient selection for proton radiotherapy. Biomarker development and validation featured as high research priorities by our survey participants. Our ultimate aim should be to improve lung cancer patient outcomes and healthcare delivery through a multidisciplinary approach involving clinicians, physicists, biologists, commissioners and health economists. “*authored by Ahmed Salem.*

4.2.5 Conclusions

This gap analysis has identified key areas to further investigate in lung cancer proton research. Priorities have been stratified to guide trial resources and encourage globally co-ordinated future efforts by the proton community.

- *The complete and revised version of this manuscript is planned for submission to Clinical Oncology- Appendix 8.*

4.3 Planning study- Retrospective planning study of patients with superior sulcus tumours comparing pencil beam scanning protons to volumetric modulated arc therapy

One of the highest research priorities from the gap analysis survey was to conduct studies identifying patients most likely to benefit from proton therapy. This planning study was undertaken to explore if patients with superior sulcus tumours (SSTs), a rare subset of stage III disease, might benefit from pencil beam scanning protons. By assessing the feasibility and dosimetric benefits of robust PBS planning thereby laying the foundation for conducting a clinical trial in patients with SSTs using PBS protons.

4.3.1 Introduction

Superior sulcus tumours (SSTs) are rare subtypes of locally advanced non-small cell lung cancers (NSCLCs), representing 5% of all bronchogenic carcinomas. Outcomes are poor with local recurrence in 40-50% of patients[16], [17], [199] and 5 year overall survival between 5-30% [200], [201]. They present a unique treatment challenge by characteristically invading the chest-wall and structures of the thoracic inlet, including the parietal pleura, 1st and 2nd ribs and vertebral bodies; as well as (but not necessarily) the brachial plexus and stellate ganglion [27]–[29]. This makes surgical resection difficult and their close proximity to the spinal canal, means that dose coverage by photon radiotherapy is often compromised. When disease is unresectable, radiotherapy (with or without chemotherapy) is the principal treatment modality.

Proton-beam therapy (PBT) has a number of advantages over state-of-the-art photon-based volumetric-arc therapy (VMAT). Its physical characteristics result in a relatively low entrance dose and minimal exit dose, potentially achieving superior target conformality whilst reducing dose to surrounding tissues [18]–[20]. Pencil beam scanning (PBS) is the latest technology whereby narrow proton beams are magnetically scanned across the tumour volume, promising better conformality than passively-scattered protons [158]. Reservations regarding PBT, particularly PBS, are due to motion and tissue heterogeneity. These impact uncertainties in radiological path-lengths [18], [79], [104], [202]and subsequently robustness of treatment delivery, as motion results in interplay-related dose degradation [160] and potential overdose to organs-at-risk (OARs).

Although an increasing number of studies investigating the use of PBT in locally advanced NSCLC have emerged over the last decade very few have used PBS [186], the vast majority utilising passively-scattered protons [21], [22], [26], [170], [171], [173], [184], [203]. From limited studies that do exist, PBS is suggested to better spare OARs [158], [168]. A number of ongoing single-arm [175], [176], [178] and randomised control trials [177], [180] intend to report toxicity following thoracic irradiation with PBT. The ongoing PRONTOX trial specifically

aims to establish if dose-sparing translates into reduced radiation-induced toxicity [145]. Of particular interest is the potential for PBT to improve survival outcomes by sparing dose to the heart, thereby minimising risk of cardiac toxicity, and limiting dose to additional lymphopenia-related organs such as the lungs and thoracic vertebra. Disappointingly, Liao's recent trial reported no reduction in local failure after passively-scattered protons [173]. However, this may be due to heterogeneity of disease stages treated (II-IV), outdated technology, or inadequate image-guidance at the time the study was conducted. It is clear that we have yet to identify key niche cohorts where the advantages of advanced proton techniques can be fully exploited.

Patients with SSTs seem likely candidates to benefit from scanning protons and present an opportunity to develop PBS techniques in locally advanced NSCLCs because 1) their invasion of local structures limits motion, circumventing the challenging issues of interplay 2) their apical location results in smaller volumes of aerated tissue surrounding them, reducing heterogeneity along proton paths.

This retrospective planning study will explore robust PBS planning of SSTs, assessing if target coverage is improved and if dose to normal tissue can be significantly spared compared to VMAT.

4.3.2 Methods

Patients with SSTs treated with radical radiotherapy between 2010-2015 were identified. All patients were positioned supine on wing boards, arms above the head and immobilised with customised vacuum bags. Four-dimensional-CTs using the Real-time Position Management system were used to acquire their free-breathing trace during acquisition and treatment delivery.

Patients were excluded if tumour motion was >5mm (figure 6). All were planned to 64 Gy (RBE) in 32 fractions using Eclipse (Varian Medical Systems, *Palo Alto, CA*), version: 13.7.33 for VMAT plans and version: 13.7 for proton plans. PBS plans were recalculated using the Monte Carlo dose calculation algorithm as a verification dose check.

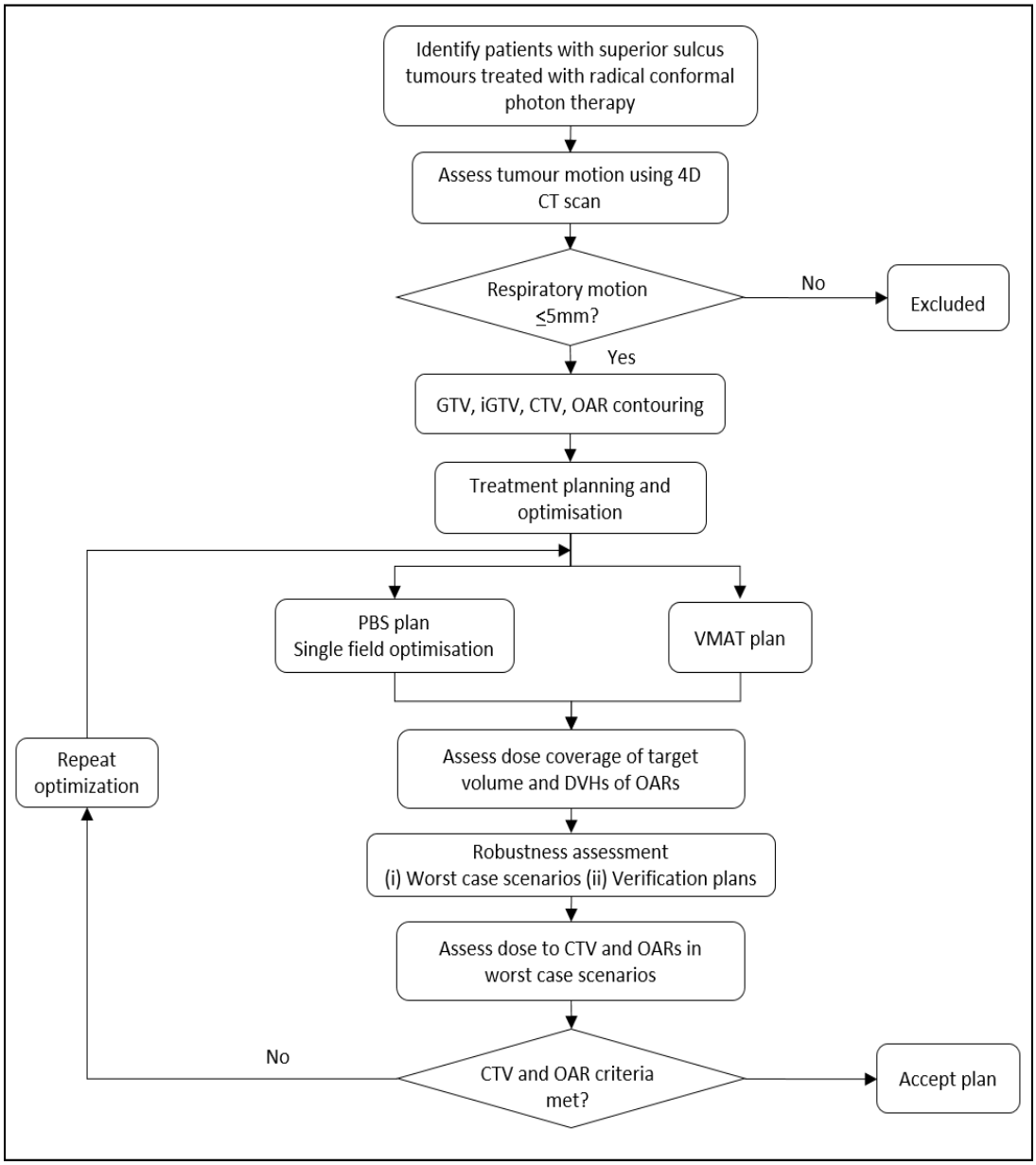

Figure 6. Flowchart of case selection and planning procedures. GTV (gross tumour volume). iGTV (internal gross tumour volume as assessed by 4DCT). CTV (clinical target volume). OAR (organs at risk).

i) Tumour motion assessment

Range of tumour motion was verified to be ≤5 mm, which was considered acceptable [204]–[206] by assessing z-axis motion of the most inferior part of tumour and delineating the Gross Tumour Volume (GTV) in each phase of the 4DCT scan to assess centre-of-mass movement in the x, y and z-axis.

For one test case, the OARs were also contoured on CT0 (max-inhalation) and CT50 (max-exhalation) and their centre-of-mass location noted so that their range of motion could be assessed.

ii) Volume delineation

The internal GTV (iGTV) was defined as the envelope of GTV motion and delineated using the Maximum-Intensity Projection (MIP) dataset. In cases where the tumour moved into nearby soft tissues of a similar density the MIP was not appropriate. Here delineation was aided by all phases, especially max-inspiration and -expiration. The clinical target volume (CTV) was defined as the iGTV+5 mm in all directions- as such, the CTV is synonymous with the internal target volume (ITV). A technical optimisation volume was created to account for external variation in set-up, as per department tolerance guidelines, and was defined as the CTV+ 5 mm in all directions.

iii) Organs at risk tolerances

OARs were delineated on the average intensity projection image datasets and tolerances are defined in table 6 [207].

Tumour target volumes were delineated by two clinicians, one of whom delineated all the OARs. All final patient volumes were verified by a third independent clinician.

Organs at Risk	Method of Delineation	Dose constraint (2Gy/#)
Spinal canal	Contoured on the bony limits of the canal.	Dmax $_{\text{point dose}}$ ≤46Gy
Spinal canal planning risk volume	SC+5mm	≤ 50Gy to 1cc
Mean lung dose	As above	<20Gy
Lungs	Contoured using lung windows and include inflated and collapsed lung. GTV and trachea and ipsilateral bronchi should be excluded.	V20 ≤ 30% V10 < 50% V5 < 50- 60% considered desirable but not at the expense of target coverage
Contralateral lung	As above	As low as reasonably possible
Heart	Contoured along the pericardial sac, starting from the superior aspect of the pulmonary artery, extending inferiorly to the apex of the heart.	V40 < 30%
Oesophagus	Contoured on mediastinal windows. Start from the cricoid to the gastro-oesophageal junction.	V35 < 50%
Brachial plexus	Contouring using a 0.5cm paint tool from C8-T1 nerve roots extending to the main trunks, divisions and cords. Higher cervical nerve roots may need to be contoured depending on how superior the technical optimisation volume extends. The subclavian and axillary vessels are used as surrogates. Both the artery and vein are contoured to ensure the whole neurovascular bundle is encompassed. Medially, begin at the neural foramen and extend laterally to and encompass the space between the anterior and medial scalene muscles. On slices where there is no neural foramen imaged, delineate the space between the anterior and medial scalene muscles alone. Inferiorly, the lateral extent of the volume is where the neurovascular bundle passes the 1st rib.	Dmax ≤66Gy to 1cc

Table 6. Dose constraints to OARs and method of contouring. All OARs were delineated on the average intensity projection image datasets. Lung V5, V10, V20 (percentage combined normal lung volume receiving 5 Gy, 10 Gy and 20 Gy, respectively). Heart V40 (percentage volume of the heart receiving 40 Gy). Oesophagus V35 (percentage volume of the oesophagus receiving 35 Gy).

iv) Planning method

VMAT plans were generated as per our departmental protocols using target and OAR structures and dose constraints, as above (table 6), to set planning objectives. Two partial-arcs were used to minimise unnecessary dose to normal lung.

For lung proton plans it has become commonplace to apply an inhomogeneity correction (IC) to ensure density correction and target coverage [208] but this may not be necessary for SSTs. Thus, for cases 1-3 two nominal plans were created with either an IC applied to the whole iGTV (by assessing the average density within the tumour's centre and assigning a uniform CT Hounsfield unit override); or no IC (fig 7). Only if robustness analysis demonstrated an advantage of applying an IC would we continue for the remaining cases.

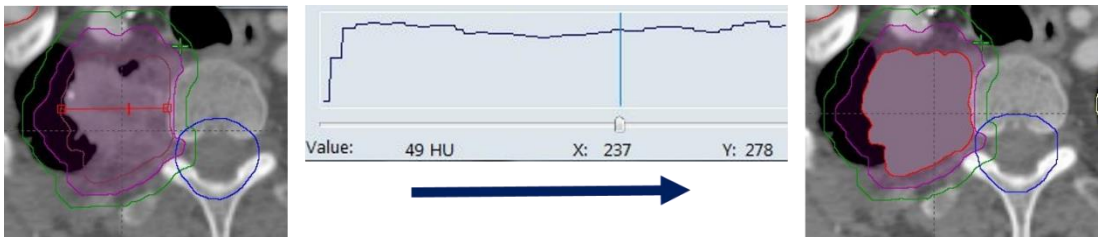

Figure 7. Diagram showing method of applying an inhomogeneity correction. The density across the central tumour mass is assessed and an averaged density override is uniformly applied to the whole iGTV.

Two to three beams of equal weighting were used for all plans. Beam angles were selected with consideration of robustness and conformality. The aim was to ensure: 1. shortest, most homogenous path to the target based on a visual check; 2. beam entry through stable tissue; 3. avoiding critical OARs immediately distal to the target [209]; 4. avoiding high-Z materials (such as metal clips or prostheses). If it was felt that the more robust option resulted in compromise to conformality that was clinically unacceptable, then angles were adjusted. Beams did not overlap at the skin surface, to avoid skin toxicity, and not more than 2 of 3 of prescribed dose came from beams directed towards a critical structure.

A single-field optimisation (SFO) approach was used rather than multi-field optimisation (MFO) despite limited reports that it might have a dosimetric advantage [26] as MFO is exquisitely sensitive to motion and therefore considered potentially less robust.

The spot- and layer-spacing was nominally set to 5mm.

v) Optimisation approach

Inverse plan optimisation was used for both photon and proton plans. The technical optimisation volume was used to optimize CTV coverage. The optimisation went through iterations in order to achieve OAR tolerances (highest priority) and target coverage. The target coverage assessment is described in the following paragraphs.

Dose distribution was calculated on the average CT datasets.

vi) Robustness assessment

Two strategies were used to assess robustness for both VMAT and PBS plans. Firstly, we performed robustness analysis based on worst-case scenario. A geometric uncertainty of 5mm, based on our centre's lung set-up tolerance, was done for proton and photon plans [210]. Range uncertainty of 3.5% was considered for protons only [202], [211]–[213]. The worst-case scenarios (defined as the minimum target coverage and maximum dose to OAR across the various scenarios) were assessed to ensure adequate target coverage and that dose tolerances were met. The spinal canal dose constraints were more restrictive for the nominal plan optimisation (point dose $\leq$46 Gy (RBE)) as a pragmatic decision to ensure it would pass robustness assessment, where up to 50 Gy (RBE) to 1cc of the spinal canal was accepted.

Secondly, verification plans were calculated in order to assess the impact of motion. These were recalculations of the nominal plan on CT0 (max-inhalation) and CT50 (max-exhalation) keeping the exposure parameters constant. Dosimetric changes affecting target coverage led to further optimisation iterations and if necessary, beam angle changes.

vii) Plan evaluation

Nominal plans were considered acceptable if the CTV D95 was $\geq$95%, acknowledging that SST CTVs can infiltrate the spinal canal, creating a conflict of dose limitations; and OAR criteria were met.

Plans passed robustness assessment if the maximum percentage difference in target coverage (difference between CTV D95 in the worst-case scenario and CTV D95 in the nominal plan) was $\leq$5%; and if OAR tolerances were maintained.

viii) Statistical Analysis

The Mann-Whitney U test was used to calculate statistical significance (p-values) of mean dose parameters from the VMAT compared to PBS plans using the statistics software programme R.

A value of $p<0.05$ was considered statistically significant.

4.3.3 Results

Ten patients were identified as suitable out of seventeen- four patients were excluded as they did not have 4D-CTs and three had large tumours extending into the lower lobes where motion was >5 mm. The median CTV volume was 274.4 cm^3 (101.4cm^3- 645.8 cm^3) (table 7, figure 8).

	Patient									
	1	2	3	4	5	6	7	8	9	10
TNM stage (AJCC 7th Ed)	T3N0M0	T4N2M0	T4N0M0	T4N3M0	T3N2M0	T3N2M0	T3N2M0	T4N2M0	Locally recurrent disease	T3N3M0
Histological confirmation of diagnosis	Adenocarcinoma	Squamous cell carcinoma	Adenocarcinoma	Squamous cell carcinoma	Squamous cell carcinoma	Adenocarcinoma	Adenocarcinoma	Adenocarcinoma	Squamous cell carcinoma	Adenocarcinoma
OTV volume (cm^3)	200.13	958.79	286.48	595.52	585.83	766.30	315.86	499.39	223.30	389.00
Tumour location	Right apex	Right apex and mediastinum	Left apex	Right apex and mediastinum	Right apex and mediastinum	Right apex and mediastinum	Right apex and mediastinum	Left apex and mediastinum	Left apex	Right apex and mediastinum
Abutting or invasion of structures	Invades mediastinal pleura medially. No brachial plexus invasion.	Involves mediastinal and peripheral pleura. Encases superior vena cava.	Abuts mediastinal and peripheral pleura. Infiltration of mediastinum at the level of the aorto pulmonary window.	Abuts 2nd rib, 4 vertebral bodies and pericardial sac superiorly to bottom of pulmonary trunk	Invades 3rd rib posteriorly	Abuts 3rd - 6th ribs posteriorly and the T4-6 thoracic vertebral bodies anteriorly	Abuts chest wall and 1st-2nd ribs anteriorly over a longitudinal length of 2.5cm	Invades chest wall along 1st -4th ribs posteriorly	Abuts 1st- 3rd ribs posteriorly and invades 2nd rib	Abuts 1st- 3rd ribs and the thoracic vertebral bodies anteriorly over a length of 2.25cm
Minimum GTV- to-spinal canal distance (cm)	0.75	1.55	3.00	0.91	1.50	0.70	3.50	1.00	0.50	1.50
Minimum GTV- to-brachial plexus distance (cm)	Abutting the brachial plexus on 1 CT slice	Abutting and displacing the brachial plexus	Abutting the brachial plexus	Abutting the brachial plexus and within 0.5cm over a length of 1.00 cm	1.54	0.40cm at two points	Within 0.5cm over a length of 1.50cm	Abutting and within 0.5cm over a length of 1.50cm	Abutting and within 0.5cm over a length of 1.75cm	1.50
Minimum GTV- to- heart distance (cm)	3.25	0.25	Abutting pericardiac sac superiorly to bottom of pulmonary trunk	Abutting pericardial sac superiorly to bottom of pulmonary trunk over a length of 2.75cm	Abutting and overlapping pericardium superiorly over a length of 5cm	Abutting and within 0.5cm over a length of 2.25cm	Abutting and within 0.5cm over a length of 5.25cm	Abutting over a length of 3.00cm	5.00	Abutting and within 0.5cm over a length of 1cm
Minimum GTV- to-oesophagus distance (cm)	2.30	1.04	Abutting for 1cm length	Abutting and within 0.5cm over a length of 5cm	Within 0.5cm from oesophagus over a length of 1.25cm	Within 0.5cm over a length of 1cm	Abutting or overlapping oesophagus over a length of 4cm	Within 0.5cm over a length of 2cm	Abutting and within 0.5cm over a length of 2.75cm	0.60
Minimum GTV- to- rib distance (cm)	Adjacent to 2nd rib extending to the costovertebral junction but no bone invasion	Abutting 1st, 2nd and 3rd ribs posteriorly	Abutting 1st and 2nd rib	Abutting 2nd rib	Invading 3rd rib posteriorly, tracking along 2nd and 4th ribs posteriorly	Abutting 3rd to 6th ribs posteriorly	Within 0.5cm of 1st and 2nd ribs anteriorly over a longitudinal length of 2.5cm	abutting the 1st to 4h ribs posteriorly over a length of 5.75cm	abutting 1st to 3rd ribs posteriorly and invading 2nd rib	Abutting the 1st, 2nd and 3rd ribs
Minimum GTV- to-thoracic vertebrae distance (cm)	Adjacent to thoracic vertebra. Within 0.5cm over a length of 2.50cm	Adjacent to thoracic vertebra. Within 0.5cm over a length of 5.25cm	Within 1.3cm over a length of 0.25cm	Abutting and within 0.5cm of the anterior part of the thoracic vertebra over a length 6.25cm	Within 0.5cm over a length of 0.25cm	Abutting the anterior part of the thoracic vertebra over a length 6cm	Within 0.5cm over a length of 4.00cm	Within 0.5cm over a length of 5.00cm	Abutting the anterior bodies of the thoracic vertebra over a length of 5.00cm	Within 0.5cm of the anterior bodies of the thoracic vertebrae along a length of 2.25cm
CTV immediately adjacent to or overlapping spinal canal	Yes	No	No	No	No	Yes	No	No	Yes	No
OTV immediately adjacent to or overlapping spinal canal PRV	Yes	Yes	No	Yes	Yes	Yes	No	Yes	Yes	Yes
CTV immediately adjacent to or overlapping brachial plexus	Yes	Yes	Yes	Yes	No	Yes	Yes	Yes	Yes	No
OTV immediately adjacent to or overlapping brachial plexus	Yes	Yes	Yes	Yes	No	Yes	Yes	Yes	Yes	Yes

Table 7. Showing anatomical tumour characteristics for each case. Optimisation target volume (OTV). Gross tumour volume (GTV). Clinical target volume (CTV). All patients had histological confirmation of their diagnosis of non- small cell lung cancer. All patients had PET CT and brain imaging as part of their staging imaging. Patient 1 had an MRI thorax as additional imaging.

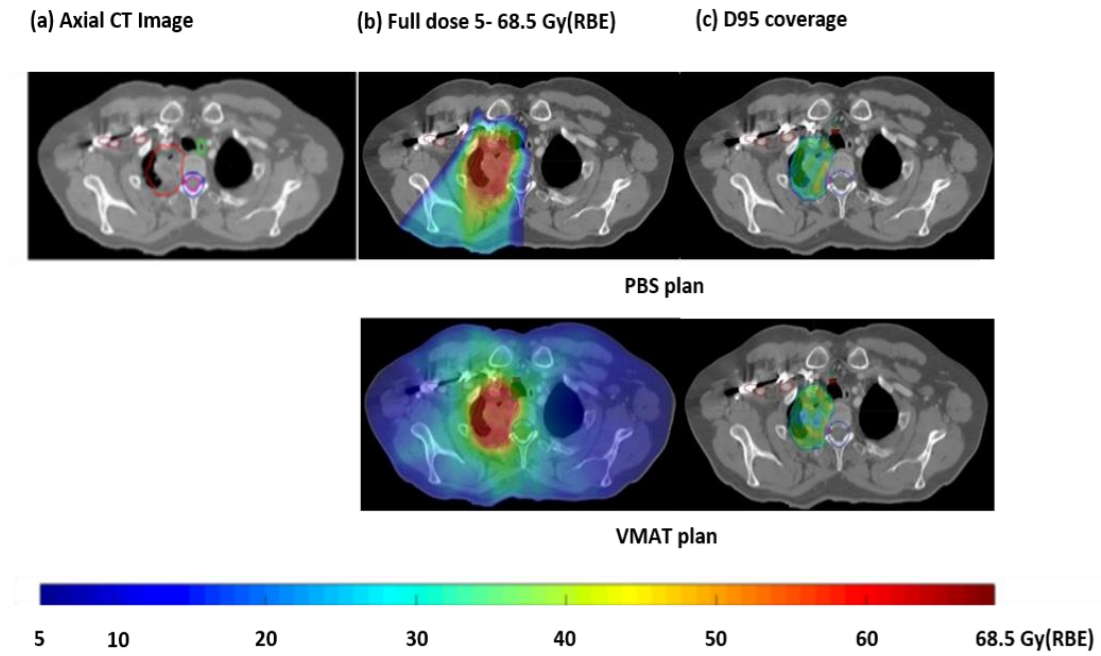

Figure 8. Graphic showing (a) axial images (b) full doses 5- 68.5 Gy (RBE) (c) D95 coverage of case 1. The PBS plan is shown in the top row. The VMAT plan is shown in the bottom row. Series (a) shows the tumour's proximity to the spinal canal and canal planning at risk volume in each case. Structures seen include: CTV (magenta), brachial plexus (red), spinal canal (pink), canal PRV (dark blue), oesophagus (light green).

4.3.3.1 Effect of inhomogeneity correction (IC) on target coverage

Applying the IC had little effect on target volume coverage and OARs. Mean CTV D95 was 98.0% (range 97.6-98.7%) compared to 98.1% (range 97.5-98.7%) with no correction. Importantly, there was minimal effect on the robustness of target coverage- mean maximum percentage difference in CTV D95 (no IC) of 1.65% (range 0.93- 2.23%) compared to a mean of 3.74% (range 1.54-7.37%) when IC was used (figure 9). Surprisingly, applying the IC for case 1 made robustness worse, resulting in a CTV D95 deviation from the nominal plan of up to 7.37% (IC) versus 1.79% (no IC). Based on these findings, the override method was not used for the remaining 7 cases.

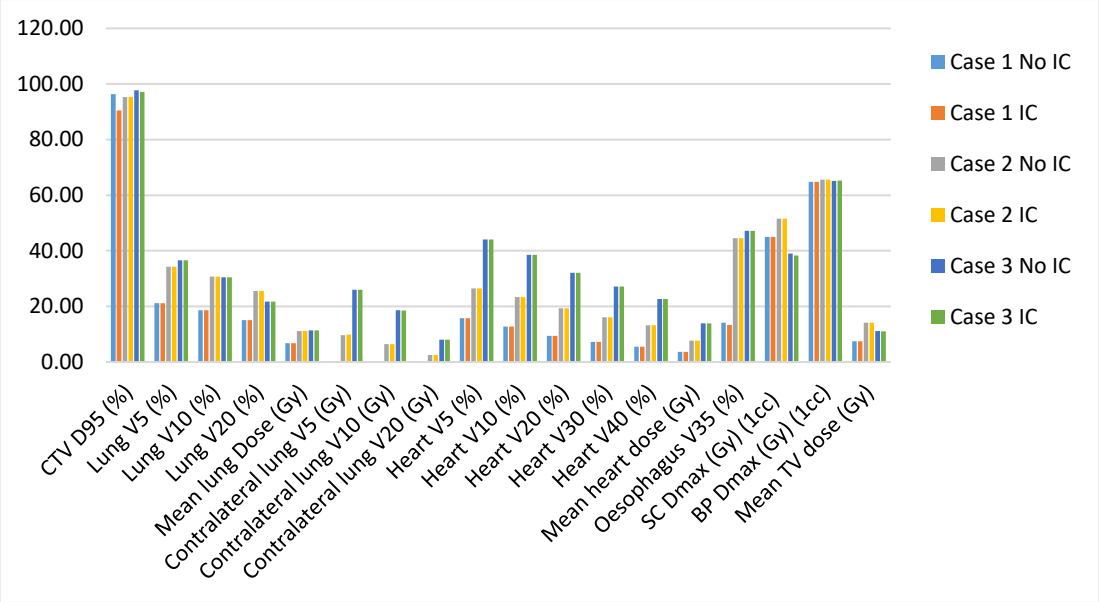

Figure 9. Graph showing the worst case scenario doses to the target and OARs for the nominal PBS plans with and without an inhomogeneity correction. CTV (clinical target volume). TV (thoracic vertebra). BP (brachial plexus). SC (spinal canal).

4.3.3.2 Dosimetric Assessment

For all plans Dmax was <107%. CTV D95 was >97% for all cases and all the mean of the dose parameters of OARs for proton plans were lower than those for VMAT plans, except heart V40 (mean: 7.1% versus 6.3%, p=0.24) and brachial plexus Dmax (1cc) (mean: 62.3 Gy versus 62.0 Gy, p=0.23).

Proton plans almost completely spared the contralateral lung, on average, reducing the V5 by 79.0% (p<0.01). Compared to VMAT plans, proton plans reduced the mean lung dose by 21.7% (mean 9.4 Gy (RBE), p<0.01), lung V20 by 12.1% (mean 17.4%, p<0.05), lung V10 by 36.4% (mean 21.8%, p<0.01), lung V5 by 47.9% (mean 25.5%, p<0.01), mean heart dose by 21.4% (mean 6.4 Gy (RBE), p<0.05) and mean thoracic vertebra dose by 29.2% (mean 10.0 Gy (RBE), p<0.01) (table 8, fig 10). The Monte Carlo dose check revealed a 3.9% reduction in mean CTV D95, as expected.

		VMAT		PBS		Difference (%)
	Assessment parameter	**Mean**	**Range**	**Mean**	**Range**	
CTV	D95 (%)	98.4± 0.2	98.1-98.9	98.1 ± 0.4	97.5-98.8	0.3
	D98 (%)	97.5± 1.2	94.1-98.1	97.2 ±0.6	96.2- 98.2	0.3
Lung	V5 (%)	48.9 ± 15.4	13.9-68.7	25.5 ±9.9	7.8- 43.4	47.9**
	V10 (%)	34.3 ± 12.8	8.9-50.2	21.8 ±8.4	6.4- 36.7	36.4**
	V20 (%)	19.8 ± 8.3	4.7-29.6	17.4 ±6.3	4.7- 25.8	12.1*
	Mean dose (Gy[RBE])	12.0 ± 4.1	3.6-16.3	9.4 ±3.4	2.7- 13.2	21.9**
Contralateral lung	V5 (%)	48.6± 16.5	10.4-71.1	10.2 ±15.0	0.0- 49.6	79.0**
	V10 (%)	27.4 ± 14.1	5.9-59.0	6.7 ±12.2	0.0- 39.9	75.4**
	V20 (%)	7.4 ± 8.5	0.0-31.4	3.2 ±7.2	0.0- 23.3	56.5**
Heart	V5 (%)	26.1± 13.2	0.0-50.3	19.3 ±11.3	0.0- 37.8	26.0
	V10 (%)	20.6 ± 10.9	0.0-41.3	15.9 ±9.7	0.0- 32.6	23.0
	V20 (%)	14.7± 8.1	0.0-28.0	11.8 ±7.7	0.0- 26.3	19.8
	V30 (%)	9.8 ± 5.7	0.0-17.5	9.2 ±6.4	0.0- 21.6	6.7
	V40 (%)	6.3 ± 4.0	0.0-12.3	7.1 ± 5.1	0.0- 17.2	+12.8
	Mean dose (Gy[RBE])	8.1 ± 3.9	0.4-13.5	6.4 ± 4.1	0.0- 14.0	21.4*
Thoracic vertebra	Mean dose (Gy[RBE])	14.1 ± 3.4	9.2- 18.1	10.0 ±2.8	5.5- 14.1	29.2**
Oesophagus	V35 (%)	32.8 ± 9.9	14.6-43.1	29.8 ±12.0	8.2- 43.3	9.2
Brachial plexus	Dmax (1cc)(Gy[RBE])	62.0 ± 5.0	48.2-65.0	62.3 ±5.4	47.2- 65.1	+0.5
Spinal canal	Dmax (point dose) (Gy[RBE])	43.4 ± 2.2	38.6-45.6	41.4 ±3.6	33.6- 45.3	4.6
	PRV Dmax (1cc) (Gy[RBE])	45.9 ± 3.8	40.5-49.6	45.1 ±3.9	35.6- 48.3	1.6

Table 8. Mean dose to target and OARS for the nominal photon VMAT and PBS single field optimization plans. CTV (clinical target volume). All percentage differences show a reduction in dose or volume in the PBS plans compared to the VMAT except for values preceded by (+) indicating a percentage increase in the PBS plan compared to the VMAT plan.*p(<0.05). **p(<0.01).

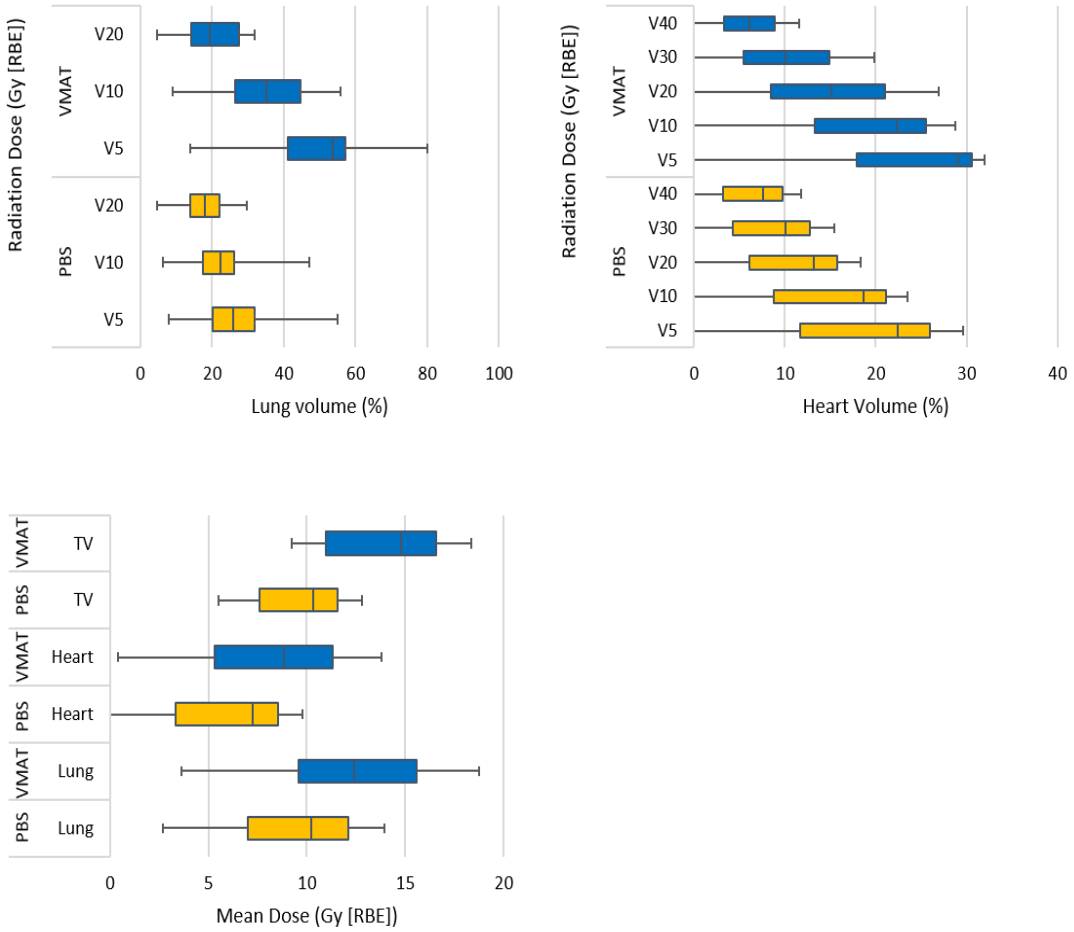

Figure 10. Box plot of distributions of dose-volume indices for the lungs, heart and thoracic vertebrae (TV) when planned with PBS protons compared to VMAT for 10 patients with superior sulcus tumours. Whiskers show range and boxes show quartile 1, 2, and 3. PBS protons reduced the mean lung dose by 21.9% (mean 9.4 Gy (RBE), p<0.01), lung V20 by 12.1% (mean 17.4%, p<0.05), lung V10 by 36.4% (mean 21.8%, p<0.01), lung V5 by 47 .9% (mean 25.5%, p<0.01), mean heart dose by 21.4%(mean 6.4 Gy (RBE), p<0.05) and mean thoracic vertebra dose by 29.2% (mean 10.0 Gy (RBE), p<0.01).

4.3.3.3 Robustness Assessment

Six scenarios were generated for the photon plans following isotropic shifts. Incorporating range uncertainty as well resulted in twelve scenarios being generated for the proton plans. Figure 11 shows the resulting CTV and OAR variation for case 1 as an example. On robustness analysis the mean CTV D95, in the worst-case scenario, was 93.9% $\pm$3.0 (range 89.5-97.8%) for proton plans (maximum percentage difference 0.9-9.0%) and 97% $\pm$1.3 (range 93-98%) for VMAT plans (maximum percentage difference 0.26-5.49%). For all photon and proton verification plans, the CTV D95 was >95%, except the proton plan for case 9 where CTV D95 was 91.9%.

Relative OAR motion at the extremes of breathing on the test-case was <3 mm, except for the heart and lungs (table 9). As such, OAR dosimetry on verification plans were not done, especially as uncertainty scenarios identified breaches in OAR constraints.

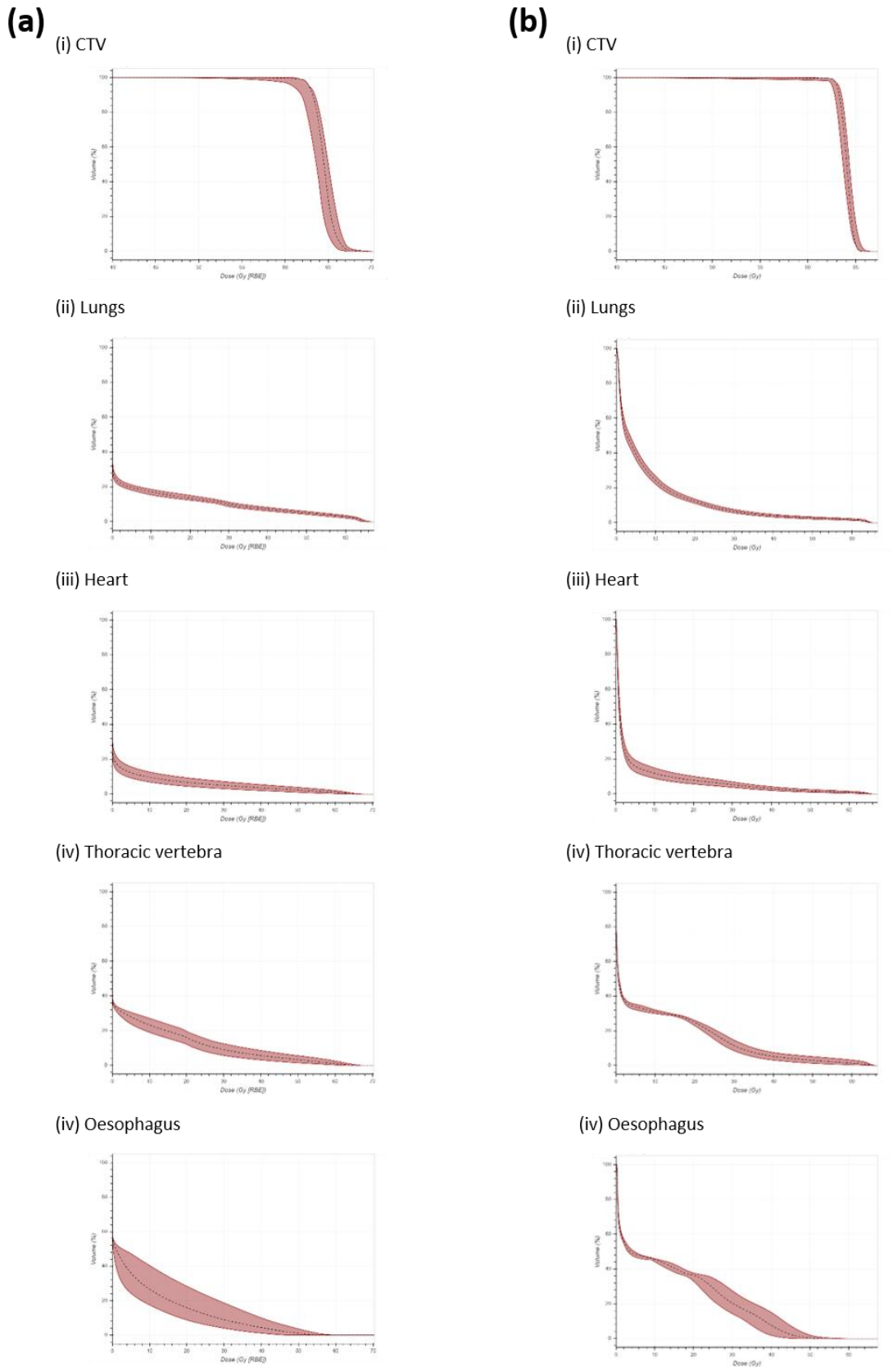

Figure 11. (a) proton and (b) photon plan dose volume histograms for (i) CTV (ii) lung (iii) heart (iv) thoracic vertebrae and (v) oesophagus generated from robustness scenarios for patient 1 as a case example. Robustness analysis for the proton plan involved 12 scenarios of varying 5 mm isocentre shifts and ±3.5% range uncertainty. Robustness analysis for the photon plans involved 6 scenarios of varying 5 mm isocentre shifts.

	CTAve-CT0 Change in Centre- of- Mass			CTAve-CT50 Change in Centre- of- Mass			CT0- CT50 Change in Centre- of- Mass		
	x axis (cm)	y axis (cm)	z axis (cm)	x axis (cm)	y axis (cm)	z axis (cm)	x axis (cm)	y axis (cm)	z axis (cm)
CTV	0.04	0.03	-0.05	-0.03	-0.04	0.01	0.07	0.07	-0.06
Ipsilateral Lung	0.04	-0.25	0.17	-0.03	0.00	0.01	0.07	-0.25	0.16
Contralateral Lung	-0.02	-0.06	1.00	0.08	0.18	-1.60	-0.1	-0.24	2.6
Heart	-0.23	0.18	0.16	-0.05	-0.16	-0.35	-0.18	0.34	0.51
Oesophagus	0.00	0.06	-0.07	0.13	-0.06	0.15	-0.13	0.12	-0.22
Spinal Canal	0.00	0.00	0.00	0.00	0.00	0.00	0.00	0.00	0.00
Brachial plexus	0.09	0.03	0.02	0.11	0.01	0.06	-0.02	0.02	-0.04
Thoracic vertebra	-0.01	0.00	-0.01	-0.01	0.00	-0.01	0.00	0.00	0.00

Table 9. Changes in centre- of- mass of the clinical target volume (CTV) and organs- at-risk (OARs) for case 2. Within the resolution limits of the planning CT, minimal change in the centre- of- mass position is demonstrated at the extremes of breathing relative to their position as seen on the CT Ave. In particular, there is <2mm change in the centre-of-mass position of the brachial plexus. The maximal change in position at the extremes of breathing was seen in lungs and heart.

The same 4 proton and photon plans failed robustness assessment (table 10). Cases planned using VMAT primarily failed due to lung V20 tolerance being exceeded in 1 scenario, whereas inadequately robust CTV coverage was the dominant reason for the proton-planned cases not passing assessment. Both VMAT and PBS plans failed robustness assessment for case 9, a likely result of the CTV abutting the spinal cord.

Case	VMAT	PBS
	Reason(s) for failing robustness assessment	Reason(s) for failing robustness assessment
2	Lung V20 tolerance exceeded on 1 worst case scenario from robustness analysis	Spinal canal tolerance exceeded on 1 worst case scenario from robustness analysis
4	Lung V20 tolerance exceeded on 1 worst case scenario from robustness analysis	Maximum percentage difference in CTV coverage on robustness analysis >5%
7	Lung V20 tolerance exceeded on 1 worst case scenario from robustness analysis	Maximum percentage difference in CTV coverage on robustness analysis >5%
9	Maximum percentage difference in CTV coverage on robustness analysis >5%	Maximum percentage difference in CTV coverage on robustness analysis >5%

Table 10. VMAT and PBS plans that failed robustness assessment.

4.3.4 Discussion

Our results suggest it is feasible to deliver robust PBS treatment in select SST cases where tumour motion ≤5mm and tissue heterogeneity along the proton paths is minimal. Comparable CTV coverage and considerable reduction in lung, mean heart dose and mean thoracic vertebra dose can be achieved.

Most studies investigating proton beam therapy in LA NSCLC have used passive scattering techniques [21], [22], [26], [171], [172], [182], [214], [215] and Liao's recent study comparing IMRT to passive scattering protons concluded no difference in treatment failure rates between the two groups [182].

SSTs are a rare subset of LA NSCLC which present similar challenges for photons and protons. These include image quality needed for accurate tumour and OAR delineation, motion and the proximity of critical organs. Additional considerations for protons are inherent uncertainties such as range, lateral scattering and exquisite sensitivity to changes in anatomy [18], [79], [104], [202].

Magnetic resonance imaging (MRI) helps evaluate SSTs as higher contrast resolution results in superior anatomical visualisation, especially the brachial plexus. MR image-guided radiotherapy (MR-linac) is an evolving technology incorporating MRI sequences to improve delineation accuracy. It can enable uncertainty margins to be reduced, thus better sparing OARs [216]. However, respiratory motion can cause ghosting artefacts and compromise resolution [217]. Furthermore, although advanced MRI-to-4DCT registration algorithms exist, they are not used in clinical practice yet [218] and assessment on an individual basis, in order to minimise error propagation, is recommended [219]. Studies comparing MR-linac and PBT for SSTs should be explored.

Motion is problematic for any form of high-precision radiotherapy where steep dose gradients can result in dose uncertainty. Our motion monitoring strategy relied on external devices tracking chest wall movement but this can be smaller than that of the tumour [77], [79]. Subsequent analysis assessed overall and maximal motion but rotational or tumour deformity analysis, was not possible. Our study only included apical tumours with motion ≤5 mm, therefore negating the need to evaluate interplay [204]–[206], [220]. The impact of motion on dosimetry was analysed by robustness assessment and considered for both VMAT and PBS. To our knowledge, this has not been performed in previous comparative lung planning studies.

Protons are particularly sensitive to motion as their radiological path length is effected, not only by tumour movement but also normal lung tissue- at different phases of breathing, variable filling of airways and blood vessels results in variable relative stopping power ratio values [211]. This interplay between the scanned beam and target motion not only causes degradation of dose homogeneity, due to misplacement of individual spots relative to planned positions, but it also affects the dose to critical organs [202], [221], [222]. Dose-repainting has been proposed to reduce this but it is not effective alone [204],[222] and questions remain about the effect of washout [160], [220], [223], [224].

Our proton planning approach focused on maximising robustness. Considerations included defining margins, choosing robust beam angles and investigating the use of an IC. The concept of beam-specific margins that incorporate proximal and distal uncertainties have been implemented in passive scattering protons but their translation to PBS is not well established [225] so was not applied here. Another strategy to allow for uncertainties is to use minimax optimization [226]. Here, uncertainties are entered into the planning system and multiple scenario-based plans are generated. This bypasses the need for a technical optimisation volume and coverage is thought to be equivalent to technical optimisation volume-based plans [227]–[229]. Although it is recognised that technical optimisation volume margins effectively only take lateral uncertainties into account, we compensated for this by retrospectively assessing target coverage before re-optimising areas of under-coverage [230].

All proton plans were achieved using a 2-3 field arrangement, which is in keeping with previous studies [19], [154], [168], [231], [232] who have used between 2-4 beams. In principle, an increased number of beams increases robustness, at the expense of an increased integral dose and dose to certain OARs.

The main purpose of an IC is to account for motion-induced tissue density variation to minimise the risk of under-dosing the target and widely used in passively scattered techniques [222], [233], [234]. However, this is an artificial scenario and our study showed that its effect on plan robustness was minimal-likely due to SSTs being more fixed and their apical location. Unexpectedly, the IC resulted in reduced CTV robustness for one case due to the complex geometry and relative position of the tumour limiting choices of beam angles. This meant part of a beam was directed through the shoulder blade. Under uncertainties, the amount of bone in the path increased. The effect was less detrimental when no IC was used as the extra bone was counteracted by more lung in the path length. This extra lung was overridden with the IC and resulted in under coverage observed. On visual assessment, it was clear that the IC effect became more noticeable in parts of tumours that were spiculated and extended lower into the thorax where movement was greater. The most important factor affecting target coverage and

robustness was the target volume overlapping with the spinal canal. The need to compromise target coverage in order to adhere to spinal canal tolerance remains as much a problem for PBS protons as it does for VMAT. This lack of improved target conformality may be explained by the lateral penumbra for PBS being worse than for photons and range straggling blunting the sharpness of distal dose fall-off such that safety margins are still needed [5]. In contrast to other reports [171], our results did not demonstrate size impacting target coverage or robustness.

Robustness analyses tools within treatment planning systems are commonly used for assessment of proton plans [158] and can be applied to photon plans [210]. In Chang et al's study (2014) comparing PBS-MFO, passive scattering protons and intensity-modulated radiotherapy (IMRT) for thoracic tumours, robustness was assessed by verification plans and 9 scenarios of $\pm$3 mm shifts (although set-up error was 5mm) and $\pm$3.5% range uncertainty, with a prescription criteria of CTV D95 >95%. They concluded that MFO enabled a dosimetric advantage in sparing OARs but no advantage in CTV coverage [158]. Similarly, we used a combination 12 scenarios with various permutations of $\pm$5 mm isocentre shifts and $\pm$3.5% range uncertainty [211] as well as verification plans at CT0 and CT50. In this way target coverage and OAR doses could be assessed in worst-case scenarios and at the extremes of the breathing cycle- a necessary 2-step check. Verification plans on repeat CT datasets were not calculated, however, so the impact of inter-fractional rotational variation was not accessed with this initial cohort.

The same 4 cases failed robustness assessment for photon and proton planning- the photon plans primarily due to lung V20 tolerance being exceeded and the proton plans due to CTV D95 variation being unacceptable, highlighting the specific challenges faced by both techniques. It was not possible to create VMAT or PBS plans that robustly covered the CTV for case 9, emphasising that the most critical factor effecting target robustness was the CTV entering the spinal canal. One proton-planned case failed due to an uncertainty scenario where the isocentre shift resulted in the spinal canal being placed into the beam's path resulting in an excess dose to it. In reality, such a scenario would be avoided by ensuring patients are shifted to "0" position following verification imaging prior to each fraction- this technique is applied to all patients with tumours close to the spinal canal. These results demonstrate that it is not practically possible to resolve all uncertainties in the planning phase and it does not diminish the need for diligent image-guidance and adaptive strategies during treatment.

The most significant dosimetric advantage of protons was in sparing central structures such as the heart and thoracic vertebra (in addition to lungs), suggesting that SSTs with associated

mediastinal involvement are likely to show the greatest benefit from PBS. There is accumulating evidence correlating low-dose to lungs and heart to poorer survival [235]. This is thought to be a result of irradiation of circulating lymphocytes [66], [70], [71] as well as cardiac toxicity. Tang et al 2014 demonstrated significant correlation between lung V5-10 and lymphocyte nadir [76] and Joseph et al 2017 showed in their retrospective analysis that higher integral heart doses correlated with decline in post-treatment lymphocyte counts [72]. Additionally, limiting dose to the thoracic vertebra, where 35% of haematopoietic bone marrow is located, also reduces the risk of lymphopenia. Based on previous studies, if the lung V5, V10, V20 and mean thoracic vertebra dose are kept under approximately 65%, 55%, 45% and 23 Gy, respectively, the risk of grade 3 (or higher) haematological toxicity can be dramatically reduced [73]–[75]. We demonstrated a significant reduction in dose to these lymphopenia-related organs which may be the most advantageous role of PBS-PBT in this era of immunotherapy.

Limitations

The Monte Carlo calculation algorithm is considered more accurate in heterogeneous environments like the lung cohort [236]. As expected, Monte Carlo calculations had little effect on the OARs but demonstrated an approximate 5% reduction in mean CTV D95 compared to the clinical algorithm utilised, which is in agreement with other reports [237], [238]. Unfortunately, Monte-Carlo-based optimisation is not currently available within the Eclipse treatment planning system but follow-up studies utilising this are warranted.

4.3.5 Conclusions

In our planning study we demonstrated that robust PBS plans are achievable in carefully selected patients. Significant dose reductions to the lung, heart and thoracic vertebra are possible without compromising target coverage. Sparing these lymphopenia-related organs may be particularly important in this era of immunotherapy. Identifying suitable cases most likely to benefit from scanning protons is crucial and further analyses on a larger patient cohort is required.

- *Manuscript accepted for publication in the Clinical Oncology journal- Appendix 6*

Chapter 5

Study of photon and proton radiotherapy treatment of non-small cell lung cancer cells

5.1 Background

The physical advantages of proton therapy and its potential role in treating locally advanced NSCLC have been discussed in chapters 3 and 4. In this chapter, I will examine biological differences in the responses of NSCLC cells to proton irradiation compared to photon irradiation.

Following definitive radiotherapy treatment, relapse occurs in up to 40% of NSCLC patients [1], [2] due to innate or acquired radioresistance. For proton beam therapy, it is known that the physical advantages of the Bragg peak, makes it possible to safely escalate dose to the tumour to overcome radioresistance, whilst sparing adjacent normal tissue [18], [20], [239]. However, at a cellular level, it is crucial to consider differences in ionization patterns between protons and photons and subsequent differences in cellular responses. The density of ionization events, or linear energy transfer (LET), is higher for PBT than X-rays and this increased relative biological effectiveness (RBE) results in lower cell survival for the same absorbed dose[30].

Key biological differences, particularly in the context of high and low LET proton irradiation, have not been comprehensively assessed and effects are thought to be tissue-, cell line- and endpoint-specific [5]–[9]. In-vitro studies have only compared high LET irradiation from heavy ion particles [38] or low LET protons [39], [40] to XRT, the findings of which may not be directly translatable to clinical practice. Moreover, within a clinical proton beam, there is non-uniformity: high LET occurs at the lateral edges of the beam and in the distal regions of the spread-out Bragg peak (SOBP), becoming maximal in the distal fall- off of the Bragg-peak, resulting in different biological consequences to both the tumour and normal tissues lying in close proximity [35]–[37], [240].

Ionizing radiation (IR) induces single strand breaks (SSBs) and double strand breaks (DSBs). Irreparable or mis-repaired DSBs [6], [9] are the major cause of cell death. DSBs can be repaired via 2 pathways: Homologous repair (HR), responsible for 20% of DBS repairs; and non- homologous end joining (NHEJ), responsible for 80% of DSB repairs [241], [242]. High and low LET radiation cause distinct patterns of DNA damage, with the former causing more complex clustered lesions, making them more lethal [31]–[33]. Some studies have suggested differential induction of DNA damage repair pathways following XRT and PBT with enhanced susceptibility to proton irradiation in the setting of homologous recombination deficiency. However, reports have been conflicting, which may be a consequence of different LET radiation being delivered or reflect differences in cell line-specific responses [5]–[9], [242]. The nature and severity of DNA injury affects the modality of induced cell death. These death

mechanisms can substitute for each other and include apoptosis, necrosis, mitotic catastrophe (MC), autophagy, senescence or necroptosis [121], [243].

5.1.1 Aims

By examining major cell death pathways following XRT in radioresistant and radiosensitive NSCLC cell lines, we aimed to identify key differences in their cellular responses to high and low LET proton therapy.

5.1.2 Objectives

- Hypothesis Tested:
    - Photon and high and low LET proton irradiation result in different mechanisms of cell kill and different cellular responses to DNA damage.

- All results presented were from experiments I independently designed, conducted and analysed.

5.2 Cell death mechanisms

5.2.1 Apoptosis

Apoptosis is the most well- described form of programmed cell death and is initiated when DNA damage is slow or incomplete. It is composed of 2 pathways: the extrinsic and intrinsic pathway, induced through activation of caspase-8 or caspase-9, respectively [244]. Caspase-independent apoptosis can also occur, mediated through apoptosis-inducing factor (AIF) but it is only seen in certain cells [244].

Apoptosis only accounts for up to 20% of radiation-induced cell death [245] and the contribution of other modes of cell death are becoming increasingly apparent. Tumour suppressor gene *TP53* plays a central role in apoptosis. Phosphorylation at Ser46 results in its transcriptional activation and pro-apoptotic target gene expression [246]. Additionally, p53 can stimulate mitochondrial outer membrane permeabilization and caspase activation, after translocating to the cytoplasm, as well as directly antagonizing anti-apoptotic Bcl-2 and BCl-X_L [247]. *TP53*-independent mechanisms involving p53 homologs, p63 and p73, can also activate apoptosis in response to DNA damage: 1. by the mitochondrial pathway as well as p73 sharing pro-apoptotic target genes with p53 e.g. *Noxa*, *casp-6* and *CD95* [248]; or 2. via the nuclear transactivation of protein Nur77 (also known as TR3 or NGFI-B) [249].

Importantly, p53 is a critical regulator that can direct cell fate towards apoptosis, senescence or autophagy. However, precise molecular mechanisms governing this, particularly those concerning mitotic catastrophe [246], [250]–[252]and necroptosis [253], are yet to be elucidated.

Methods of analysing apoptosis

Different methods for analysing apoptosis include Annexin V- FITC and PI staining for FACs, detecting cells with sub-G1 content by flow cytometry, terminal deoxynucleotidyl transferase dUTP nick-end labelling (TUNEL) staining, caspase activation and cleaved PARP detectable by western blotting, DNA laddering and identification of morphological characteristics by electron microscopy [254].

Apoptosis can be of variable duration, lasting between 1-8 hours and tending to peak within the first 24 hours, depending on inducer and cell type. Choice of assay method can affect optimal time windows for analysis and can also result in different percentages of apoptotic cells for same population.

5.2.2 Senescence

Senescence, a state of permanent cell cycle arrest, is critical for homeostasis and plays an important role in ageing, fibrosis and cancer [255]. It is a terminal stress- activated programme controlled by p53 and $p16^{INK4a}$ tumour suppressor proteins, and their expression is required to induce the characteristic senescence-associated secretory phenotype following irradiation [121], [256], [257]. Active p53 is needed for both the establishment and maintenance of senescence; and $p16^{INK4a}$ expression usually increases at the late stage of senescence.

DNA damage induces expression of p53 via ATM/ATR kinase activation. $P21^{waf}$ is a cyclin-dependant kinase inhibitor whose transcription is activated by p53. This results in the inhibition of cyclin-CDK2,-CDK1 and CDK4/6 complexes leading to cell cycle arrest at G1/S [258]. Whilst $p21^{waf}$ can also be induced by several p53-independent signalling pathways, it is the p53-dependent activation thought to be particularly important for senescence after IR- induced DNA damage [259], [260] (fig 12).

The $p14^{ARF}$ of the Ink4a/p16 locus has a central role in senescence via its reciprocal relationship with p53. It negatively regulates p53 by reducing its transcription and increasing Mdm2- mediated p53 degradation[261]; whilst also being the target of p53-mediated suppression [258], [262], [263]. Following senescence-inducing stimuli, p16 demonstrates

delayed expression, only being observed once p53 levels start to decline back to baseline levels. P16 inhibits cyclin D-dependent kinase CDk4 activity and CDK6 [264], [265], which prevents phosphorylation of Rb (as well as suppressing transcription of *RB*) and subsequent release of transcription factor E2F that is required for G1 to S progression and DNA replication [266].

There is also evidence suggesting p16 serves as a back-up tumour suppressor to p53 [267]. Studies have observed that stress-induced premature senescence (SIPS) induction in p16 deficient cells are associated with p53/p21 pathway induction and nuclear accumulation of p21; whilst cell lines proficient in p16 and deficient in p53 show nuclear accumulation of p16 [268]–[270]. Absence of expression of $p16^{INK4a}$, due to methylation or homozygous deletion, is seen in more than 70% of NSCLC [271], [272] and making p53/p21 the main pathway through which SIPS is induced in the majority of NSCLC.

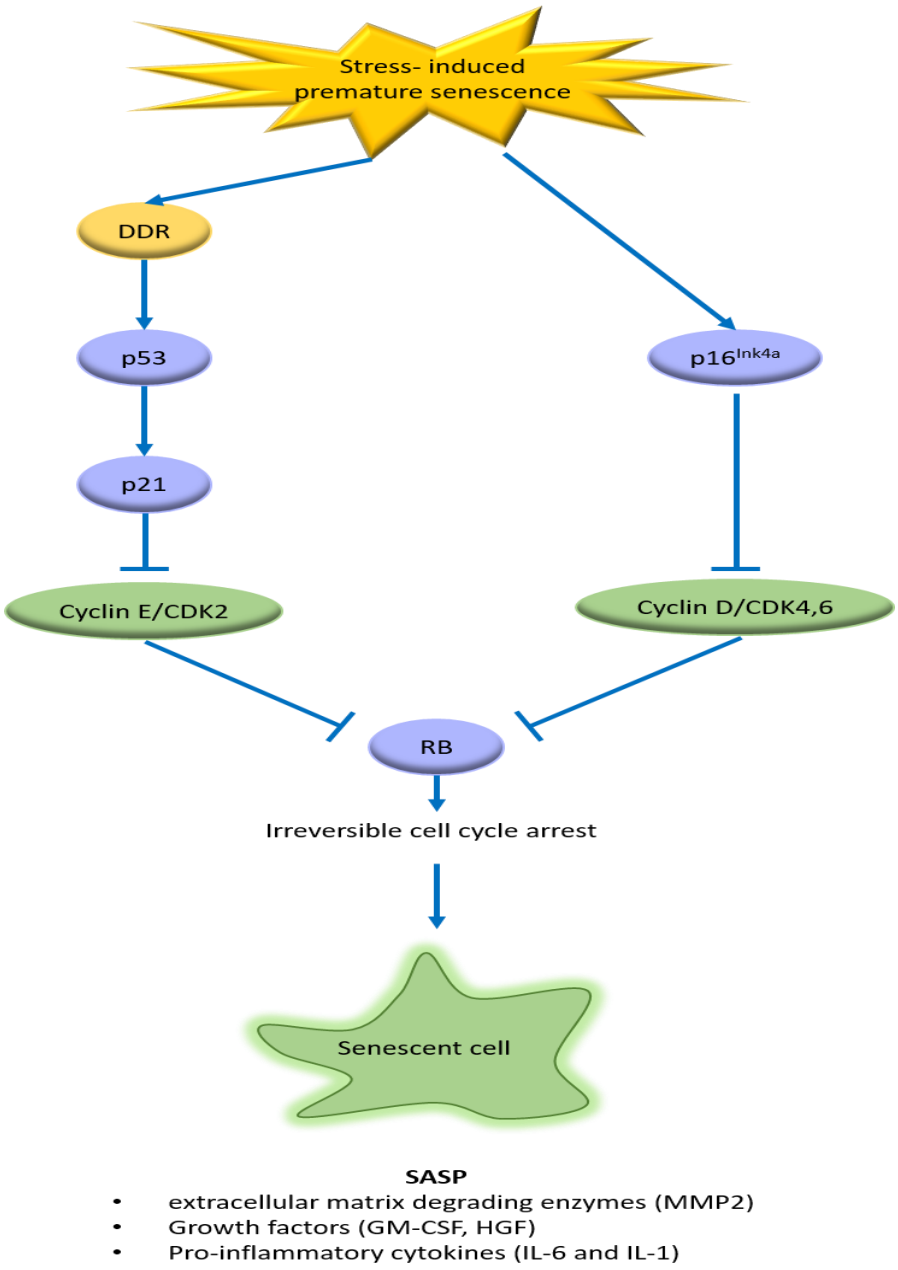

Figure 12. Diagram summarising mechanisms underlying ionizing radiation-induced senescence in non-small cell lung cancer cell lines. Senescence is controlled by p53 and $p16^{INK4a}$ tumour suppressor proteins: DNA damage induces expression of p53 via ATM/ATR kinase activation. P53 induces transcription of p21, which results in the inhibition of cyclinE/CDK2 complex leading to cell cycle arrest at G1/S. P16 inhibits cyclin D-dependent kinase CDk4 activity and CDK6 [264], [265], which prevents phosphorylation of Rb and suppression of its transcription, resulting in cell cycle arrest at G1/S. SASP (senescence associated secretory phenotype). DDR (DNA damage response).

Methods of analysing senescence

Senescent cells are a heterogeneous population and several phenotypic traits are used to identify cells undergoing senescence. Markers used to assess stress-induced premature senescence include permanent cell cycle arrest [273], persistent DNA damage response [274], senescence-associated heterochromatic foci (SAHFs) [275], senescence associated secretory phenotype (SASP) [276] and increased lysosomal and proteasomal activity [277]. Senescence-associated gene expression profiles have also been considered but appear to be cell-specific and stimuli-specific, making their use as a comparative biomarker limited [278].

	Biomarker	**Indicator**	**Detection method**	**Limitations**
Secretory profile	SASP	Enables evaluation of general tissue or cell culture senescence	FACS, ELISA	SASP may vary between cell types and at different stages of senescence. Not able to isolate single-cell secretory phenotypes. [279]
Damage and repair	B galactosidase activity	Increased lysosomal activity	Cytochemical or histochemical detection Fluorescence detection [280]	B-galactosidase activity increases in quiescence and in response to other forms of stress resulting in false-positives[281]
Cell cycle genes	P53/p21 pathway	Expression is required to induce cell cycle arrest	Western blotting	P53 is also responsible for apoptosis so cannot discriminate cells undergoing apoptosis or senescence[282] Cells in quiescence also depend on p53 induction
	P16/Rb pathway	Expression is required to induce cell cycle arrest and thought to be a back-up tumour suppressor to p53[267]		
DNA-associated	Telomere length		Quantitative PCR, FISH	
	DNA damage markers (eg.ϒH2AX, RAD51, 53BP1, ATM, ATR)	DNA damage which is a key trigger of senescence	Immunohistochemistry	Not a direct measure of senescence and not exclusive to senescence [283]

Table 11. Summary of senescence biomarkers, methods of analysis and limitations.

There is no singular biomarker for senescence used across the majority of studies. A combination of β-galactosidase activity with p53/p21 and p16/Rb pathway analyses and telomere length assessment is considered the most reliable method to accurately identify cells undergoing senescence [284].

5.2.3 Necrosis

Necrosis is a rapid nonspecific form of unregulated cell death triggered by energy loss and loss of membrane permeability. Primary necrosis occurs within the first hour following toxic stimuli and secondary necrosis occurs beyond 24 hours later when apoptotic cells are not efficiently cleared, resulting in loss of membrane integrity and associated release of danger associated molecular patterns (DAMPs) [285]. A third form of necrosis is regulated necrosis and includes necroptosis, which will be discussed later. There is no simple test able to distinguish between primary and secondary necrosis [286].

High dose per fraction radiotherapy regimens (greater than 8-10 Gy per fraction) has been demonstrated to cause preferential cell death via necrosis, in contrast to doses of 5 Gy per fraction that are thought to primarily induce MC, apoptosis and autophagy [287], [288].

Methods of analysing necrosis

Dual staining combinations for flow cytometry or cytochemical analysis are commonly used to identify and quantify necrosis.

Annexin-V PI staining, as previously described, can discriminate necrotic from apoptotic cells. Here, loss of membrane permeability allows the impermeable nuclear dye, PI, to bind to necrotic cells (Annexin V+/PI+) and not apoptotic (Annexin V+/PI-) or viable cells (Annexin V-/ PI-). However, at later stages, apoptotic cells also lose membrane permeability as well as their ability to bind Annexin-V due to severe membrane damage [289].

Another very common approach is dual staining with PI/Hoechst. Hoechst 33342 is a cell permeable DNA binding dye used to observe nuclear condensation. When Hoechst binds to DNA complex it fluoresces light blue. Propidium iodide (PI) specifically binds double-stranded nucleic acids in apoptosis and necrosis and cannot enter normal living cells. When PI binds the DNA complex, it fluoresces light red. When living cells are stained with Hoechst and PI at same time, nuclei that stain with high Hoechst (and low PI) are viable. Nuclei that stain with

low Hoechst (and low PI) are apoptotic. Cells that stain with high PI are in secondary necrosis or necrosis.

5.2.4 Mitotic catastrophe

Mitotic catastrophe (MC), an aberrant form of mitosis, resulting from defective cell-cycle checkpoints that fail to arrest ineffectively repaired DNA before they enter mitosis. The final step characteristically features the formation of chromatin surrounded by their own nuclear envelope or cytosolic DNA, also known as micronuclei. It is sometimes considered more of a process leading to apoptosis, rather than a distinct mechanism of cell death itself as aberrant chromosomal segregation initiates the activation of caspase-2 and/or mitochondrial membrane permeabilization, release of cytochrome C and ultimately apoptosis [244], [246].

MC is typically demonstrated 2-6 days post-irradiation [290]. Studies have suggested that MC is the main avenue of cell death induced by ionizing radiation, especially in p53-deficient cells and where Chk1/2 are depleted or inhibited. However, the precise mechanisms directing cell fate towards MC, such as the nature of DNA damage or presence of dysfunctional alternative cell death machinery, are yet to be fully elucidated [246], [250]–[252].

It is well known that at the same dose, densely ionizing particles are more effective at inducing micronuclei formation [122] than XRT. Studies have shown that the concentration of cytosolic DNA increases with increasing radiation dose up to approximately 15-18 Gy, beyond which it decreases due to degradation by activated DNA exonuclease Trex1 [122].

Methods of analysing mitotic catastrophe

Mitotic catastrophe can be analysed using immunofluorescence staining for mitotic markers, including MPM2, TUNEL staining and time- lapse video microscopy to observe cells in real time [254], [291]. The most common method is by light or electron microscopy to identify the presence of micronuclei [292], multilobulated nuclei, and multinucleated cells. However, this method is limited in that micronuclei only indicate that cells have undergone an aberrant mitosis- so some cells with micronuclei may not undergo MC because they survive and do not die.

5.2.5 Necroptosis

Necroptosis is a form of programmed necrotic cell death that morphologically appears like necrosis but is induced by apoptotic death stimuli such as TNF-alpha and Fas ligand [244], [293]. However, it remains a caspase- independent pathway and the precise mechanisms leading to necroptosis are currently poorly understood.

Key proteins involved in necroptosis are: Mixed-lineage kinase domain-like protein (MLKL), receptor interacting protein kinase 3 (RIP3), receptor interacting protein kinase 1 (RIP1), caspase 8 [294]–[296] and lack of expression determined by IHC analysis or silencing confers resistance to necroptosis [294].

Protein	Role in necroptosis	Notes
RIPK1	Protein kinase that recruits RIPK3 to the necrosome, resulting in mutual phosphorylation of RIPK1 and RIPK3	RIP1 involvement in apoptosis & necroptosis RIP1 is not always required for necroptosis[297]
RIPK3	Protein kinase that phosphorylates MLKL. Activated when phosphorylated by RIPK1 and subsequent oligomerization	Functions solely in necroptosis Inhibition of RIP3 expression results in reduced sensitivity of lung cancer cells to high dose radiotherapy [294] RIP3 deficiency contributes to necroptosis resistance in malignant melanomas [298]
MLKL	Phosphorylation by RIPK3 results in MLKL translocating to cell membrane to mediate cell death	
Caspase 8	Inhibits necroptosis by proteolytic cleavage and inactivation of RIP1 and RIP3 leads to pro-apoptotic caspase activation instead of a pro-necrotic cascade	Inhibition may be required for necroptosis induction under some circumstances but is not crucial: Some in vivo studies have shown necroptosis in presence of caspase 8 [299]–[301] Deficiency in caspase 8 results in increased RIP3 expression [302]

Table 12 Key proteins in the necroptotic pathway.

Wang et al's 2018 [294] study in NSCLC in vitro and in vivo suggested that ablative hypofractionated radiotherapy (≥10 Gy per fraction) resulted in preferential cell death via necroptosis in a RIP3-dependent manner, a finding that is consistent with previous studies [287], [288], [303], and that inhibition of *RIP3* expression results in reduced sensitivity to high dose radiation.

Methods of analysing necroptosis

There is no one specific marker distinguishing necroptosis from other cell death modalities so a combination of approaches are generally required [304]–[306]. These are summarised in the table below.

Key feature of necroptosis	Reagents for detection	Method
Loss of membrane integrity	DAPI, Hoechst, PI	Flow cytometry, microscopy
Phosphatidylserine flipping **(Distinguishes from apoptosis)**	Annexin-V conjugates	Flow cytometry, microscopy
Morphology	Swelling of cell and cytoplasmic organelles, followed by rapid loss of plasma membrane integrity	Microscopy
Key protein detection	RIPK3, RIPK1, MLKL, procaspase-8 cleaved caspase-8	Western blot, microscopy, flow cytometry
Death receptor activation	TNFR1,TNFR2, FAS, TWEAK receptor, TRAIL receptors	Western blot, flow cytometry

Table 13. Assays for detecting hallmarks of necroptosis[304]–[306]

5.2.6 Autophagy

Autophagy is an intracellular degradation and recycling system whereby cellular component are wrapped within double- membrane autophagosomes and delivered to lysosomes for degradation. It is a complex process, involving more than 16 proteins, that also acts to promote cell survival during starvation and other stresses [307].

Key protein	Role in Autophagy
LC3-I (Microtubule-associated protein 1A/1B light chain 3B)	LC3 forms stable association with membrane of autophagosomes. LC3-I found in cytoplasm
LC3-II (LC3- phosphatidylethanolamine conjugate)	Membrane-bound and is converted from LC3-I, to initiate formation and lengthening of autophagosome. Differs from LC3-1 in that it is covalently modified with lipid extensions and has undergone removal of a short amino acid.
Beclin1	Promotes autophagosome formation

Table 14. Key proteins involved in autophagy [307], [308]

Autophagic cell death is also known as type II programmed cell death and a major intracellular degradation and recycling system- cellular components are enwrapped within double-membranes autophagosomes and delivered to lysosomes for degradation [309]. The autophagic response is characterised by two fluxes: the first being a survival response in an attempt to remove dead unwanted protein, and the second is a pro-death response. When there is increased autophagy beyond a threshold point, cells undergo autophagic death. If the autophagic response is inadequate, then cells undergo senescence [255].

The role of autophagy in lung cancer are currently limited with contradicting results. It is known to exhibit a pro-survival response, in an attempt to remove dead unwanted proteins, followed by a pro-death response that ensues when the autophagic response increases beyond a threshold. Studies support both positive correlations with radiosensitivity, whereby increased autophagy, via mammalian target of rapamycin (mTOR) inhibitors, radiosensitize A549 cells due to delayed DNA damage repair and downregulation of RAD51 and Ku80 expression [310], [311]; and negative correlation, whereby p53 upregulation, mediated by reduced autophagy increases radiosensitivity [312].

Methods of analysing autophagy

Autophagic activity can be assessed by Western blotting of key related proteins such as microtubule-associated proteins 1A/1B light chain 3B (LC3-1) and LC3-phosphatidylethanolamine conjugate (LC3-II) - the conversion of intracytoplasmic soluble LC3-I to lipid-bound LC3-II, indicates autophagosome formation [311], [313].

Quantification of autophagy can be done via transient transfection with green fluorescent protein (GFP)-LC3 plasmid whereby autophagic cells show increased punctuate pattern of LC3 fluorescence in immunofluorescence positive cells [313]; or using green detection reagents that fluoresce when incorporated into pre-autophagosomes, autophagosomes and autolysosomes [314].

5.3 Materials and Method

5.3.1 Cell culture

Four human non-small cell lung cancer cell lines obtained from The Francis Crick Institute, UK (A549 [ATCC CCL-185], H2122 [ATCC CRL-5985], H1975 [ATCC CRL-5908] and H1792 [ATCC CRL-5895]) (table 15) were cultured in RPMI media supplemented with 10 % FBS and 100 units/ml penicillin and 100 ug/ml streptomycin (all from Gibco, USA) and maintained in a 5 % CO_2/ 95 % air atmosphere humidified incubator at 37°C. Cells were grown as monolayers in 75 cm^2 flasks maintained in exponential growth.

Cell Line	Derivation	P53 status	Kras status	Other mutations	MSI/MSS
A549	Carcinoma-primary	WT	Mut Gene sequence: substitution missense p.Gly12Ser Zygosity: Homozygous		MSS
H1975	Adenocarcinoma- primary	Mut Gene sequence: c.818G>A Protein sequence: p.R273H (GAIN FUNCTION) substitution - Missense Zygosity: Homozygous	WT	EGFR Gene sequence: c.2369C>T Protein sequence: p.T790M Heterozygous EGFR Gene sequence: c.2573T>G Protein sequence: p.L858R Heterozygous	MSS
H1792	Adenocarninoma-metastases pleural effusion	Mut Intron Gene sequence: c.672+1G>A Protein sequence: p.? Zygosity: Homozygous	Mut Gene sequence: c.34G>T Protein sequence: p.G12C substitution - Missense Zygosity: Homozygous		MSS
H2122	Adencarcinoma- pleural effusion	Mut Gene sequence: c.47A>T amino acid mutation: p.Q16L Substitution - Missense, position 16, Q➞L) gene mutation: c.527G>T amino acid mutation: p.c176F Zygosity: Heterozygous (substitution missense for both)	Mut Gene sequence: c.34G>T amino acid mutation: p.G12C Substitution - Missense Zygosity: Homozygous		MSS

Table 15. Human non-small cell lung cancer cell lines studied.

5.3.2 Irradiation

5.3.2.1 X-ray irradiation

All cells were seeded a day prior to irradiation. Cells were irradiated at room temperature with single doses of 2-15 Gy per fraction and analysed 24-144 hours after irradiation.

Photon irradiation was delivered by a Small Animal Radiation Research Platform (Xstrahl, USA) at a dose rate of 2.83 Gy/min (220 kVp, 13 mA, filtered with 0.15 mm Cu) at a source-to-surface distance of 35 cm, with 1.25 cm backscatter. Quality assurance checks on output and targeting were performed every two months. Dosimetry was measured using a PTW 30012 Farmer ionisation chamber, and a UNIDOSE electrometer (both from PTW- UK Ltd.), corrected and calibrated to the National Physical Laboratory (Teddington, UK) primary X-ray reference standard. Reference conditions: open field; source to surface distance (SSD), 33 cm; phantom thickness, 5.5 cm; detector's geometric centre at 2 cm depth, 35 cm; and half-value layer, 0.658 mm Cu.

5.3.2.2 Proton irradiation

Cell death assays were first optimised for XRT irradiation. The dominant death mechanisms and their peak time points were identified and comparative proton irradiation experiments carried out under these conditions.

All cells were seeded a day prior to irradiation. Cells were irradiated at room temperature and analysed at optimal time points after irradiation. A horizontal, passively scattered beam line of 60 MeV maximal energy from the Douglas Cyclotron at Clatterbridge was used for proton irradiation of cells, as previously described [315]. Low LET (high energy) PBT was delivered by a 1 keV/um pristine beam, of 59 MeV effective energy (dose rate of approximately 10 Gy/min). High LET (low energy) proton irradiation was achieved using a modulator to generate a 27 mm spread-out Bragg peak (SOBP) and a 24.4 mm Perspex absorber to position the cells at the distal edge of the SOBP, corresponding to a mean energy of 11 MeV at a dose-averaged LET of 12 keV/µm.

The dosimetry of the proton beam was performed at the beginning of each irradiation session. The collimator was made of a 43 mm diameter annulus which was inserted into the brass nozzle. Measurements were performed with a flat ion chamber (PTW Classic Markus) placed at the isocentre situated on the beam axis, 70 mm from the collimator. The proton calibration factor (in Gy/nC) was previously obtained using the IAEA TRS-398 Code of Practice and a local secondary standard chamber traceable to the National Physical Laboratory. Prior to

irradiations, the beam area homogeneity was checked by X-Y scanning with compact diode, and making corrections with the final steering magnets, as required.

All cell plating needed to be in 35 mm dishes or 96 well plates in order to fit specially tailored mounting slides required for irradiation by the horizontal beam.

5.3.3 Cell survival

Colony- forming assays were performed as described in Franken et al [316]. Briefly, for X-ray irradiation, 1500 exponentially growing cells were plated in 10 cm petri dishes and irradiated with increasing doses of 0, 2, 4 and 6 Gy (RBE) X-rays. Cells were cultured until colonies were visible. The surviving fraction was determined by dividing the number of colonies following irradiation by the number of non- irradiated colonies grown.

For PBT irradiation, up to 1500 exponentially growing cells were plated in 35 mm dishes and subjected to the same conditions and analysed as described above.

5.3.4 Apoptosis analysis

Cells were seeded at a density of 5x 10^5 cells per 6cm petri dish and mock irradiated or irradiated with a single doses of 5 Gy and 10 Gy XRT. At 24 hours, 48 hours and 72 hours after irradiation, cells were harvested and the Alexa Fluor® 488 Annexin V/Dead Cell Apoptosis Kit (ThermoFisher) was used to detect apoptotic cells in accordance with the manufacturer's instructions.

Briefly, cells were washed with cold PBS, resuspended in 100 µl of 1X binding buffer and incubated with 5 µL AlexaFluor 488 annexin V and 1 µL 100 µg/mL PI working solution for 15 minutes at room temperature in the dark. Immediately after, binding buffer (1X, 400 µl) was added to each sample tube and the sample analysed by flow cytometry using the BD Fortessa X20B flow cytometer.

Cells that stain positive for fluorescein (FITC) Annexin V and negative for PI are undergoing apoptosis. Percentage of apoptotic cells were quantified using FlowJo version 10 software. Three sets of independent experiments were performed.

5.3.5 Senescence analysis

5.3.5.1 Senescence- associated β galactosidase staining

Cells were seeded not to exceed 50 % confluency in 24 well plates and mock irradiated or irradiated with a single doses of 5 Gy (RBE) and 10 Gy (RBE) of X-rays. At 72 hours and 144 hours after irradiation, cells were stained with senescence β-Galactosidase staining kit (#9860 Cell Signaling) following the standard protocol outlined by manufacturer. Briefly, cells were PBS-washed, fixed in paraformaldehyde, and stained overnight incubated at 37 °C, wrapped in parafilm to minimise CO_2 exposure.

Senescent cells were identified as those with blue cytoplasmic staining and counted as a percentage of at least 100 cells from randomly sampled fields under a light microscope at x20 magnification. The results are shown as the average percentages from 3 independent experiments.

For proton irradiation, cell-seeding was adapted to a 96-well plate formation, subjected to the same conditions and analysed as described above.

5.3.5.2 Western blotting

Cells were seeded at a density of $5x10^5$ cells per 35 mm culture dish plate and mock irradiated or irradiated with single doses of 10 Gy (RBE) of X-rays or protons. Cells were collected and lysed with RIPA lysis buffer at 4 hours, 24 hours and 96 hours. Samples were centrifuged and total protein concentrations determined from supernatants using the BCA protein assay kit (#500-0206 Bio-Rad). Thereafter, samples were separated by denaturing gel electrophoresis on NuPAGE Novex 4-12 % Bis-Tris gels (Invitrogen, UK), and analysed by quantitative Western blotting using the Odyssey image analysis system (Li-cor Biosiences, Cambridge, UK). The antibodies employed in this study were mouse anti-p53 (ab1101, Abcam), rabbit anti-p21 (ab109520, Abcam), rabbit anti-p16 (ab108349, Abcam), rabbit anti-phospho-Rb (D59B7, Cell Signaling), mouse anti-RB (554136, Becton Dickinson), rabbit p14ARF (A300-340A-2, Bethyl laboratories) and rabbit anti-beta-tubulin (ab108342, Abcam). Primary antibody incubation was conducted overnight at 4 °C.

Further primary antibodies used to analyse related pathways were anti-phospho-STING (Ser366) (D7C3S, Cell Signaling), anti-LKB1 (ab 15095 abcam), and anti-GATA4 antibody (ab84593 abcam).

Secondary antibodies conjugated with Alexa Fluor 680/800 (Invitrogen, UK) were incubated for 1 hour at room temperature.

5.3.6 Necrosis analysis

Cells were seeded at a density of 10,000 cells per well on 12 well plates and mock irradiated or irradiated with single doses of 5 Gy, 10 Gy and 15 Gy of XRT. At 24 hours, 72 hours and 144 hours after irradiation, cells were dual stained with 4 µg/mL propidium iodide (PI) and 1 µg/mL Hoechst.

Cells undergoing necrosis were identified as those with high PI and counted as a percentage of at least 100 cells from randomly sampled fields under an Evos FL Auto confocal microscope using DAPI and RFP filters at x20 magnification. The results are shown as the average percentages from 3 independent experiments.

5.3.7 Mitotic catastrophe analysis

Cells were seeded at a density of 5000 cells per well in a 24 well plate and mock irradiated or irradiated with single doses of 2 Gy (RBE), 5 Gy (RBE) and 10 Gy (RBE) of X-rays or protons. At 48 hours, 72 hours and 96 hours after irradiation, cells were fixed with methanol/acetone for 15 minutes at 4°C. Cells were then washed with PBS twice, stained with 4', 6-diamidino-2-phenylindole (DAPI) for 15 minutes at room temperature and washed again with PBS twice.

Cells with multinucleated enlarged nuclei, micronuclei and multilobulated nuclei were considered to be in mitotic catastrophe [256], [317]. Cells in MC were counted as a percentage of at least 100 cells from randomly sampled fields under a Zeiss Z1 Inverted confocal microscope at x20 magnification. The results are shown as the average percentages from 3 independent experiments.

For proton irradiation, cell were seeded in 96 well plates at a density of 3000 cells per well, subjected to the same conditions and analysed as described above.

5.3.8 Necroptosis analysis

Cells were seeded at a density of 5x10e5 cells per 6 cm culture dish and mock-irradiated, irradiated with 10 Gy XRT or treated with cisplatin 10 µM (as a positive drug control). Protein extraction from cells and western blotting were done as described earlier at 4 hours, 24 hours, 48 hours and 72 hours following treatment. The antibodies employed in this study were rabbit anti-mixed lineage kinase domain-like (MLKL) (ab187091, Abcam), rabbit anti-receptor-interacting protein kinase 3 (RIP3) (ab209384, Abcam), rabbit-anti pro-caspase 8 (ab32397, Abcam) and mouse anti-GAPDH (ab8245, Abcam). Primary antibody incubation was conducted overnight at 4 °C. Secondary antibodies conjugated with Alexa Fluor 680/800 (Invitrogen, UK) were incubated for 1 hour at room temperature.

5.3.9 Autophagy analysis

Cells were seeded at a density of 3000 cells per well in a 96 well plate and mock irradiated or irradiated with a single dose of 5 Gy (RBE) and 10 Gy (RBE) of X-rays or protons. At 72 hours and 96 hours after irradiation, cells were stained with green detection reagent (autophagy detection kit (ab139484, Abcam) following the standard protocol outlined by manufacturer. Cells with multiple (more than 2) green vacuoles around nucleus and staining in the cytoplasm, indicating incorporation of green detection reagent into pre-autophagosomes, autophagosomes and autolysosomes, were considered to be undergoing autophagy. Autophagic cells were counted as a percentage of at least 100 cells from randomly sampled fields under an Evos FL Auto confocal microscope using DAPI and GFP filters at x20 magnification. The results are shown as the average percentages from 3 independent experiments.

5.3.10 Micronuclei assay

When DNA damage occurs fragments can get separated from the nucleus due to mis-segregation of DNA during cell division. The result is the formation of chromatin surrounded by their own nuclear envelope or cytosolic DNA, also known as micronuclei. This triggers rapid accumulation of cGAS which can penetrate these micronuclei and bind to DNA, activating the cGAS-STING pathyway that initiates inflammation.

5.3.11 Immunofluorescence staining of DNA damage response foci

Cells were grown on coverslips in 35 mm dishes overnight and mock irradiated or irradiated with 5 Gy (RBE) of photons or protons. At 0.5 hours, 4 hours and 24 hours after irradiation cells were washed with PBS, fixed in methanol-acetone for 10 minutes in 4 °C and washed twice with PBS.

Cells were incubated with primary antibodies mouse anti-γH2AX (JBW301, EMD Millipore Corp), rabbit anti-53BP1 (A300-272A, Bethyl) and rabbit anti-Rad51 (ab133534, Abcam) overnight at 4 ºC. Secondary antibodies conjugated with Alexa Fluor 680/800 (Invitrogen, UK) were incubated for 1 hour at room temperature. Cells were then washed 3 times with PBS before being mounted in DAPI. Images were obtained using a Zeiss Z1 Inverted confocal microscope at x40 magnification.

A mean number of foci per cell was determined by analysing 25 cells in randomly sampled fields from 3 independent experiments using ImageJ.

5.3.12 Statistical Analysis

All experiments were repeated at least 3 times and the values shown on graphs represent the means +/- SD. The statistics software programme Prism version 7.0a was used to perform two- way ANOVA, Tukey's multiple comparisons tests, to compare percentages of cells undergoing MC, autophagy or senescence following XRT, low LET and high LET PBT.

A value of $p<0.05$ was considered statistically significant.

5.4 Results

5.4.1 XRT predominantly induces mitotic catastrophe, autophagy and senescence

The major cell death pathways induced by XRT in the NSCLC cell lines studied were MC, senescence and autophagy (fig 14. D). Percentage cell death by these modes of death increased with increasing IR dose. Relatively low levels of apoptosis and necrosis were observed following XRT (fig 13. B, C). Peak apoptosis was seen at 72 hours and necrosis at 144 hours (fig 13. Di, ii). No necroptosis was demonstrated due to low expression of *RIP3*, which is needed to phosphorylate MLKL, a critical step in necroptosis. A549 cells transfected with *RIP3* subjected to the same treatment did express phosphorylated MLKL, confirming that RIP3-deficiency confers resistance to necroptosis [298] (fig 13. E).

Clonogenic survival assays following XRT identified A549 and H2122 as the most radioresistant and radiosensitive cell lines, respectively (fig 13. A). Examining differences in modes of death in these two cell lines, we found that H2122, showed higher levels of autophagy and senescence, whereas A549 showed higher levels of MC (fig 14. D). Percentage autophagy in H2122 cells compared to A549 at its peak of 96 hrs following 10 Gy was 54.0 % versus 33.0 % ($p<0.01$) (fig 14. B, E ii); and percentage senescence at its peak following 10 Gy at 144 hours was 38.0 % versus 19.2 % ($p<0.01$) (fig 14. C, E iii). Percentage MC in A549 cells compared to H2122 at its peak was 47.4 % versus 32.3 % ($p< 0.05$) (fig 14. A, E i).

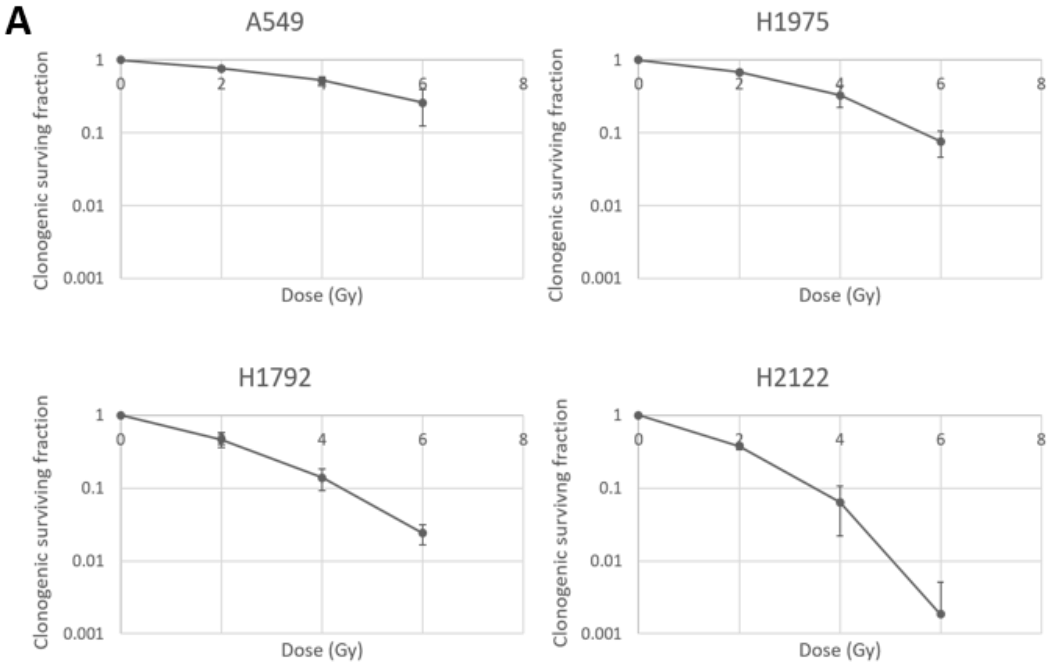

Fig 13. A. Clonogenic survival following increasing doses of XRT.

B

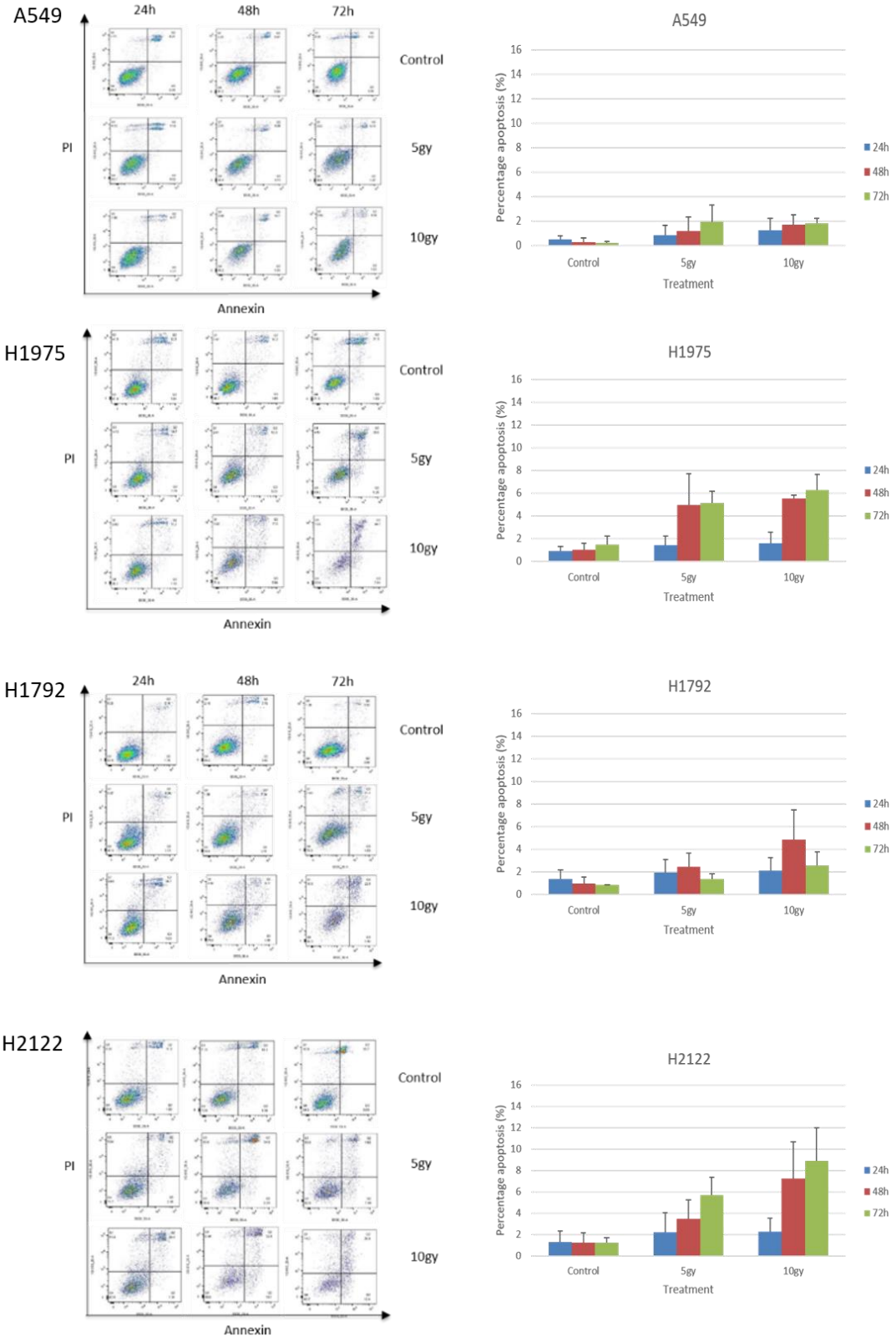

Fig 13. B. Quantification of cells undergoing apoptosis following XRT irradiation.

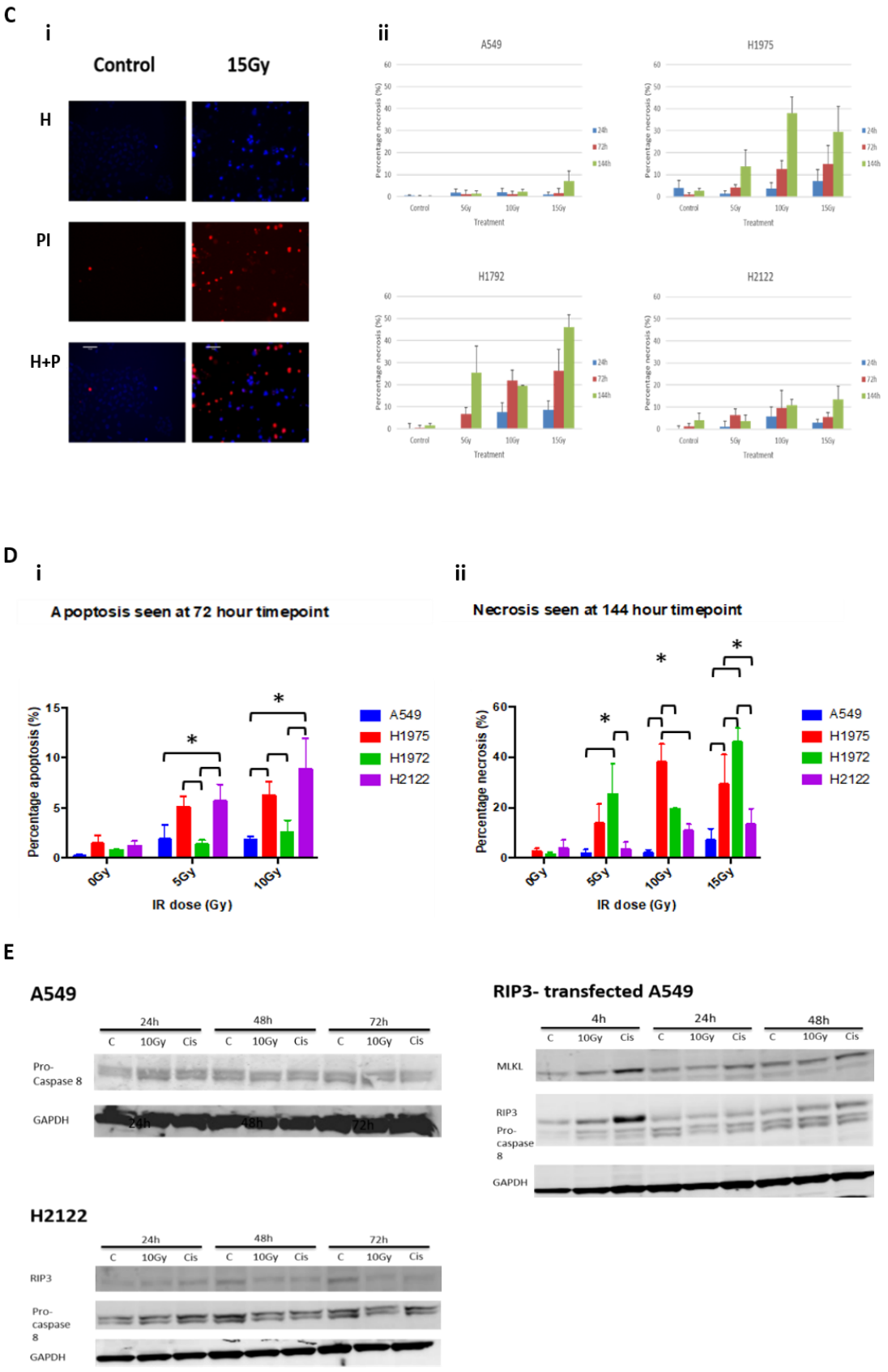

Fig 13. C. (i) Hoescht/ PI staining of H1792 cells 72 h following 0 Gy and 15 Gy XRT. (H) Hoescht staining. (PI) Propidium iodide. (H+P) Combined staining. (ii) Quantification of cells undergoing necrosis following XRT irradiation. **D.** Comparative quantification of cells undergoing (i) apoptosis following XRT irradiation at peak time point of 72 h (ii) necrosis following XRT irradiation at peak time point of 144 h. *Indicates a significant difference of $p<0.05$. **E.** Western

blot of A549, H2122 and RIP3- transfected A549 cells treated with 10 Gy XRT and 10uM cisplatin. No RIP3 expressed in A549 and very low RIP3 expression in H2122 making them necroptosis- resistant. RIP3- transfected A549 cells show increased RIP3 and phosphorylated MLKL following irradiation and cisplatin indicative of necroptosis. The RIP3-transfected A549 cell line was obtained from a partner laboratory.

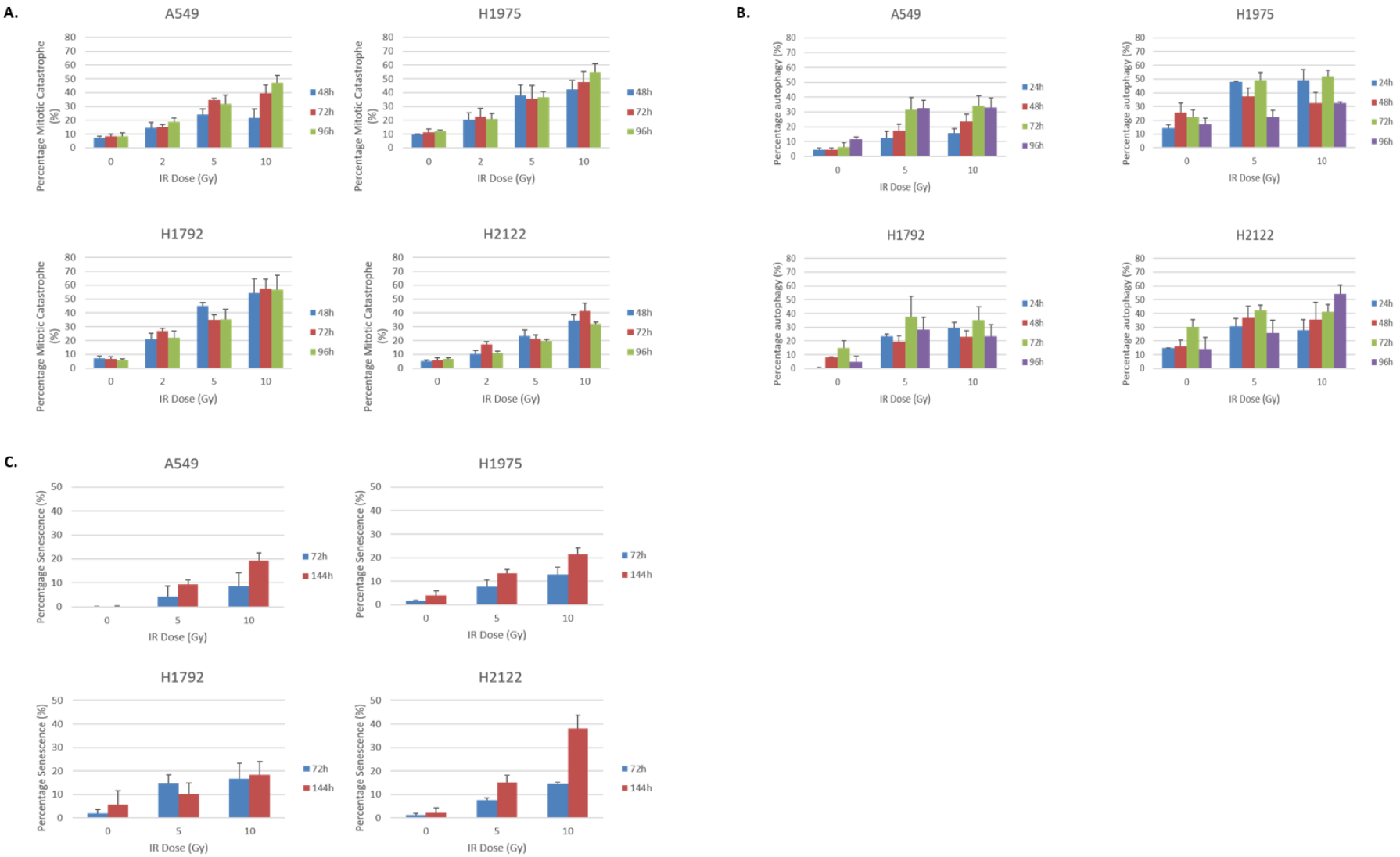

Fig 14. A. Quantification of cells undergoing mitotic catastrophe following XRT irradiation. **B.** Quantification of cells undergoing autophagy following XRT irradiation. **C**. Quantification of cells undergoing senescence following XRT irradiation.

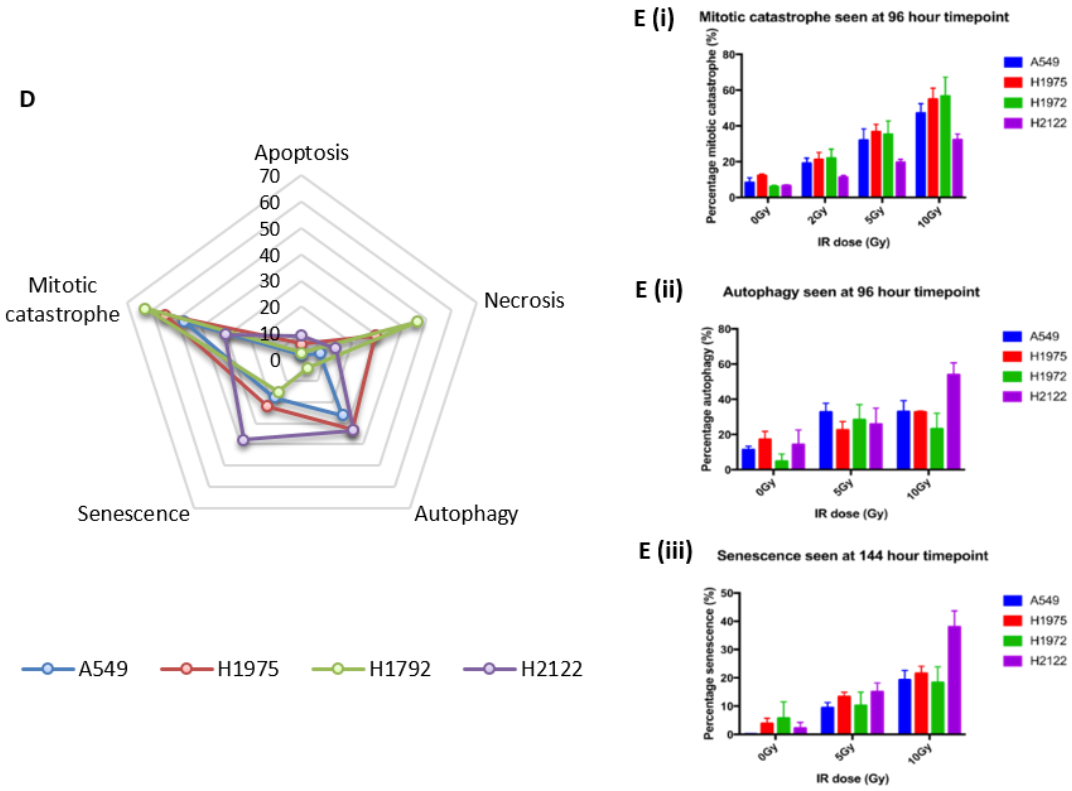

Fig 14. D. Comparative cell death pathways induced by XRT in A549, H1975, H1792 and H2122 cell lines at peak time points (Apoptosis: at 72h following 10 Gy; necrosis: at 144 h following 15 Gy; Autophagy: at 96 h following 10 Gy; Senescence: at 144 h following 10 Gy; Mitotic catastrophe: at 96 h following 10 Gy). **E.** In the cell lines studied, XRT-induced cell death was predominantly via MC (observed maximally at 96 h), autophagy (observed maximally at 96 h) and senescence (observed maximally at 144 h). **(i).** Comparative quantification of cells undergoing mitotic catastrophe following XRT irradiation at peak time point of 96 h. **(ii).** Comparative quantification of cells undergoing autophagy following XRT irradiation at peak time point of 96 h. **(iii)**. Comparative quantification of cells undergoing senescence following XRT irradiation at peak time point of 144 h. Compared to the radioresistant cell line A549, the radiosensitive H2122, showed higher levels of autophagy, statistically significant at 96 h following 10 Gy (54.0% versus 33.0% ($p<0.01$); and senescence following 10 Gy at 144 h (38.0% versus 19.2% ($p<0.01$). A549 cells showed a higher percentage of MC compared to H2122 following 10 Gy at 96 h (47.2% V 32.3%, $p<0.01$).

Having identified the major XRT-induced cell death mechanisms, we assessed these pathways following proton irradiation of the radioresistant A549 cell line so that responses could be compared to the radiosensitive H2122 cell line.

5.4.2 High LET proton irradiation more effectively induces senescence compared to low LET proton and X-ray irradiation

Clonogenic survival assays showed a trend toward proton irradiation inhibiting colony formation more effectively than XRT in both cell lines, with high LET PBT resulting in the greatest reduction in survival fraction (fig. 15. A). Senescence was the major cell death pathway responsible for this for both cell lines. High LET PBT caused significantly more senescence compared to low LET PBT and XRT and this increase was most significant at 144 hours and greater at 10 Gy (RBE) than 5 Gy (RBE) (fig 15. B i). In A549, the percentage of senescent cells following 10 Gy (RBE) high LET PBT compared to XRT at 144 hours, was 38.5 % versus 19.2 % ($p<0.01$) (fig 15. B ii). In H2122, the percentage senescent cells was significantly increased following 5 Gy (RBE) and 10 Gy (RBE) at 72 hours and 144 hours. Percentage senescence at 144 hours following 5 Gy (RBE) high LET PBT compared to XRT was 29.3 % versus 15.1 % ($p<0.01$); and 56.5 % versus 38.0 % ($p<0.01$) after 10 Gy (RBE) (fig 16. B).

On the other hand, similar levels of MC was induced following PBT compared to XRT in H2122 cells (fig 15. C iii- iv). In A549 cells, less MC was shown following 5 Gy (RBE) PBT compared to XRT but was only statistically significant at 96 hours following low LET PBT (9.4 % versus 32.1 %, $p<0.01$) (fig 15. C i- ii).

Interestingly, IR-induced autophagy observed at 72 hours following 5 Gy (RBE) was higher in both cell lines for XRT compared to PBT (fig 15. D i and iii). By 96 hours, 5 Gy (RBE) high LET showed a higher percentage of autophagy, although not statistically significant, compared to XRT (fig 15. D ii and iv). These results suggest the autophagic response following 5 Gy (RBE) high LET PBT may be delayed compared to XRT. Following 10 Gy (RBE) there was no statistically significant difference following XRT or PBT except in H2122 cells where high LET irradiation was associated with a relatively dramatic reduction in autophagic response compared to XRT (32.0 % V 54.0 %, $p<0.01$).

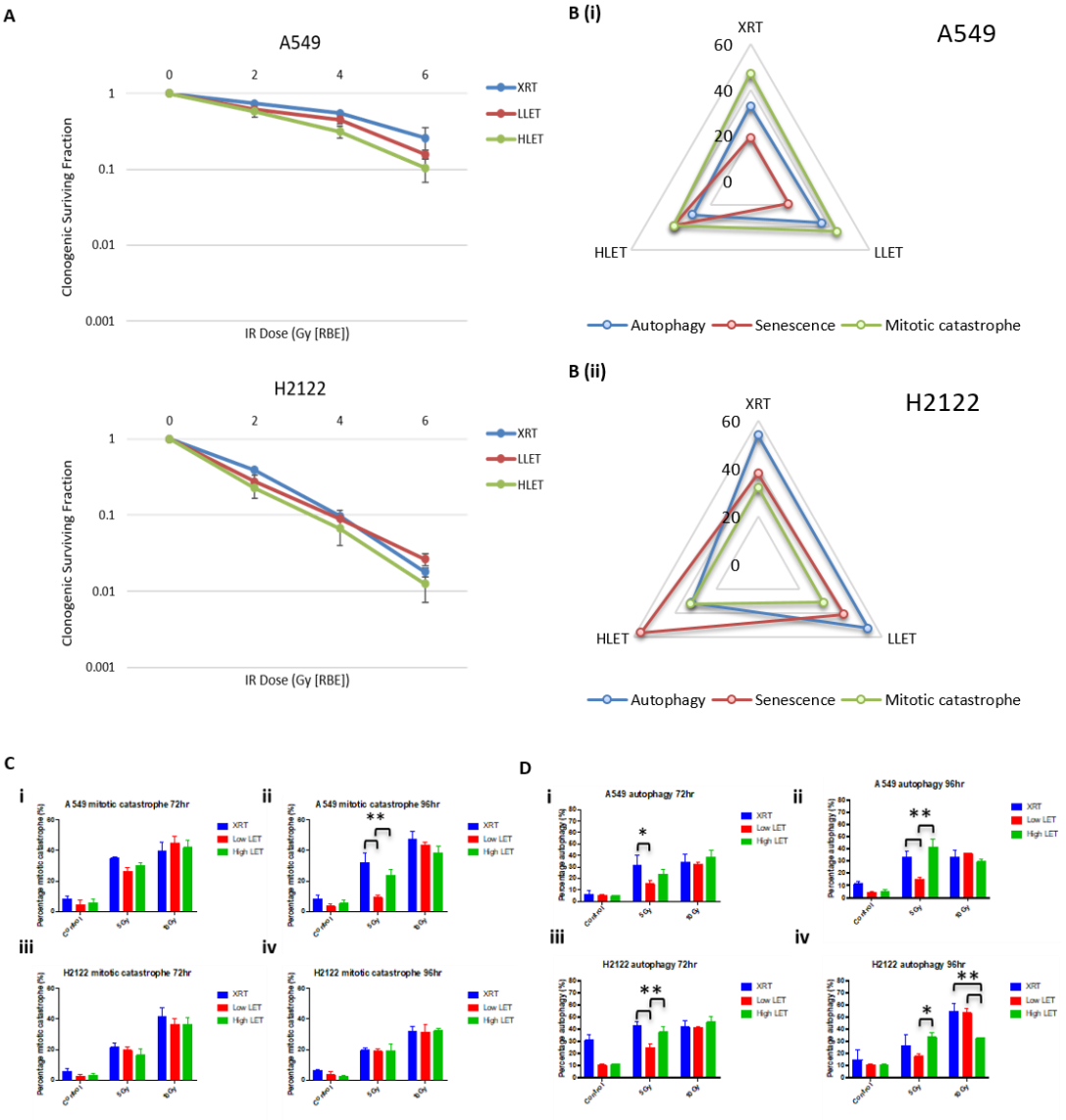

Fig 15. Increased radiosensitivity of non- small cell lung cancer cell lines to PBT compared to XRT irradiation is not due to differences in mitotic catastrophe or autophagy. A. Clonogenic survival following increasing doses of high (HLET) and low LET (LLET) PBT compared to XRT for A549 and H2122. At least 3 sets of independent colony-forming assays were performed and error bars represent standard error. The dose following XRT, LLET PBT and HLET PBT irradiation required for 10% and 20% survival was interpolated and a one-way ANOVA, Dunnett's multiple comparisons statistical test for significance following those doses for A549 and H2122 was conducted. A trend towards increased lethality following HLET compared to LLET and XRT was seen but no statistically significant difference was demonstrated. Only the dose required for 20% survival in A549 cells was statistically significant following HLET compared to XRT ($p<0.05$) (but not LLET compared to XRT). **B.** Comparative cell death pathways induced by XRT, LLET protons and HLET protons in (i) A549 and (ii) H2122 cell lines at peak time points (Autophagy: at 96 h following 10 Gy (RBE); Senescence: at 144 h following 10 Gy (RBE); Mitotic catastrophe: at 96 h following 10 Gy (RBE)).**C.** Quantification of cells undergoing mitotic catastrophe following irradiation: A549 cells at **(i)** 72h and **(ii)** 96 h; and in H2122 cells at **(iii)** 72 h and **(iv)** 96 h. **D.** Quantification of cells undergoing autophagy following irradiation: A549 cells at **(i)** 72 h and **(ii)** 96 h; and in H2122 cells at **(iii)** 72 h and **(iv)** 96 h. ***Indicates a significant difference of $p<0.05$. **indicates a significant difference of $p< 0.01$.

Our results suggest that senescence is the major pathway responsible for the increased lethality of high LET proton irradiation.

5.4.3 Senescence is mainly established through p53/p21 pathway

We investigated the contribution of senescence-associated cell-cycle proteins to the observed increase in senescence following PBT. We demonstrated up-regulation of p53 and p21 that persisted at high levels for longer after proton irradiation (fig 16. C). Although RB and pRB (phosphorylated RB) protein levels were down-regulated, $p16^{INK4a}$ protein levels were hardly detectable in cells, regardless of treatment.

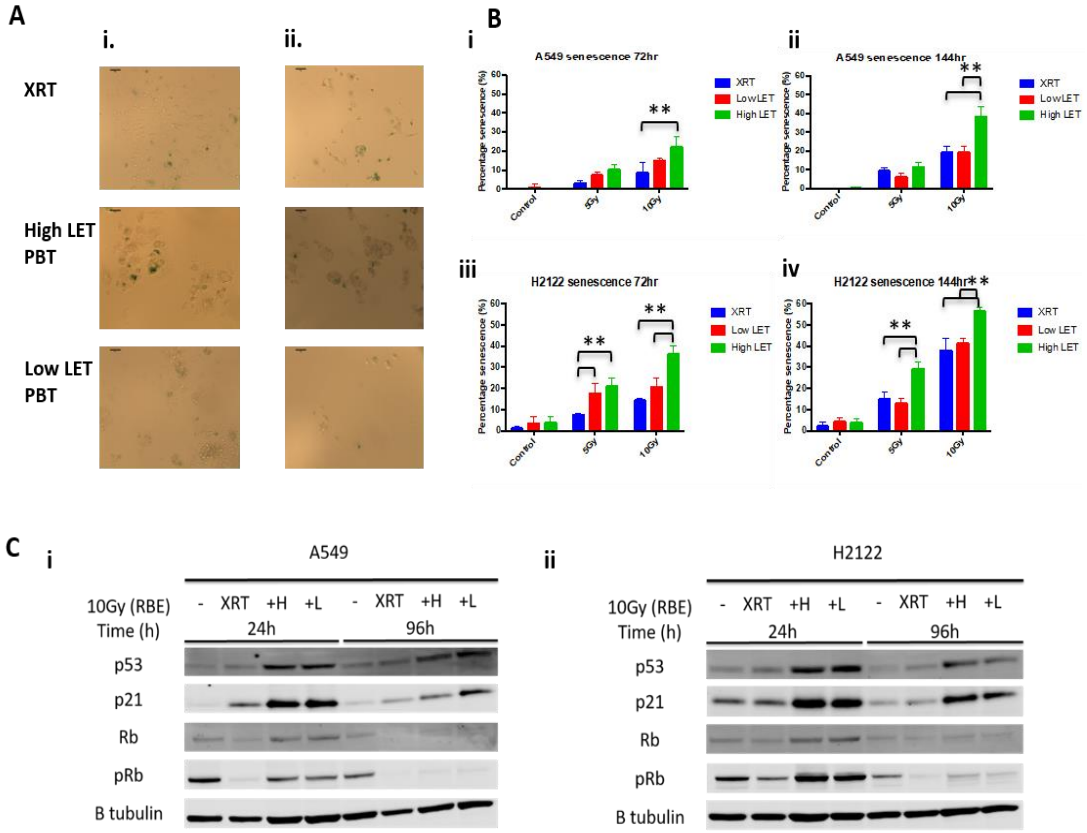

Fig 16. Senescence is the major cell death pathway by which PBT more effectively inhibits clonogenic survival compared to XRT in NSCLC cell lines. **A.** SA- β- Gal staining of H2122 cells 6 days following irradiation with **(i)** 5 Gy (RBE) and **(ii)** 10 Gy (RBE). **B.** Quantification of mean number of SA- β- Gal positive cells in A549 cells following irradiation at **(i)** 72 h and **(ii)** 144 h; and in H2122 cells at **(iii)** 72 h and **(iv)** 144 h. Both cell lines show increased senescence following 10 Gy (RBE) HLET compared to XRT (**p< 0.01). Peak response at 144 h following 10 Gy (RBE). **C.** Western blot showing senescence induction following 10 Gy (RBE) **(i)** Western blot of irradiated A549 cells and; **(ii)** Western blot of irradiated H2122 cells at 24 h and 96 h. (+H) denotes high LET irradiation. (+L) denotes low LET irradiation. (-) denotes mock- irradiated cells. No p16 or p14 expression was seen on the blots, regardless of treatment.

Our results suggest that radiation- induced cellular senescence in A549 and H2122 is mainly established through the p53/p21 pathway.

5.4.4 Difference in radiation- induced cellular senescence is not related to differential repair machineries

We used DNA double strand break (DSB) marker, γ-H2AX foci, and DSB repair markers 53BP1 and RAD51 (fig 17. A) to investigate if proton irradiation influenced differential induction of the 2 major DSB repair machineries- non-homologous end joining (NHEJ) and homologous repair (HR); and if the increased senescence was related to persistent DSB.

In A549 cells, rapid induction of the DNA damage response (DDR) machineries was observed, following both XRT and PBT, with the peak in mean number of foci per cell seen at 0.5 hours (fig 17. B). In H2122 cells, the peak in mean ϒH2AX and RAD51 foci/cell occurred later at 4 hours following XRT. PBT irradiation was associated with faster DNA repair foci induction, peaking at 0.5 hours (fig 17. C). No clear differential DDR machinery induction was observed between XRT and high or low LET PBT in either cell line.

Mean foci levels that had not returned to untreated levels at 24 hours were considered to be indicative of persistent DNA damage. Following XRT, both A549 and H2122 cells showed persistently raised RAD51 ($p<0.05$) and 53BP1 ($p<0.01$) foci at 24 hours. After high LET PBT, only H2122 cells demonstrated a statistically significant increased mean number of RAD51 foci ($p<0.01$) 24 hours after irradiation; whilst all foci reached untreated levels by 24 hours in A549 cells (fig. 17 B, C. This suggests more persistent DNA damage and delayed HR repair kinetics following high LET PBT in H2122 cells compared to A549.

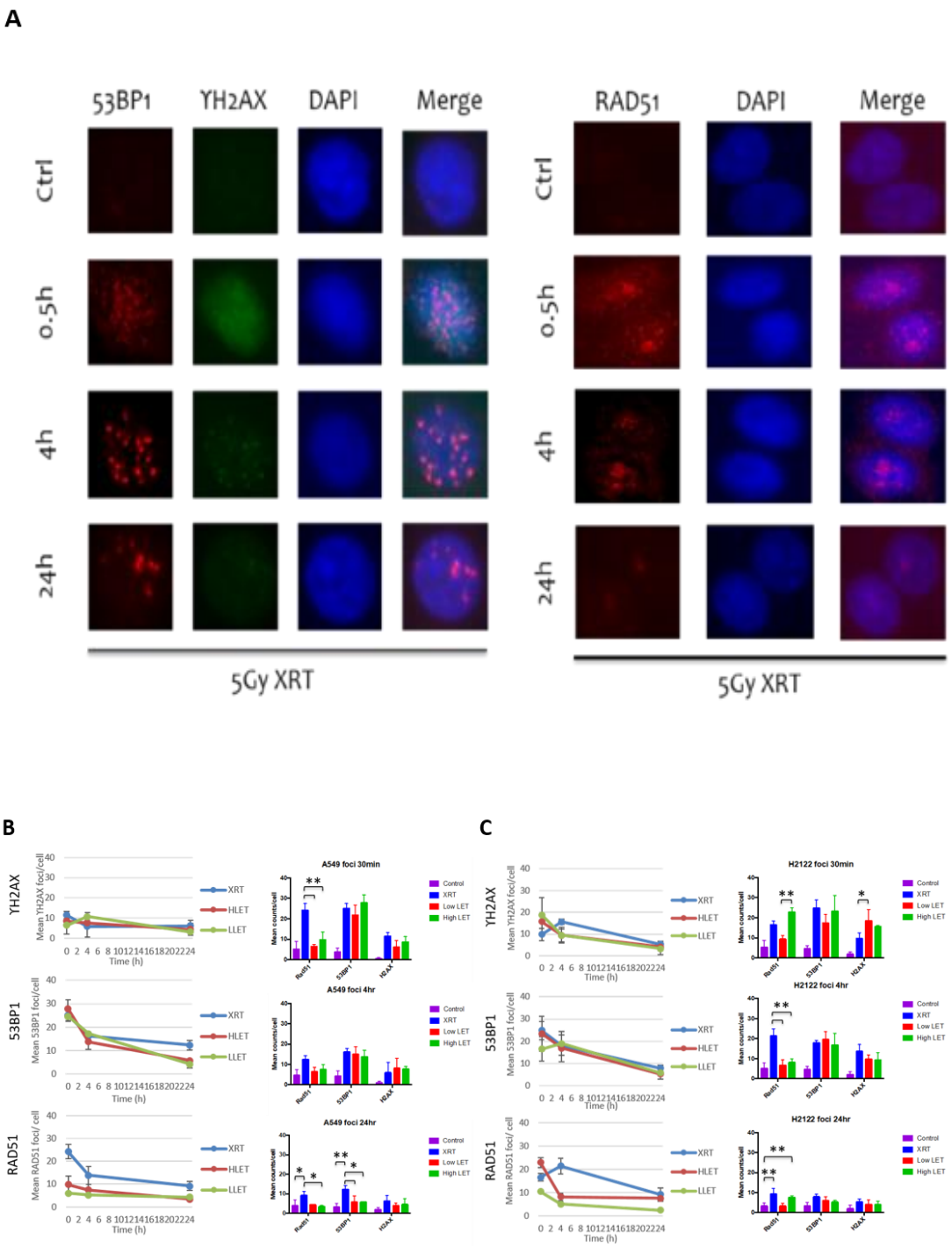

Fig 17. Difference in radiation- induced cellular senescence is not related to activation of differential repair machineries. A. Representative micrographs of YH2AX, 53BP1 and RAD51 foci in A549 cells exposed to 5 Gy XRT at indicated time points. **B.** Average number of DNA foci per cell in A549 cells following 5 Gy (RBE) XRT and high LET (HLET) and low LET (LLET) proton irradiation at 0.5 h, 4 h and 24 h**. *** Indicates a significant difference of p<0.05. ** indicates a significant difference of p< 0.01. **C.** Average number of DNA foci per cells in H2122 cells following 5 Gy (RBE) at 0.5 h, 4 h and 24 h.

5.4.5 Difference in radiation- induced cellular senescence is not related to differences in micronuclei formation or activation of STING pathway

We investigated if the LET-associated increase in senescence was related to increased MN formation and activation of the cGAS-STING pathway following high LET PBT compared to low LET PBT or XRT. Whilst HLET PBT showed a trend towards an increase in MN formation, this was not statistically significant.

No STING expression was observed in A549 cells, regardless of treatment. Increased STING expression was demonstrated in H2122 cells following PBT compared to XRT. High LET PBT resulted in an early (24 h) and sustained increased expression of STING. Low LET PBT was observed to cause a late (96 h) increased expression of STING (fig 18). However, there was no associated changes in LKB1 expression detectable in either cell lines with or without treatment, suggesting LKB1-independent activation of the STING pathway.

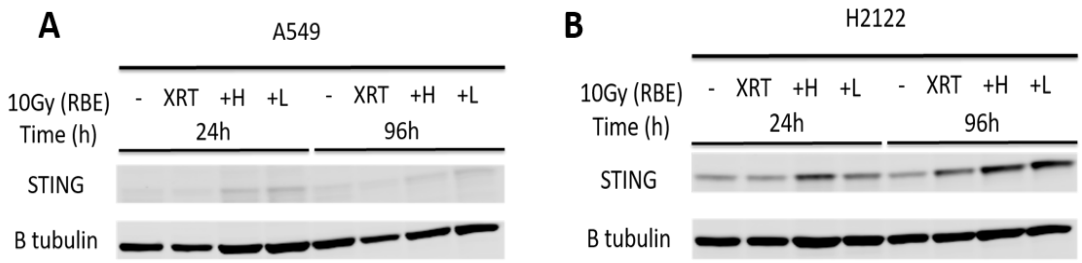

Fig 18. Western blot showing changes in STING expression following 10 Gy (RBE) irradiation of (A) A549 cells and (B) H2122 cells at 24 h and 96 h. (+H) denotes high LET proton irradiation. (+L) denotes low LET proton irradiation. (-) denotes mock- irradiated cells. No STING expression was seen in A549 cells with or without irradiation treatment. LKB1 expression was undetectable in both cell lines regardless of treatment.

5.4.6 Difference in radiation- induced cellular senescence is not related to changes in GATA4 expression

We investigated if a change in GATA4 expression, a key switch linking senescence and autophagy, following XRT compared to high and low LET PBT might contribute to the increase in senescence following high LET PBT. No GATA4 expression was found in either A549 or H2122 cells, regardless of treatment.

5.5 Discussion

Key findings from this study are that MC, autophagy and senescence are the dominant cell death mechanisms induced by XRT; and senescence is the major cell death pathway by which PBT more effectively reduces clonogenic potential compared to XRT in NSCLC cell lines grown in vitro. Proton- induced cellular senescence is mainly established through the p53/p21 pathway and is both LET- and dose-dependent but does not appear to be related to differential DNA repair machineries.

Previous in vitro studies have shown MC, apoptosis, senescence and autophagy to be the dominant modes of cell death following low to moderately fractionated XRT (1.8-8 Gy per fraction) and necrosis or necroptosis following hypofractionated XRT (greater than or equal to 10 Gy per fraction) [287], [288], [303], [318]. In the NSCLC cell lines studied, our findings agree that MC, senescence and autophagy are dominant mechanisms but not apoptosis; no necroptosis was observed due to RIP3-deficiency; and we did not observe a clear dose-dependent differentiation of cell death mechanisms. Reasons for these incongruences are likely to be tissue and cell line-specific.

The relatively low percentages of apoptosis seen is not surprising as many cancers have an inherent resistance to apoptosis, reportedly only accounting for up to 20 % of radiation-induced cell death [245]. Instead, senescence was more prominent and is an alternative cell fate to apoptosis, although the ultimate determinants switching from one to the other are unclear. Some studies have shown that the decision is related to cell type-specific regulators [319], [320]; whilst Probin et al demonstrated that busulfan, an agent that produces bulky DNA adducts, causes senescence but not apoptosis irrespective of dose in lung fibroblasts, suggesting it is the nature of DNA damage driving a preference for senescence [321].

Autophagy in lung cancer is not well understood and evidence is conflicting. It is known to exhibit a pro-survival response, in an attempt to remove dead unwanted protein, followed by a pro- death response that ensues when the autophagic response increases beyond a threshold. Studies support both positive correlations with radiosensitivity, whereby increased autophagy, via mammalian target of rapamycin (mTOR) inhibitors, radiosensitizes A549 cells due to delayed DNA damage repair and downregulation of RAD51 and Ku80 expression [310], [311]; and negative correlation, whereby p53 upregulation, mediated by reduced autophagy increases radiosensitivity [312]. Our study showed more autophagy in the radiosensitive H2122 cell line compared the radioresistant A549 following XRT. However, both cell lines showed similar percentages of autophagy following XRT and high LET PBT, despite increased clonogenic death from high LET PBT. The only exception to this was in H2122 cells following

high LET PBT of 10 Gy (RBE) at 96 hours where a significant reduction in autophagy was noted. Associated with this was an increase in senescence, a known consequence of an inadequate autophagic response [255]. These results suggest that autophagic cell death is context- and cell-dependent.

The observed trend of increased lethality of protons compared to XRT has previously been demonstrated [30], [40]. A statistically significant difference was only seen for the dose required for 20 % survival in the A549 cells following HLET compared to XRT; and none was seen in the H2122 cell line. Whilst both cell lines have known genomic instability [322]–[324], clonogenic survival reproducibility in the H2122 cell line was particularly challenging, which may be due to requiring a longer incubation period for cell attachment. We showed that senescence was the principle cause of the increased lethality. Similarly, in their study of head and neck cancer cells, Wang et al [40] showed senescence and also MC to be the major types of cell death induced by 4 Gy (RBE) of both XRT and low LET PBT, but reported PBT was more effective. In contrast to our findings, others have reported high LET PBT to result in earlier and more MC than XRT in V79 Chinese hamster cells [325].

Mitotic catastrophe one of the main avenues of cell death induced by IR [246], [250]–[252]. It is an aberrant form of mitosis following DSB, characterised by the formation of chromatin surrounded by their own nuclear envelope or cytosolic DNA, also known as micronuclei. It is well known that densely ionizing particles more effectively induce micronuclei than XRT [122]. Furthermore, studies have shown that the concentration of cytosolic DNA increases with increasing radiation dose up to approximately 15-18 Gy, beyond which it decreases due to degradation by activated DNA exonuclease Trex1 [122]. So, it is unclear why proton irradiation was not associated with an increase in percentage MC in our study, even following high LET PBT. However, MC can direct defective cells to various anti-proliferative fates, one of which is senescence [292]. Therefore, one possibility is that the peak response following PBT was much earlier than the time at which the cells were analysed for MC. Another reason might be because irradiation was delivered as single fractions, which may be less effective than fractionated treatment at inducing micronuclei formation [6].

We demonstrated that increased stress- induced premature senescence (SIPS) in these NSCLC cell lines was dose and LET-dependent and established through the p53/p21 pathway. Zhang et al reported similar findings following irradiation of human uveal melanoma 92-1 cells, although much higher LET-associated carbon ions (LET 80 keV/µm) and iron ions (LET 400 keV/µm), were used to compare against XRT [38].

Senescence is controlled by p53 and $p16^{INK4a}$ tumour suppressor proteins, and their expression is required to induce the characteristic senescence-associated secretory phenotype (SASP) following irradiation [121], [256], [257]. DNA damage induces expression of p53 via ATM/ATR kinase activation, which subsequently activates transcription of p21. This results in the binding of CDK4 and cyclin E dependant kinase CDK2, inhibiting their kinase activities leading to cell cycle arrest at G1/S [258]. Whilst p21 can also be induced by several p53-independent signalling pathways, it is the p53-dependent activation that is particularly important for senescence after IR-induced DNA damage [259], [260].

The $p14^{ARF}$ of the Ink4a/p16 locus also has an important role in senescence via its reciprocal relationship with p53. It negatively regulates p53 by reducing its transcription and increasing Mdm2- mediated p53 degradation [261]; whilst also being the target of p53-mediated suppression [258], [262], [263]. P16 inhibits cyclin D-dependent kinase CDk4 activity and CDK6[264], [265], which prevents phosphorylation of Rb (as well as suppressing transcription of RB) and subsequent release of transcription factor E2F that is required for G1 to S progression and DNA replication [266]. Evidence suggests that p16 serves as a back-up tumour suppressor to p53 [267].

The expression of $p16^{INK4a}$ is absent in more than 70 % of NSCLCs, due to methylation or homozygous deletion [271], [272]. Studies have shown that SIPS induction in p16 deficient cells are associated with p53/p21 pathway activation and nuclear accumulation of p21; whilst cell lines proficient in p16 and deficient in p53 show nuclear accumulation of p16 [268]–[270]. Unsurprisingly, we found p53/p21 to be the main pathway through which SIPS was established- A549 cells (wild-type p53 and p16 deficient) and H2122 cells (although known to be *TP53*- mutant) both demonstrated p53 and p21 induction that was maintained at high levels but no p16 expression. This also proves that H2122 cell line's Q16L and C176F p53 mutations (considered as neutral and partially deleterious mutations) allows it to retain some p53/p21 pathway functions [326].

5.5.1 Senescence and DNA damage

We investigated the cause of the increased senescence by analysing DSB as the DNA damage response is a critical event triggering senescence. Whilst PT and PBT result in similar initial DNA damage, high LET irradiation has been shown to cause more complex clustered DNA damage which is more difficult to repair, resulting in persistent damage [327], [328]. Reports have suggested that low LET irradiation preferentially induces NHEJ whilst high LET irradiation predominantly induces HR [6], [9], [242], [329].

However, we did not demonstrate predominant DDR machinery induction and no preferential switching following XRT compared to high or low LET PBT. This may be because *KRAS*-mutant cell lines, such as A549 and H2122, are known to be relatively autophagy- impaired and therefore tend to rely mostly on NHEJ, given autophagy is required for HR function [330]. Also, high LET-induced DNA damage studies have mostly used heavy particle therapy, in the form of Fe ions and C ions [38], [242], which have much higher LET than the high LET PBT used here. Additionally, complex cluster DNA lesions can be non-DSB oxidative clustered DNA lesions, which can be a mixture of base modifications and SSB [331], or DSB [31]. Our study focused on analysing DSB but it may be that non-DSB complex clusters were occurring from the high LET protons used and this should be further investigated.

Alternative potential causes for the observed LET-dependent senescence are related to the complex interplay between senescence and autophagy and MC [332], [333]. Understanding these pathway interactions and key mechanisms directing cell fate could help exploit additional biological advantages over the known physical advantages of protons.

We investigated if radiation quality affected key switches that link senescence, autophagy and MC.

5.5.2 Senescence and autophagy

There is increasing evidence that autophagy is both a negative and positive regulator of senescence [255], [334]. The tumour suppressor gene, GATA4, has been identified as a key link connecting autophagy and DDR to senescence and inflammation [335]. It is widely epigenetically silenced in lung cancer [335]–[337] and normally regulated by p62-dependent selective autophagy. DDR releases GATA4 from p62 control by ATM-induced phosphorylation allowing the activation of NF-κB and resulting in the release of senescence associated secretory proteins (SASP) [334]. It acts independently of the typical executors p53/p21 and $p16^{INK4a}$/pRB pathways [335]. Decreased GATA4 levels in clinical specimens are significantly associated with poor prognosis and ectopic expression of GATA4 has been shown to significantly inhibit colony formation in A549 cells and increase senescence [335].

No GATA4 expression was found in either A549 or H2122 cells, regardless of treatment suggesting alternative mechanisms driving senescence.

5.5.3 Senescence and mitotic catastrophe

A key link between MC and senescence is the cytosolic DNA by cGMP-AMP synthase (cGAS)-Stimulator of Interferon Genes (*STING*) signalling pathway. It is triggered when cGAS senses MN, which is more strongly induced by high LET irradiation, and results in a type 1 immune response [338]–[340], leading to further accumulation of cytosolic DNA, amplification of DDR and induction of senescence. *KRAS*-driven lung cancers frequently inactivate *LKB1*, which supresses *STING* expression via the epigenetic silencing enzymes EZH2 and DNMT1 [341]. Low expression of cGAS and *STING* is correlated with poor survival in human lung adenocarcinoma patients [342]. Interestingly, Kitajima et al further reported that if *STING* expression was undetectable, as in A549 cells, then they could not be rescued by *LKB1* reconstitution. However, if *STING* expression was just downregulated, as in H2122 cells, this could be rescued by *LKB1* reconstitution. Because *KRAS-LKB1* mutant lung cancers also tend to lack PD-L1 receptors that are restored upon re-induction of *LKB1* and *STING,* therapies that stimulate *STING* expression might also sensitize such tumours to immune check point [341].

We investigated if the LET-associated increase in senescence was related to changes in expression of these key proteins, enabling the activation of the cGAS-STING pathway and if there was evidence of increased MN formation following high LET PBT compared to low LET PBT or XRT.

Whilst there was a trend towards an increase in MN formation following high LET PBT compared to XRT and low LET PBT, this was not statistically significant. This may be because irradiation was delivered as a single fraction and fractionated treatment may be more effective at triggering the STING- interferon pathway [6].

As expected, A549 cells showed no evidence of *STING* expression regardless of treatment. However, in the strongly senescent H2122 cells we did observe a late and persistent increase in *STING* expression following high LET PBT compared to low LET PBT and XRT. This was most obvious at 96 hours. No detectable change in *LKB1* expression was associated proving that *LKB1*-independent pathways can release *STING* expression from suppression. These observations show PBT triggers different signal responses compared to XRT, which are both LET-associated and cell-specific. Previous studies have demonstrated that expression of proteins associated with inflammation, cellular defence and cell cycle to be influenced by PBT irradiation compared to XRT [343]–[345].

The ability for PBT to trigger different protein expression profiles compared to XRT has previously been demonstrated. Park et al reported increased *EGFR* expression in radioresistant NSCLC cells when proton- irradiated, supporting combination treatment with PBT and EGFR inhibitor to enhance radiation sensitivity [39]. Further studies characterising epigenetic reprogramming and changes in expression of key switches that link these major pathways following XRT and high and low LET PBT will be critical to identifying optimal combination treatments although these are likely to be tumour and cell-specific [122].

Further studies characterising radiation-induced chromosomal aberrations as well as identifying optimal doses and fractionations for sufficient MN formation and immune stimulation via sGAS-STING versus *Trex1* activation will be key to optimal radiotherapy protocols during immunotherapy but are likely to be tumour and cell-specific [122].

5.5.4 Therapeutic implications

Our findings have a number of therapeutic implications. Firstly, the differential lethality and biological consequences of high LET PBT further justifies LET-based optimisation for proton radiotherapy planning, whereby physical and biological dose planning are integrated [346]. Furthermore, the observed LET-dependent senescence suggests that increased senescence might be expected at the end and edge of the SOBP, where LET is greatest. Secondly, senolytics that target senescent cells by inducing apoptosis [347] should enhance tumour control if combined with high LET PBT irradiation. However, depending on cell type, multiple anti-apoptotic pathways may be induced in senescent cells, resulting in significant variation in the senolytic effect of these drugs. Navitoclax (ABT263), for example, has shown limited success in small cell lung cancer (NCT00445198). Lastly, is the epigenetic reprogramming triggered by high LET PBT that results in the senescent phenotype, which itself can drive gene expression changes [348].

Further potential causes for the observed LET-dependent senescence are related to the complex interplay between senescence and autophagy and MC [332], [333]. It was not possible to fully investigate this via RNA analysis due to constraints of the proton irradiation set-up and limited available beam-time in Clatterbridge Hospital.

Our findings can be validated using 3D cell culture as an intermediate model prior to xenografts [349], [350]. Whilst many pre-clinical studies begin with 2D cell culture, its limitations in adequately representing the cellular environment in organisms are recognised. Several 3D cultures systems have been developed, including scaffolds, matrix gels and hanging drops, some of which have been used in lung cancer studies [351]–[353]. This

organoid technology means that cell-cell and cell-matrix interactions more closely represent the original tumour *in vivo*, enabling more accurate data about response to mechanical and biochemical cues and changes in gene expression profiles [351], [354]. Such preclinical models will also enable the hypotheses generated by our experiments to be further examined.

Understanding these pathway interactions and key mechanisms directing cell fate could help exploit additional biological advantages over the known physical advantages of protons.

5.6 Conclusions

In the NSCLC cell lines studied, MC, autophagy and senescence are the major cell death pathways following XRT. High LET PBT results in lower cell survival than low LET PBT or XRT as a result of more effective senescence induction, established via the p53/p21 pathway. The mechanisms driving the LET- and dose-dependent senescence in these NSCLC cells is unclear but it may be due to non- DSB complex clusters or epigenetic reprogramming affecting cell death pathway dynamics.

The impact of these different cell death modalities include varying immunogenicity and clonogenic potential. Understanding how they differ in response to high and low LET protons can help guide radiotherapy optimisation and enable more advantage to be taken of the biological benefits of proton therapy by identifying optimal drug-radiotherapy combinations that will maximise tumour cell kill.

Chapter 6

General Discussion and Final Conclusions

The unmet need to improve outcomes in patients with locally advanced non-small cell lung cancer has been has spurred intensive research efforts to develop new treatment strategies. The large amounts of data generated during cancer management and trials need to be synthesised and analysed efficiently to facilitate the pace of study developments and to guide decision-making.

My novel approach of using routine datasets to estimate survival outcomes, refined by a back-dating interval optimisation process, correlates well with that derived from the gold standard manual data. This shows it is a reliable method that can be modelled by an algorithm to determine survival outcomes for patients treated with locally advanced NSCLC and can be adapted for other stages of lung cancer as well as other tumours. This single-institution-level of data extraction, synthesis, and analysis is the first step in a multi-level process. To reach the goal of a "live" automated decision support system that incorporates ongoing prospective data farming and retrospective data mining, there needs to be broadening of data elements in standardised extractable formats, aggregation of data across multiple institutions, and implementation of artificial intelligence algorithms that are supported by deep learning mechanisms.

Currently, the Public Health England's National Cancer Registration and Analysis Service (NCRAS) holds a vast network of data systems including Cancer Outcomes and Service Dataset (COSD) feeds, such as the systemic anti-cancer therapy data (SACT) and radiotherapy data set (RTDS); the Lung Cancer Data Audit (LUCADA) and the National Lung Cancer Audit (NLCA), hospital episode statistics (HES) and diagnostic imaging dataset (DID) making it a very rich data resource [355].

An important expansion of this network would be the incorporation of a next-generation sequencing (NGS) database. NGS enables the detection of germline and somatic driver mutations, resistance mechanisms and quantification of mutational burden. Advances in NGS techniques, has driven the "genomic era" of cancer research and promises to enable personalising treatment to an individual's unique molecular profile, as well as being used to identifying new biomarkers for early diagnosis of lung cancer [356]. As a consequence, huge amounts of data is amassed requiring organisation into work-flows that are easy to navigate and clinically relevant- the "Clinical NGS Database" is an example of one such model [357]. Ultimately, the usability of datasets, is dependent on data integrity and the evolution of practical Big Data systems [358].

Data-sharing across institutions, within and across nations, diversifies databases but is notoriously difficult. The Personal Health Train is a proposed infrastructure that promises a secure global data-sharing network set to enable rapid and easy analysis across separate databases, without the need for data centralisation, via Distributed Learning [359].

Ultimately, the usability of routine datasets and breadth of clinical scope, is dependent on data integrity; enriched and expanding clinical databases via global data-sharing infrastructures; and the evolution of practical Big Data systems [358]. As part of future work, my methodology can be applied to software programmes (eg. Python) written to automate analysis, which can then be applied to a secure global data-sharing infrastructure, such as the Personal Health Train [359].

Significant advances in photon radiotherapy over the past one to two decades and the emergence of immunotherapy continue to shape the treatment landscape for unresectable locally advanced NSCLC. Currently, clinical evidence for proton therapy is lacking but the gap analysis has identified key research priorities. Those considered to be particularly high priority include the need for high quality randomised controlled trials comparing proton and photon technology to justify PBT with particular focus on patients with locally advanced disease; identification of patients most likely to benefit using predictive biomarkers or model-based approaches; improved reporting on radiation dose to organs at risk, acute and late toxicity and patient-reported outcome measures; comprehensive analysis of the biological consequences of PBT in lung cancer; examination of the immunological effects of proton irradiation; and health economic evaluation.

There are nine ongoing prospective trials investigating proton therapy in lung cancer that collectively address some of the gaps identified, such as randomized comparative photon and proton clinical trials (*NCT02731001, NCT01629498, NCT01993810*); and trials investigating various sequencing of combination proton and immunotherapy (*NCT03818776, NCT01993810, NCT03087760).* All the trials intend to report on acute toxicity and survival outcomes. However, critical gaps remain unaddressed and/ or require further examination. Only two trials intend to use IMPT, the latest in proton technology *(NCT01629498, NCT01770418)*; and only one trial states clear intentions for translational biomarker development *(NCT01629498).* As identified by the gap analysis, there is a clear need for further studies in these current themes, particularly improving patient selection by developing predictive biomarkers or model-based approaches; as well as evaluation of the health economic implications of proton therapy, reporting on patient-related outcome measures, investigation of optimal fractionation regimes, robustness of planning, and characterisation of DNA damage induced by low and high LET protons. The scope for future trial development remain vast.

My retrospective planning study demonstrates that robust PBS plans are achievable in selected patients with SSTs, a rare subset of locally advanced NSCLC. The most significant dosimetric advantage of protons is the sparing of lymphopenia-related central structures such as the heart, lungs and thoracic vertebra, without compromising target coverage. This work indicates that the greatest benefit from scanning protons is likely to be in well-defined tumours where motion is ≤5 mm with associated mediastinal involvement. This may have particularly important therapeutic implications when combining with immunotherapy.

Considering the dose-sparing capabilities of protons, a reasonable hypothesis is that tumour geometry fundamentally influences which patients are mostly likely to benefit, although there is currently no clear evidence that normal-tissue dose reduction actually improves patient outcome. The Dutch health authorities accept the practice of using a normal tissue complication probability (NTCP) model to select patients for proton therapy based on predicted reduction of side effects. These model-based approaches, such as the one described by Langendijk et al [360] could help improve patient selection and be incorporated into trial design [361] but have recognised limitations. These include the need for dual planning which is time-consuming, inability to account for individual prognostic or confounding factors and the need for NTCP-models that have been developed in patients treated with photons to be validated in those treated with protons before direct comparisons of toxicity rates [360].

Future work includes not only using Monte Carlo-based optimisation for a more accurate representation of what is realistically achievable, but also assessing if an NTCP-model predicts less toxicity using PBS protons in the SST cohort, as well as comparative studies with advanced photon-based MR-Linac technology. These findings will form the basis for prospective clinical trials.

My study of cell death mechanisms induced by high and low LET proton therapy compared to XRT in NSCLC cell lines revealed differential lethality and biological consequences of these distinct radiation qualities. High LET PBT most effectively inhibited colony formation and this was done predominantly by senescence-induction through the p53-p21 pathway. The more radiosensitive H2122 cell line showed more senescence following XRT that was augmented further still following high LET PBT compared to the radioresistant A549 cell line. These results support that response to radiation is biologically driven and allude to why individuals' responses can vary quite significantly. Identifying biomarkers of increased radiosensitivity to PBT would improve selection of patients for this treatment. However, biomarker development can be a long and iterative process.

Based on my study, one approach would be to look for differentially expressed genes in these cell lines before and after XRT and high and low LET PBT using RNA sequencing. Particular attention would be paid to markers of senescence and key links between the different cell death modalities, for example, changes in *LKB1 and STING* expression (as discussed in chapter 5). Knowing that downregulated (but not absent) STING expression can be rescued by LKB1 reconstitution (otherwise frequently inactivated in KRAS-driven lung cancers) and that this is associated with PD-L1 receptor restoration [341], examining for differential changes in STING expression in the context of senescence might elucidate the major mechanisms by which increased lethality is achieved. Furthermore, this could be used to help identify which cell lines are most likely to respond to high LET PBT in this manner and identify additional biomarkers for cancers where PBT-enhanced immunotherapy is possible.

Another approach would be to focus on identifying biomarkers for impaired DNA repair capacity, particularly those involved in complex clustered ssDNA break repair, which may be the main mechanism of damage from high LET PBT, given no differential induction of dsDNA repair mechanisms were observed in my study. This could be used to predict which patients might benefit from specific DNA-repair inhibitors, in combination with PBT.

Collectively, these findings support the need to develop LET-based proton planning optimisation and prompt future work to further elucidate precise mechanisms that result in different cell death modalities and their impact on immunogenicity that will drive biologically based clinical trials.

The incorporation of software programmes designed to automate analysis into healthcare systems and proton radiotherapy for lung cancer treatment are two major broad themes that will dominate research efforts in the immediate future. My novel methodology to estimate survival outcomes for patients locally advanced NSCLC contributes to research efforts into big data processing in oncology. From the gap analysis, critical gaps in lung proton therapy research were identified and two of the work streams included in this thesis address two of the major gaps: 1. the retrospective planning study in patients with SSTs forms part of the work needed to help identify sub-groups within the locally advanced NSCLC group who might benefit, but also highlighted the limitations of PBS protons; 2. my study of cell death mechanisms in NSCLC cell lines following high and low LET protons contributes to the international efforts for comprehensive analysis of the biological consequences of PBT in lung cancer. Ultimately, multi-disciplinary inputs are essential to cover the huge scope of future work still needed.

Final Conclusions

Proton radiotherapy is likely to play a pivotal role in improving outcomes for patients with locally advanced NSCLC. My retrospective planning study has highlighted the physical dosimetric advantages of PBS protons and shown that robust plans are achievable in patients with SSTs. My study of cell death mechanisms following XRT and PBT has demonstrated biological advantages of high LET PBT. My methodology to determine outcome indicators using routine data shows that it can be incorporated into an algorithm to reliably estimate survival. Such AI applications will support the pace of evolving research in pre-clinical physics-driven and radiobiology studies and will facilitate their translation into clinical trial designs.

With the advancement of proton radiotherapy technology, concerted global research efforts, accumulating knowledge of proton radiobiology, supported by evolving AI infrastructures and emerging immunotherapeutic agents, there are many promising treatment strategies that will continue to be developed and every reason to be optimistic about the future of LA NSCLC outcomes.

References and Bibliography

[1] A. Verdecchia *et al.*, “Recent cancer survival in Europe: a 2000-02 period analysis of EUROCARE-4 data,” *Lancet Oncol.*, vol. 8, no. 9, pp. 784–796, 2007.

[2] M. Coleman *et al.*, “Cancer survival in Australia , Canada , Denmark , Norway , Sweden , and the UK , 1995 – 2007 (the International Cancer Benchmarking Partnership): an analysis of population-based,” *Lancet*, vol. 377, no. 9760, pp. 127–138, 2011.

[3] J. R. Molina, P. Yang, S. D. Cassivi, S. E. Schild, and A. A. Adjei, “Non-small cell lung cancer: epidemiology, risk factors, treatment, and survivorship.,” *Mayo Clin. Proc.*, vol. 83, no. 5, pp. 584–94, 2008.

[4] S. J. Antonia *et al.*, “Overall Survival with Durvalumab after Chemoradiotherapy in Stage III NSCLC,” *N. Engl. J. Med.*, vol. 379, no. 24, pp. 2342–2350, 2018.

[5] H. Paganetti, “Relative biological effectiveness (RBE) values for proton beam therapy. Variations as a function of biological endpoint, dose, and linear energy transfer.,” *Phys. Med. Biol.*, vol. 59, no. 22, pp. R419-72, 2014.

[6] F. Tommasino and M. Durante, “Proton Radiobiology,” *Cancers (Basel).*, vol. 7, pp. 353–381, 2015.

[7] N. Grosse *et al.*, “Deficiency in homologous recombination renders mammalian cells more sensitive to proton versus photon irradiation,” *Int. J. Radiat. Oncol. Biol. Phys.*, vol. 88, no. 1, pp. 175–181, 2014.

[8] M. Niemantsverdriet *et al.*, “High and low LET radiation differentially induce normal tissue damage signals,” *Int. J. Radiat. Oncol. Biol. Phys.*, vol. 83, no. 4, pp. 1291–1297, 2012.

[9] A. Gerelchuluun *et al.*, “The Major DNA Repair Pathway after Both Proton and Carbon- Ion Radiation is NHEJ, but the HR Pathway is More Relevant in Carbon Ions,” *Radiat Res.*, vol. 183, no. 3, pp. 345–356, 2015.

[10] S. J. Antonia *et al.*, “Durvalumab after Chemoradiotherapy in Stage III Non–Small-Cell Lung Cancer,” *N. Engl. J. Med.*, p. NEJMoa1709937, 2017.

[11] H. J. de Koning *et al.*, “Reduced Lung-Cancer Mortality with Volume CT Screening in a Randomized Trial,” *N. Engl. J. Med.*, vol. 382, no. 6, pp. 503–513, 2020.

[12] The National Lung Screening Trial Research Team, “Reduced Lung-Cancer Mortality with Low-Dose Computed Tomographic Screening,” *N. Engl. J. Med.*, vol. 365, no. 5, pp. 395–409, 2011.

[13] The National Lung Screening Trial Research Team, “Lung Cancer Incidence and Mortality with Extended Follow-up in the National Lung Screening Trial,” *J. Thorac. Oncol.*, vol. 14, no. 10, pp. 1732–1742, 2019.

[14] “The SUMMIT Study: Cancer Screening Study With or Without Low Dose Lung CT to Validate a Multi-cancer Early Detection Test,” *NCT03934866*. [Online]. Available: https://www.clinicaltrials.gov/ct2/show/NCT03934866.

[15] N. B. Leighl *et al.*, “Pembrolizumab in patients with advanced non-small-cell lung cancer (KEYNOTE-001): 3-year results from an open-label , phase 1 study,” *Lancet Respir.*, vol. 7, no. 4, pp. 347–357, 2019.

[16] R. Dillman, J. Herndon, S. Seagren, W. J. Eaton, and M. Green, “Improved survival in stage III non-small-cell lung cancer: Seven-year follow-up of cancer and leukemia group b (CALGB) 8433 trial.,” *J. Natl. Cancer Inst.*, vol. 88, pp. 1210–1215, 1996.

[17] F.-M. Kong *et al.*, “High-dose radiation improved local tumor control and overall survival in patients with inoperable/unresectable non-small-cell lung cancer: long-term results of a radiation dose escalation study.,” *Int. J. Radiat. Oncol. Biol. Phys.*, vol. 63, no. 2, pp. 324–333, 2005.

[18] H. Giap, D. Roda, and F. Giap, “(Review) Can proton beam therapy be clinically relevant for the management of lung cancer ?,” *Transl. Cancer Res.*, vol. 4, no. 4, pp. 3–15, 2015.

[19] J. Chang, X. Zhang, X. Wang, Y. Kang, B. Riley, and S. Bilton, “Significant reduction of normal tissue dose by proton radiotherapy compared with three-dimensional conformal or intensity-modulated radiation therapy in Stage I or Stage III non-small-cell lung cancer.,” *Int J Radiat Oncol Biol Phys.*, vol. 65, pp. 1087–96, 2006.

[20] D. De Ruysscher and J. Y. Chang, “Clinical controversies: Proton therapy for thoracic tumors,” *Semin. Radiat. Oncol.*, vol. 23, no. 2, pp. 115–119, 2013.

[21] B. S. Hoppe *et al.*, “A Phase 2 Trial of Concurrent Chemotherapy and Proton Therapy for Stage III Non-Small Cell Lung Cancer: Results and Reflections Following Early Closure of a Single-Institution Study,” *Int. J. Radiat. Oncol. Biol. Phys.*, vol. 95, no. 1, 2016.

[22] Q. N. Nguyen *et al.*, “Long-term outcomes after proton therapy, with concurrent chemotherapy, for stage II-III inoperable non-small cell lung cancer,” *Radiother. Oncol.*, vol. 115, no. 3, pp. 367–372, 2015.

[23] H. Iwata *et al.*, “High-dose proton therapy and carbon-ion therapy for stage I nonsmall cell lung cancer,” *Cancer*, vol. 116, no. 10, pp. 2476–2485, 2010.

[24] J. Y. Chang *et al.*, “Proton beam radiotherapy and concurrent chemotherapy for

unresectable stage III non–small cell lung cancer: Final results of a phase 2 study," *JAMA Oncol.*, vol. 3, no. 8, pp. 1–9, 2017.

[25] J. Chang, R. Komaki, C. Lu, and H. Wen, "Phase 2 study of high dose proton therapy with concurrent chemotherapy for unresectable stage III nonsmall cell lung cancer," *Cancer*, vol. 117, no. 20, pp. 4707–4713, 2011.

[26] E. J. Koay, D. Lege, R. Mohan, R. Komaki, J. D. Cox, and J. Y. Chang, "Adaptive/nonadaptive proton radiation planning and outcomes in a phase II trial for locally advanced non-small cell lung cancer," *Int. J. Radiat. Oncol. Biol. Phys.*, vol. 84, no. 5, pp. 1093–1100, 2012.

[27] J. Tobias, "Sindrome apico-costo-vertebral doloroso por tumor apexiano: su valor diagnostico en le cancer primitive pulmonary (Spanish).," *Rev Med Lat Am*, vol. 19, pp. 1552–6, 1932.

[28] V. W. Rusch, "Management of Pancoast tumours," *Lancet Oncol.*, vol. 7, no. 12, pp. 997–1005, 2006.

[29] C. N. Foroulis *et al.*, "Superior sulcus (Pancoast) tumors: Current evidence on diagnosis and radical treatment," *J. Thorac. Dis.*, vol. 5, no. SUPPL.4, pp. S342–S358, 2013.

[30] D. Schulz-Ertner and H. Tsujii, "Particle radiation therapy using proton and heavier ion beams," *J. Clin. Oncol.*, vol. 25, no. 8, pp. 953–964, 2007.

[31] M. HADA and A. G. GEORGAKILAS, "Formation of Clustered DNA Damage after High-LET Irradiation: A Review," *J. Radiat. Res.*, vol. 49, no. 3, pp. 203–210, 2008.

[32] I. V. Mavragani *et al.*, "Complex DNA damage: A route to radiation-induced genomic instability and carcinogenesis," *Cancers (Basel).*, vol. 9, no. 7, pp. 1–21, 2017.

[33] Y. Lorat, S. Timm, B. Jakob, G. Taucher-Scholz, and C. E. Rübe, "Clustered double-strand breaks in heterochromatin perturb DNA repair after high linear energy transfer irradiation," *Radiother. Oncol.*, vol. 121, no. 1, pp. 154–161, 2016.

[34] S. R. Gameiro *et al.*, "Tumor Cells Surviving Exposure to Proton or Photon Radiation Share a Common Immunogenic Modulation Signature, Rendering Them More Sensitive to T Cell-Mediated Killing," *Int. J. Radiat. Oncol. Biol. Phys.*, vol. 95, no. 1, pp. 120–130, 2016.

[35] H. Hojo *et al.*, "Difference in the relative biological effectiveness and DNA damage repair processes in response to proton beam therapy according to the positions of the spread out Bragg peak.," *Radiat Oncol.*, vol. 12, no. 1, p. 111, 2017.

[36] T. Marshall *et al.*, "Investigating the Implications of a Variable RBE on Proton Dose Fractionation Across a Clinical Pencil Beam Scanned Spread-Out Bragg Peak.," *Int J*

Radiat Oncol Biol Phys., vol. 95, no. 1, pp. 70–77, 2016.

[37] J. J. Cuaron *et al.*, “Exponential Increase in Relative Biological Effectiveness Along Distal Edge of a Proton Bragg Peak as Measured by Deoxyribonucleic Acid Double-Strand Breaks,” *Int J Radiat Oncol Biol Phys.*, vol. 95, no. 1, pp. 62–69, 2016.

[38] X. Zhang, C. Ye, F. Sun, W. Wei, B. Hu, and J. Wang, “Both complexity and location of DNA damage contribute to cellular senescence induced by ionizing radiation,” *PLoS One*, vol. 11, no. 5, 2016.

[39] H. J. PARK, J. S. OH, J. W. CHANG, S.-G. HWANG, and J.-S. KIM, “Proton Irradiation Sensitizes Radioresistant Non-small Cell Lung Cancer Cells by Modulating Epidermal Growth Factor Receptor-mediated DNA Repair,” *Anticancer Res*, vol. 36, pp. 205–212, 2016.

[40] L. Wang *et al.*, “Proton versus photon radiation–induced cell death in head and neck cancer cells,” *Head Neck*, vol. 41, no. 1, pp. 46–55, 2019.

[41] Cancer Research UK, “Vision for radiotherapy 2014-2024,” 2014.

[42] R. Korn and J. Crowley, “Overview: Progression-Free Survival as an Endpoint in Clinical Trials with Solid Tumors,” *Clin Cancer Res*, vol. 19, no. 10, pp. 2607–2612, 2013.

[43] E. D. Saad and A. Katz, “Progression-free survival and time to progression as primary end points in advanced breast cancer: Often used, sometimes loosely defined,” *Ann. Oncol.*, vol. 20, no. 3, pp. 460–464, 2009.

[44] R. Kane, K. Wellings, C. Free, and J. Goodrich, “Uses of routine data sets in the evaluation of health promotion interventions: opportunities and limitations,” *Health Educ.*, vol. 100, no. 1, pp. 33–41, 2000.

[45] M. Coory, B. Thompson, P. Baade, and L. Fritschi, “Utility of routine data sources for feedback on the quality of cancer care: an assessment based on clinical practice guidelines.,” *BMC Health Serv. Res.*, vol. 9, p. 84, 2009.

[46] M. Hewitt and J. Simone, *Ensuring quality cancer care*. National Academies Press, 1999.

[47] G. Jamtvedt, J. Young, D. Kristoffersen, M. Thomson O’Brien, and A. Oxman, “Audit and feedback: Effects on professional practice and health care outcomes (Cochrane Review),” *Cochrane Libr.*, 2006.

[48] R. D. AK Jha, JB Perlin, KW Kizer, “Effect of the transformation of the Veterans Affairs Health Care System on the quality of care.,” *N Engl J Med*, vol. 348, pp. 2218–2227, 2003.

[49] A. Trivedi, A. Zaslavsky, E. Schneider, and E. Al, “Trends in the quality of care and racial disparities in Medicare managed care,” *New Engl J Med*, vol. 353, pp. 692–700, 2005.

[50] K. Ricketts, M. Williams, Z. Liu, and A. Gibson, “Automated estimation of disease recurrence in head and neck cancer using routine healthcare,” *Comput. Methods Programs Biomed.*, vol. 117, no. 3, pp. 412–424, 2014.

[51] Z. Liu, H. Fitzke, and M. Williams, “Using routine data to estimate survival and recurrence in head and neck cancer : our preliminary experience in twenty patients,” *Clin. Otolaryngol.*, vol. 38, no. 4, pp. 334–339, 2013.

[52] A. L. Rich *et al.*, “Lung cancer in England: Information from the National Lung Cancer Audit (LUCADA),” *Lung Cancer*, vol. 72, no. 1, pp. 16–22, 2011.

[53] N. O’Rourke, M. Roqué i Figuls, N. Farré Bernadó, and F. Macbeth, “Concurrent chemoradiotherapy in non-small cell lung cancer,” *Cochrane Database Syst. Rev.*, no. 6, 2010.

[54] C. P. Oken MM, Creech RH, Tormey DC, Horton J, Davis TE, McFadden ET, “Toxicity and response criteria of the Eastern Cooperative Oncology Group.,” *Am J Clin Oncol.*, vol. 5, no. 6, pp. 649–55, 1982.

[55] R. A. Hughes, J. Heron, J. A. C. Sterne, and K. Tilling, “Accounting for missing data in statistical analyses: Multiple imputation is not always the answer,” *Int. J. Epidemiol.*, vol. 48, no. 4, pp. 1294–1304, 2019.

[56] C. M. Nur U, Shack LG, Rachet B, Carpenter JR, “Modelling relative survival in the presence of incomplete data: a tutorial.,” *Int J Epidemiol*, vol. 39, pp. 118–28, 2010.

[57] W. I. Keogh RH, “Using full-cohort data in nested case– control and case–cohort studies by multiple imputation.,” *Stat Med*, vol. 32, pp. 4021–43, 2013.

[58] H. G. Shardell M, “Statistical analysis with missing expo_sure data measured by proxy respondents: a misclassification problem within a missing-data problem.,” *Stat Med*, vol. 33, pp. 4437–52., 2014.

[59] M. J. Cornish RP, Tilling K, Boyd A, Davies A, “Using linked educational attainment data to reduce bias due to missing outcome data in estimates of the association between the duration of breast_feeding and IQ at 15 years.,” *Int J Epidemiol*, vol. 44, pp. 937–45, 2015.

[60] S. P. Blagden, S. C. Charman, L. D. Sharples, L. R. A. Magee, and D. Gilligan, “Performance status score: do patients and their oncologists agree?,” *Br. J. Cancer*, vol. 89, no. 6, pp. 1022–7, 2003.

[61] “Lung cancer: The diagnosis and treatment of lung cancer,” *NICE Clin. Guidel. 121*,

no. February, p. 41, 2011.

[62] J. B. Sørensen, M. Klee, T. Palshof, and H. H. Hansen, “Performance status assessment in cancer patients. An inter-observer variability study.,” *Br. J. Cancer*, vol. 67, no. 4, pp. 773–775, 1993.

[63] “Everyone Counts: Planning for Patients 2014/15 to 2018/19,” *England, NHS*, pp. 1–90, 2013.

[64] D. Verellen, M. De Ridder, N. Linthout, K. Tournel, G. Soete, and G. Storme, “Innovations in image-guided radiotherapy,” *Nat. Rev. Cancer*, vol. 7, no. 12, pp. 949–960, 2007.

[65] R. Mohan and D. Grosshans, “Proton Therapy – Present and Future,” *Adv Drug Deliv Rev.*, vol. 109, pp. 26–44, 2017.

[66] J. D. Bradley *et al.*, “Standard-dose versus high-dose conformal radiotherapy with concurrent and consolidation carboplatin plus paclitaxel with or without cetuximab for patients with stage IIIA or IIIB non-small-cell lung cancer (RTOG 0617): A randomised, two-by-two factorial p,” *Lancet Oncol.*, vol. 16, no. 2, pp. 187–199, 2015.

[67] C. K. Speirs *et al.*, “Heart Dose Is an Independent Dosimetric Predictor of Overall Survival in Locally Advanced Non–Small Cell Lung Cancer,” *J. Thorac. Oncol.*, vol. 12, no. 2, pp. 293–301, 2017.

[68] R. T. Dess *et al.*, “Cardiac Events After Radiation Therapy : Combined Analysis of Prospective Multicenter Trials for Locally Advanced Non – Small-Cell Lung Cancer,” vol. 35, no. 13, 2017.

[69] A. Mcwilliam, J. Kennedy, C. Hodgson, E. Vasquez, C. Faivre-finn, and M. Van Herk, “ScienceDirect Radiation dose to heart base linked with poorer survival in lung cancer patients,” *Eur. J. Cancer*, vol. 85, pp. 106–113, 2017.

[70] C. Tang *et al.*, “Lymphopenia Association With Gross Tumor Volume and Lung V5 and Its Effects on Non-Small Cell Lung Cancer Patient Outcomes,” *Radiat. Oncol. Biol.*, vol. 89, no. 5, pp. 1084–1091, 2014.

[71] B. P. Venkatesulu, S. Mallick, S. H. Lin, and S. Krishnan, “A systematic review of the influence of radiation-induced lymphopenia on survival outcomes in solid tumors,” *Crit. Rev. Oncol. Hematol.*, vol. 123, no. January, pp. 42–51, 2018.

[72] N. Joseph, A. Mcwilliam, J. Kennedy, K. Haslett, and A. Choudhury, “Posttreatment Lymphocytopenia, Integral Heart Dose, and Overall Survival in Lung Cancer Patients Treated With Radical Radiation Therapy,” *Int. J. Radiat. Oncol. Biol. Phys.*, vol. 99, no. 2, p. S36, 2017.

[73] C. L. Barney *et al.*, “Radiation Dose to the Thoracic Vertebral Bodies is Associated

with Acute Hematologic toxicities in Patients Receiving Concurrent Chemoradiation for Lung Cancer: Results of a Single Center Retrospective Analysis," *Int. J. Radiat. Oncol.*, vol. 100, no. 3, pp. 748–755, 2017.

[74] M. P. Deek *et al.*, "Thoracic vertebral body irradiation contributes to acute hematologic toxicity during chemoradiation therapy for non-small cell lung cancer," *Int. J. Radiat. Oncol. Biol. Phys.*, vol. 94, no. 1, pp. 147–154, 2016.

[75] A. Zhang *et al.*, "Vertebral Bone Marrow Irradiation Contributes to Hematologic Toxicity During Chemoradiation Therapy for Esophageal Cancer," *Int. J. Radiat. Oncol.*, vol. 99, no. 2, p. E205, 2017.

[76] C. Tang, Z. Liao, D. Gomez, L. Levy, Y. Zhuang, and 2014. Gebremichael, R.A., et al., "Lymphopenia association with gross tumor volume and lung V5 and its effects on non-small cell lung cancer patient outcomes. Int. J. Radiat. Oncol. Biol. Phys.," vol. 89, pp. 1084–1091., 2014.

[77] S. Erridge, Y. Seppenwoolde, and S. Muller, "Portal imaging to assess set-up errors, tumor motion and tumor shrinkage during conformal radiotherapy of non-small cell lung cancer.," *Radiother Oncol.*, vol. 66, pp. 75– 85, 2003.

[78] J. J. Sonke, J. Lebesque, and H. M. Van, "Variability of four-dimensional computed tomography patient models.," *Int. J. Radiat. Oncol. Biol. Phys.*, vol. 70, pp. 590–8, 2008.

[79] H. H. Liu, "Assessing respiration-induced tumor motion and internal target volume using four-dimensional computed tomography for radiotherapy of lung cancer.," *Int. J. Radiat. Oncol. Biol. Phys*, vol. 68, pp. 531–40, 2007.

[80] A. J. Cole, G. G. Hanna, S. Jain, and J. M. O'Sullivan, "Motion management for radical radiotherapy in non-small cell lung cancer," *Clin. Oncol.*, vol. 26, no. 2, pp. 67–80, 2014.

[81] G. Distefano, A. Baker, A. J. D. Scott, and G. J. Webster, "Survey of stereotactic ablative body radiotherapy in the UK by the QA group on behalf of the UK SABR Consortium," *Br. J. Radiol.*, vol. 87, no. 1037, 2014.

[82] Y. O. Negoro *et al.*, "THE EFFECTIVENESS OF AN IMMOBILIZATION DEVICE IN CONFORMAL RADIOTHERAPY FOR LUNG TUMOR : REDUCTION OF RESPIRATORY TUMOR MOVEMENT AND EVALUATION OF THE DAILY SETUP ACCURACY," *Int. J. Radiat. Oncol. Biol. Phys*, vol. 50, no. 4, pp. 889–898, 2001.

[83] G. Bouilhol *et al.*, "Is abdominal compression useful in lung stereotactic body radiation therapy? A 4DCT and dosimetric lobe-dependent study," *Phys. Medica*, vol. 29, no. 4, pp. 333–340, 2013.

[84] W. A. Mampuya *et al.*, “The impact of abdominal compression on outcome in patients treated with stereotactic body radiotherapy for primary lung cancer,” *J. Radiat. Res.*, vol. 55, no. May, pp. 934–939, 2014.

[85] M. Partridge *et al.*, “Improvement in tumour control probability with active breathing control and dose escalation: A modelling study,” *Radiother. Oncol.*, vol. 91, no. 3, pp. 325–329, 2009.

[86] T. G. Purdie *et al.*, “Cone-Beam Computed Tomography for On-Line Image Guidance of Lung Stereotactic Radiotherapy: Localization, Verification, and Intrafraction Tumor Position,” *Int. J. Radiat. Oncol. Biol. Phys.*, vol. 68, no. 1, pp. 243–252, 2007.

[87] I. S. Grills *et al.*, “IMAGE-GUIDED RADIOTHERAPY VIA DAILY ONLINE CONE-BEAM CT SUBSTANTIALLY REDUCES MARGIN REQUIREMENTS FOR STEREOTACTIC LUNG RADIOTHERAPY,” *Int J Radiat Oncol Biol Phys*, vol. 70, no. 4, pp. 1045–1056, 2008.

[88] M. Josipovic *et al.*, “Translational and rotational intra- and inter- fractional errors in patient and target position during a short course of frameless stereotactic body radiotherapy Translational and rotational intra- and inter-fractional errors in patient and target positio,” 2012.

[89] J. R. McClelland, D. J. Hawkes, T. Schaeffter, and A. P. King, “Respiratory motion models: A review,” *Med. Image Anal.*, vol. 17, no. 1, pp. 19–42, 2013.

[90] A. Richter, J. Wilbert, K. Baier, M. Flentje, and M. Guckenberger, “Feasibility study for markerless tracking of lung tumors in stereotactic body radiotherapy,” *Int. J. Radiat. Oncol.*, vol. 78, pp. 618–27, 2010.

[91] J. H. Bryant, J. Rottmann, J. H. Lewis, P. Mishra, P. J. Keall, and R. I. Berbeco, “Registration of clinical volumes to beams-eye-view images for real-time tracking,” *Med. Phys.*, vol. 41, no. 12, p. 121703, 2014.

[92] M. Serpa, K. Baier, F. Cremers, M. Guckenberger, and J. Meyer, “Suitability of markerless EPID tracking for tumor position verification in gated radiotherapy,” *Med. Phys.*, vol. 41, p. 031702, 2014.

[93] G. Hugo, J. Liang, and D. Yan, “Marker-free lung tumour trajectory estimation from a cone beam CT sinogram,” *Phys Med Biol*, vol. 55, no. 9, pp. 2637–2650, 2010.

[94] J. H. Lewis *et al.*, “Markerless lung tumor tracking and trajectory reconstruction using rotational cone-beam projections: a feasibility study,” *Phys. Med. Biol.*, vol. 55, pp. 2505–22, 2010.

[95] J. van Sörnsen de Koste *et al.*, “Markerless tracking of small lung tumors for stereotactic radiotherapy Markerless tracking of small lung tumors for stereotactic

radiotherapy," vol. 1640, 2015.

[96] J. Yang, T. Yamamoto, S. R. Mazin, E. E. Graves, and P. J. Keall, "The potential of positron emission tomography for intratreatment dynamic lung tumor tracking: A phantom study," *Med. Phys.*, vol. 41, no. 2, pp. 1–14, 2014.

[97] A. Abravan, H. A. Eide, I. S. Knudtsen, A. M. Løndalen, Å. Helland, and E. Malinen, "Assessment of pulmonary 18 F-FDG-PET uptake and cytokine profiles in non-small cell lung cancer patients treated with radiotherapy and erlotinib," *Clin. Transl. Radiat. Oncol.*, vol. 4, no. June, pp. 57–63, 2017.

[98] M. Massaccesi *et al.*, " ^{18}F-FDG PET-CT during chemo-radiotherapy in patients with non-small cell lung cancer: the early metabolic response correlates with the delivered radiation dose.," *Radiat. Oncol.*, vol. 7, no. 1, p. 106, 2012.

[99] L. I. Cerviño, J. Du, and S. B. Jiang, "MRI-guided tumor tracking in lung cancer radiotherapy," *Phys. Med. Biol.*, vol. 56, no. 13, pp. 3773–3785, 2011.

[100] M. J. Ghilezan *et al.*, "Prostate gland motion assessed with cine-magnetic resonance imaging (cine-MRI)," *Int. J. Radiat. Oncol. Biol. Phys.*, vol. 62, no. 2, pp. 406–417, 2005.

[101] C. Plathow *et al.*, "Analysis of intrathoracic tumor mobility during whole breathing cycle by dynamic MRI," *Int. J. Radiat. Oncol. Biol. Phys.*, vol. 59, no. 4, pp. 952–959, 2004.

[102] J. Yun, K. Wachowicz, M. Mackenzie, S. Rathee, D. Robinson, and B. Fallone, "First demonstration of intrafractional tumortracked irradiation using 2D phantom MR images on a prototype linac-MR.," *Med Phys*, vol. 40, no. 5, p. 051718., 2013.

[103] J. J. Sonke and J. Belderbos, "Adaptive Radiotherapy for Lung Cancer," *Semin. Radiat. Oncol.*, vol. 20, no. 2, pp. 94–106, 2010.

[104] K. Britton *et al.*, "Assessment of gross tumor volume regression and motion changes during radiotherapy for non-small-cell lung cancer as measured by four-dimensional computed tomography Phys.," *Int. J. Radiat. Oncol. Biol.*, vol. 68, pp. 1036–46, 2007.

[105] M. Kwint *et al.*, "Intra thoracic anatomical changes in lung cancer patients during the course of radiotherapy," *Radiother. Oncol.*, vol. 113, no. 3, pp. 392–397, 2014.

[106] K. MM, H. L, N. M, and E. Al., "Daily cone-beam computed tomography used to determine tumour shrinkage and localisation in lung cancer patients. Acta Oncol," vol. 49, pp. 1077–84, 2010.

[107] J. J. Sonke, M. Aznar, and C. Rasch, "Adaptive Radiotherapy for Anatomical Changes," *Semin. Radiat. Oncol.*, vol. 29, no. 3, pp. 245–257, 2019.

[108] R. S, F. M, S. S, and E. Al:, “Local control and toxicity of adaptive radiotherapy using weekly CT imaging: Results from the lartia trial in stage III Nsclc.,” *J Thorac Oncol*, vol. 12, pp. 1122–1130, 2017.

[109] A. Hunt, V. N. Hansen, U. Oelfke, S. Nill, and S. Hafeez, “Adaptive Radiotherapy Enabled by MRI Guidance Will MRI-Guided Radiotherapy be the Ultimate Online IGRT Solution ?,” *Clin. Oncol.*, vol. 30, no. 11, pp. 711–719, 2018.

[110] O. Bohoudi *et al.*, “Fast and robust online adaptive planning in stereotactic MR-guided adaptive radiation therapy (SMART) for pancreatic cancer.,” *Radiother Oncol*, vol. 125, no. 3, p. 439e444., 2017.

[111] E. Ahunbay and X. Li, “Gradient maintenance: a new algorithm for fast online re-planning.,” *Med Phys*, vol. 42, no. 6, p. 2863e2876, 2015.

[112] E. E. Ahunbay *et al.*, “An on-line replanning scheme for interfractional variations,” *Med. Phys.*, vol. 35, no. 8, pp. 3607–3615, 2008.

[113] D. B. Doroshow *et al.*, “Immunotherapy in non-small cell lung cancer: Facts and hopes,” *Clin. Cancer Res.*, vol. 25, no. 15, pp. 4592–4602, 2019.

[114] R. Herbst and M. Sznol, “Diminished but not dead: chemotherapy for the treatment of NSCLC.,” *Lancet Oncol*, vol. 17, pp. 1464–5, 2016.

[115] C. Langer, S. Gadgeel, V. Borghaei, H Papadimitrakopoulou, A. Patnaik, and S. et al. Powell, “Carboplatin and pemetrexed with or without pembrolizumab for advanced, non-squamous non-small-cell lung cancer: a randomised, phase 2 cohort of the open-label KEYNOTE-021 study.,” *Lancet Oncol*, vol. 17, pp. 1497–508, 2016.

[116] L. Gandhi, S. Rodríguez-Abreu, D Gadgeel, E. Esteban, E. Felip, and F. et al Angelis, “Pembrolizumab plus chemotherapy in metastatic non–small-cell lung cancer.,” *N Engl J Med*, vol. 378, pp. 2078–92, 2018.

[117] M. Socinski, R. Jotte, F. Cappuzzo, and N. et al. Orlandi, F Stroyakovskiy, D Nogami, “Atezolizumab for first-line treatment of metastatic nonsquamous NSCLC.,” *N Engl J Med*, vol. 378, pp. 2288–301, 2018.

[118] V. Papadimitrakopoulou, M. Cobo, R. Bordoni, and P. Longeras, “IMpower132: PFS and safety results with 1L atezolizumabþ carboplatin/ cisplatin þ pemetrexed in stage IV non-squamous NSCLC,” in *Proceedings of the IASLC 19th World Conference on Lung Cancer*.

[119] M. Hellmann, T.-E. Ciuleanu, A. Pluzanski, J. Lee, G. Otterson, and C. et al. Audigier- Valette, “Nivolumab plus ipilimumab in lung cancer with a high tumor mutational burden.,” *N Engl J Med*, vol. 378, pp. 2093–104, 2018.

[120] M. Spaas and Y. Lievens, “Is the Combination of Immunotherapy and Radiotherapy

in Non-small Cell Lung Cancer a Feasible and Effective Approach?," *Front. Med.*, vol. 6, no. November, 2019.

[121] E. B. Golden, I. Pellicciotta, S. Demaria, M. H. Barcellos-Hoff, and S. C. Formenti, "The convergence of radiation and immunogenic cell death signaling pathways," *Front. Oncol.*, vol. 2 AUG, no. August, pp. 1–13, 2012.

[122] M. Durante and S. C. Formenti, "Radiation-induced chromosomal aberrations and immunotherapy: Micronuclei, cytosolic DNA, and interferon-production pathway," *Front. Oncol.*, vol. 8, no. MAY, 2018.

[123] C. Vanpouille-Box *et al.*, "DNA exonuclease Trex1 regulates radiotherapy-induced tumour immunogenicity," *Nat. Commun.*, vol. 8, p. 15618, 2017.

[124] S. Lin, X. Lin, D. Clay, L. Yao, I. Mok, and D. et al. Gomez, "DETERRED: phase II trial combining atezolizumab concurrently with chemoradiation therapy in locally advanced non-small cell lung cancer.," *J Thorac Oncol.*, vol. 13, pp. S320–1., 2018.

[125] S. Peters, E. FeliP, U. Dafni, M. I. A. Tufman, A Guckenberger, and E. Al., "Efficacy evaluation of concurrent nivolumab addition to a first-line, concurrent chemo-radiotherapy regimen in unresectable locally advanced NSCLC: results from the European Thoracic Oncology Platform (ETOP 6–14) NICOLAS phase II trial..," *Ann Oncol*, vol. 30, no. Suppl. 5, 2019.

[126] S. Peters, E. Felip, U. Dafni, C. Belka, and et al. Guckenberger, M Irigoyen A, "Safety evaluation of nivolumab added concurrently to radiotherapy in a standard first line chemo-radiotherapy regimen in stage III non-small cell lung cancer-The ETOP NICOLAS trial.," *Lung Cancer*, vol. 133, pp. 83–7, 2019.

[127] M. Mitchell Machtay, "A Pilot Trial of Proton Based Cardiac Sparing Accelerated Fractionated RadioTherapy in Unresectable Non-Small Cell Lung Cancer With Extended Durvalumab Therapy (PARTICLE-D)," *https://clinicaltrials.gov/ct2/show/NCT03818776*, 2019. .

[128] S. E. Schild, "Phase II Trial of Consolidation Pembrolizumab After Concurrent Chemotherapy and Proton Re-irradiation for Thoracic Recurrences of Non-small cell lung cancer NCT03087760," *https://clinicaltrials.gov/ct2/show/NCT03132532*, 2017. .

[129] "Clinical Trials Database," *https//www.clinicaltrials.gov/ct2/show/NCT01993810?term=rtog&recr=Open&rank=01993812 (accessed 29 January 2015).*

[130] M. E. Goossens *et al.*, "Is there any benefit to particles over photon radiotherapy," *ecancer*, vol. 13, p. 982, 2019.

[131] T. Sun *et al.*, "Heart and Cardiac Substructure Dose Sparing in Synchronous Bilateral

Breast Radiotherapy: A Dosimetric Study of Proton and Photon Radiation Therapy," *Front. Oncol.*, vol. 9, no. January, pp. 1–11, 2020.

[132] K. M. Menezes, H. Wang, M. Hada, and P. B. Saganti, "Radiation Matters of the Heart : A Mini Review," vol. 5, no. July, pp. 1–10, 2018.

[133] G. GAGLIARDI *et al.*, "Quantec: Organ specific paper. Radiation dose- volume effects in the heart," *Int J Radiat. Oncol. Biol Phys.*, vol. 76, no. 3, pp. 77–85, 2010.

[134] S. Darby, M. Ewertz, P. McGale, A. Bennet, U. Blom-Goldman, and D. et al Brønnum, "Risk of ischemic heart disease in women after radiotherapy for breast cancer.," *N Engl J Med.*, vol. 368, pp. 987–98, 2013.

[135] F. van Nimwegen, G. Ntentas, S. Darby, M. Schaapveld, M Hauptmann, and et al. Lugtenburg, PJ, "Risk of heart failure in survivors of Hodgkin lymphoma: effects of cardiac exposure to radiation and anthracyclines.," *Blood*, vol. 129, pp. 2257–65, 2017.

[136] Y. Shimizu, K. Kodama, N. Nishi, F. Kasagi, A. Suyama, and M. et al Soda, "Radiation exposure and circulatory disease risk: Hiroshima and Nagasaki atomic bomb survivor data, 1950–2003.," *BMJ*, 2010.

[137] W. Finch, K. Shamsa, and M. Lee, "Cardiovascular complications of radiation exposure.," *Rev Cardiovasc Med.*, vol. 15, no. 3, pp. 232–44, 2014.

[138] G. Nilsson, L. Holmberg, H. Garmo, O. Duvernoy, I. Sjogren, and B. Lagerqvist, "Distribution of coronary artery stenosis after radiation for breast cancer.," *J Clin Oncol.*, vol. 30, pp. 380–6, 2012.

[139] D. Jaffray, "Image-guided radiotherapy: from current concept to future perspectives.," *Nat Rev Clin Oncol.*, vol. 9, pp. 688–99, 2012.

[140] T. Bortfeld, "IMRT: a review and preview.," *Phys Med Biol.*, vol. 51, pp. R363–79, 2006.

[141] B. Teh, H. Ishiyama, T. Mathews, B. Xu, E. Butler, and N. et al. Mayr, "Stereotactic body radiation therapy (SBRT) for genitourinary malignancies. Discov Med.," vol. 10, pp. 255–62, 2010.

[142] T. Swanson, I. Grills, H. Ye, A. Entwistle, M. Teahan, and et al. Letts, N, "Six year experience routinely using moderate deep inspiration breath-hold for the reduction of cardiac dose in left-sided breast irradiation for patients with early-stage or locally advanced breast cancer.," *Am J Clin Oncol.*, vol. 36, pp. 24–30, 2013.

[143] A. McIntosh, A. Shoushtari, S. Benedict, P. Read, and K. Wijesooriya, "Quantifying the reproducibility of heart position during treatment and corresponding delivered heart dose in voluntary deep inhalation breath hold for left breast cancer patients

treated with external beam radiotherapy. Int J Radiat Oncol Biol Phys.," vol. 81, pp. e569–76, 2011.

[144] J. Wondergem, E. Strootman, M. Frolich, J. Leer, and E. Noordijk, "Circulating atrial natriuretic peptide plasma levels as a marker for cardiac damage after radiotherapy.," *Radiother Oncol.*, vol. 58, pp. 295–301, 2001.

[145] S. Zschaeck *et al.*, "PRONTOX – proton therapy to reduce acute normal tissue toxicity in locally advanced non-small-cell lung carcinomas (NSCLC): study protocol for a randomised controlled trial," *Trials*, vol. 17, p. 543, 2016.

[146] K. Gabriels, S. Hoving, I. Seemann, N. Visser, M. Gijbels, and et al. Pol, JF, "Local heart irradiation of ApoE(-/-) mice induces microvascular and endocardial damage and accelerates coronary atherosclerosis.," *Radiother Oncol.*, vol. 105, pp. 358–64., 2012.

[147] S. Darby, D. Cutter, M. Boerma, L. Constine, L. Fajardo, and et al. Kodama, K, "Radiation-related heart disease: current knowledge and future prospects.," *Int J Radiat Oncol Biol Phys.*, vol. 76, pp. 656–65, 2010.

[148] E. Ricciotti *et al.*, "Distinct vascular genomic response of proton and gamma radiation — A pilot investigation," *PLoS One*, vol. 14, no. 2, p. e0207503, 2019.

[149] J. Forrest, J. Presutti, M. Davidson, P. Hamilton, A. Kiss, and G. Thomas, "A Dosimetric Planning Study Comparing Intensity-modulated Radiotherapy with Four-field Conformal Pelvic Radiotherapy for the Definitive Treatment of Cervical Carcinoma," *Clin. Oncol.*, vol. 24, no. 4, pp. e63–e70, 2012.

[150] J. A. Hayman *et al.*, "Distribution of proliferating bone marrow in adult cancer patients determined using FLT-PET imaging," *Int. J. Radiat. Oncol. Biol. Phys.*, vol. 79, no. 3, pp. 847–852, 2011.

[151] J. S. Blebea *et al.*, "Structural and Functional Imaging of Normal Bone Marrow and Evaluation of Its Age-Related Changes," *Semin. Nucl. Med.*, vol. 37, no. 3, pp. 185–194, 2007.

[152] S. M. McGuire *et al.*, "Spatial mapping of functional pelvic bone marrow using FLT PET," *J. Appl. Clin. Med. Phys.*, vol. 15, no. 4, pp. 129–136, 2014.

[153] J. Lee *et al.*, "Dosimetric predictors of acute haematological toxicity in oesophageal cancer patients treated with neoadjuvant chemoradiotherapy," *Br. J. Radiol.*, vol. 89, no. 1066, pp. 7–13, 2016.

[154] R. Nichols, S. Huh, R. Henderson, N. Mendenhall, S. Flampouri, and Z. Li, "Proton radiation therapy offers reduced normal lung and bone marrow exposure for patients receiving dose-escalated radiation therapy for unresectable stage iii non-small-cell

lung cancer: A dosimetric study.," *Clin Lung Cancer.*, vol. 12, pp. 252–7, 2011.

[155] S. Warren, C. N. Hurt, T. Crosby, M. Partridge, and M. A. Hawkins, "Potential of Proton Therapy to Reduce Acute Hematologic Toxicity in Concurrent Chemoradiation Therapy for Esophageal Cancer," *Int. J. Radiat. Oncol. Biol. Phys.*, vol. 99, no. 3, pp. 729–737, 2017.

[156] R. Wilson, "Radiological use of fast protons," *Radiology*, vol. 47, pp. 487–491, 1946.

[157] J. Lawrence *et al.*, "Pituitary irradiation with high-energy proton beams: a preliminary report.," *Cancer Res.*, vol. 18, pp. 121–134, 1958.

[158] J. Y. Chang *et al.*, "Clinical implementation of intensity modulated proton therapy for thoracic malignancies," *Int. J. Radiat. Oncol. Biol. Phys.*, vol. 90, no. 4, pp. 809–818, 2014.

[159] U. Schneider and R. Hälg, "The impact of neutrons in clinical proton therapy," *Front. Oncol.*, vol. 5, no. OCT, pp. 1–5, 2015.

[160] S. Dowdell, C. Grassberger, G. C. Sharp, and H. Paganetti, "Interplay effects in proton scanning for lung: a 4D Monte Carlo study assessing the impact of tumor and beam delivery parameters.," *Phys. Med. Biol.*, vol. 58, no. 12, pp. 4137–56, 2013.

[161] B. S. Hoppe *et al.*, "Double-scattered proton-based stereotactic body radiotherapy for stage i lung cancer: A dosimetric comparison with photon-based stereotactic body radiotherapy," *Radiother. Oncol.*, vol. 97, no. 3, pp. 425–430, 2010.

[162] N. Kadoya *et al.*, "Dose-volume comparison of proton radiotherapy and stereotactic body radiotherapy for non-small-cell lung cancer," *Int. J. Radiat. Oncol. Biol. Phys.*, vol. 79, no. 4, pp. 1225–1231, 2011.

[163] S. P. Register, X. Zhang, R. Mohan, and J. Y. Chang, "Proton stereotactic body radiation therapy for clinically challenging cases of centrally and superiorly located stage i non-small-cell lung cancer," *Int. J. Radiat. Oncol. Biol. Phys.*, vol. 80, no. 4, pp. 1015–1022, 2011.

[164] D. A. Bush *et al.*, "High-dose hypofractionated proton beam radiation therapy is safe and effective for central and peripheral early-stage non-small cell lung cancer: Results of a 12-year experience at loma linda university medical center," *Int. J. Radiat. Oncol. Biol. Phys.*, vol. 86, no. 5, pp. 964–968, 2013.

[165] M. Hata *et al.*, "Hypofractionated High-Dose Proton Beam Therapy for Stage I Non-Small-Cell Lung Cancer: Preliminary Results of A Phase I/II Clinical Study," *Int. J. Radiat. Oncol. Biol. Phys.*, vol. 68, no. 3, pp. 786–793, 2007.

[166] D. A. Bush *et al.*, "Proton-beam radiotherapy for early-stage lung cancer," *Chest*, vol. 116, no. 5, pp. 1313–1319, 1999.

[167] J. Y. Chang *et al.*, “Toxicity and patterns of failure of adaptive/ablative proton therapy for early-stage, medically inoperable non-small cell lung cancer,” *Int. J. Radiat. Oncol. Biol. Phys.*, vol. 80, no. 5, pp. 1350–1357, 2011.

[168] X. Zhang *et al.*, “Intensity-modulated proton therapy reduces the dose to normal tissue compared with intensity-modulated radiation therapy or passive scattering proton therapy and enables individualized radical radiotherapy for extensive stage IIIB non-small-cell lung canc,” *Int J Radiat Oncol Biol Phys*, vol. 77, no. 2, pp. 357–366, 2010.

[169] R. C. Nichols *et al.*, “Protons safely allow coverage of high-risk nodes for patients with regionally advanced non-small-cell lung cancer.,” *Technol. Cancer Res. Treat.*, vol. 10, no. 4, pp. 317–22, 2011.

[170] H. Harada *et al.*, “Dose escalation study of proton beam therapy with concurrent chemotherapy for stage III non-small cell lung cancer,” *Cancer Sci.*, vol. 107, no. 7, pp. 1018–1021, 2016.

[171] Y. Oshiro *et al.*, “High-dose concurrent chemo-proton therapy for Stage III NSCLC: Preliminary results of a Phase II study,” *J. Radiat. Res.*, vol. 55, no. 5, pp. 959–965, 2014.

[172] Y. Oshiro *et al.*, “Results of Proton Beam Therapy without Concurrent Chemotherapy for Patients with Unresectable Stage III Non-small Cell Lung Cancer,” *J. Thorac. Oncol.*, vol. 7, no. 2, pp. 370–375, 2012.

[173] Z. X. Liao *et al.*, “Bayesian randomized trial comparing intensity modulated radiation therapy versus passively scattered proton therapy for locally advanced non-small cell lung cancer.,” *J Clin Oncol*, vol. 34, no. 15, pp. 8500–8500, 2016.

[174] D. Moher, A. Liberati, J. Tetzlaff, and D. G. Altman, “Preferred reporting items for systematic reviews and meta-analyses: The PRISMA statement,” *BMJ*, vol. 339, no. 7716, pp. 332–336, 2009.

[175] B. S. Hoppe, “Phase I/II study of hypofractionated proton therapy for stage II-III Non-small cell lung cancer NCT01770418,” *https://clinicaltrials.gov/ct2/show/NCT01770418*, 2013. .

[176] D. Gomez, “Phase I Study of Hypofractionated Proton Radiation Therapy in Thoracic Malignancies NCT01165658,” *https://clinicaltrials.gov/ct2/show/NCT01165658*, 2010. .

[177] M. Zhongxing Liao, “Phase III Randomized Trial Comparing Overall Survival After Photon Versus Proton Chemoradiotherapy for Inoperable Stage II-IIIB NSCLC NCT01993810,” *https://clinicaltrials.gov/ct2/show/NCT01993810*, 2014. .

[178] M. Bradford S Hoppe, MD, “Hypofractionated, Image-Guided Radiation Therapy With Proton Therapy for Stage I Non-Small Cell Lung Cancer (LU03) NCT00875901,” *https://clinicaltrials.gov/ct2/show/NCT00875901*, 2009. .

[179] P. Esther Troost, “Proton therapy to reduce acute normal tissue toxicity in locally advanced non-small cell lung cancer (PRONTOX,” *https://clinicaltrials.gov/ct2/show/NCT02731001*, 2016. .

[180] Z. Liao, “Phase I/II Trial of Image-Guided, Intensity-Modulated Photon (IMRT) or Scanning Beam Proton Therapy (IMPT) Both With Simultaneous Integrated Boost (SIB) Dose Escalation to the Gross Tumor Volume (GTV) With Concurrent Chemotherapy for Stage II/III Non-Smal,” *https://clinicaltrials.gov/ct2/show/NCT01629498*, 2012. .

[181] P. Pallmann *et al.*, “Adaptive designs in clinical trials : why use them , and how to run and report them,” pp. 1–15, 2018.

[182] Z. Liao *et al.*, “Bayesian Adaptive Randomization Trial of Passive Scattering Proton Therapy and Intensity-Modulated Photon Radiotherapy for Locally Advanced Non–Small-Cell Lung Cancer,” *J. Clin. Oncol.*, p. JCO.2017.74.072, 2018.

[183] J. J. H. Park *et al.*, “Systematic review of basket trials, umbrella trials, and platform trials: A landscape analysis of master protocols,” *Trials*, vol. 20, no. 1, pp. 1–10, 2019.

[184] P. Yang *et al.*, “Patterns of Local-Regional Failure After Intensity Modulated Radiation Therapy or Passive Scattering Proton Therapy With Concurrent Chemotherapy for Non-Small Cell Lung Cancer,” *Int. J. Radiat. Oncol. Biol. Phys.*, vol. 103, no. 1, pp. 123–131, 2019.

[185] A. Hudson *et al.*, “Is heterogeneity in stage 3 non-small cell lung cancer obscuring the potential benefits of dose-escalated concurrent chemo-radiotherapy in clinical trials?,” *Lung Cancer*, vol. 118, no. January, pp. 139–147, 2018.

[186] M. D. Jeter *et al.*, “Simultaneous Integrated Boost for Radiation Dose Escalation to the Gross Tumor Volume With Intensity Modulated (Photon) Radiation Therapy or Intensity Modulated Proton Therapy and Concurrent Chemotherapy for Stage II to III Non-Small Cell Lung Cancer: A P,” *Int. J. Radiat. Oncol. Biol. Phys.*, vol. 100, no. 3, pp. 730–737, 2018.

[187] M. Machtay *et al.*, “Higher Biologically Effective Dose of Radiotherapy is Associated with Improved Outcomes for Locally Advanced Non-small cell Lung Carcinoma treated with Chemoradiation: An Analysis of the Radiation Therapy Oncology Group,” *Int J Radiat Oncol Biol Phys*, vol. 82, no. 1, pp. 425–434, 2012.

[188] M. J. Parkes, S. Green, A. M. Stevens, S. Parveen, R. Stephens, and T. H. Clutton-

Brock, “Reducing the within-patient variability of breathing for radiotherapy delivery in conscious, unsedated cancer patients using a mechanical ventilator,” *Br. J. Radiol.*, vol. 89, no. 1062, 2016.

[189] M. J. Parkes, S. Green, W. Kilby, J. Cashmore, Q. Ghafoor, and T. H. Clutton-Brock, “The feasibility, safety and optimization of multiple prolonged breath-holds for radiotherapy,” *Radiother. Oncol.*, vol. 141, pp. 296–303, 2019.

[190] A. Santiago *et al.*, “Reproducibility of target coverage in stereotactic spot scanning proton lung irradiation under high frequency jet ventilation.,” *Radiother Oncol.*, vol. 109, no. 1, pp. 45–50, 2013.

[191] C. Zeng *et al.*, “Proton pencil beam scanning for mediastinal lymphoma: the impact of interplay between target motion and beam scanning.,” *Phys. Med. Biol.*, vol. 60, no. 7, pp. 3013–29, 2015.

[192] J. Miszczyk, K. Rawojć, A. Panek, J. Swakoń, P. G. Prasanna, and M. Rydygier, “Response of human lymphocytes to proton radiation of 60 MeV compared to 250 kV X-rays by the cytokinesis-block micronucleus assay,” *Radiother. Oncol.*, vol. 115, no. 1, pp. 128–134, 2015.

[193] L. M. Green *et al.*, “Response of Thyroid Follicular Cells to Gamma Irradiation Compared to Proton Irradiation. I. Initial Characterization of DNA Damage, Micronucleus Formation, Apoptosis, Cell Survival, and Cell Cycle Phase Redistribution,” *Radiat. Res.*, vol. 155, no. 1, pp. 32–42, 2001.

[194] S. M. Harding, J. L. Benci, J. Irianto, D. E. Discher, A. J. Minn, and G. A. Roger, “Mitotic progression following DNA damage enables pattern recognition within micronuclei,” *Nature*, vol. 548, no. 7668, pp. 466–470, 2017.

[195] H. Paganetti *et al.*, “Relative biological effectiveness (RBE) values for proton beam therapy,” *Int. J. Radiat. Oncol.*, vol. 53, no. 2, pp. 407–421, 2002.

[196] A. Lühr, C. Von Neubeck, M. Krause, and E. Troost, “Relative biological effectiveness in proton beam therapy - Current knowledge and future challenges.,” *Clin Transl Radiat Oncol.*, vol. 9, pp. 35–41, 2018.

[197] M. Gérard *et al.*, “Hypoxia Imaging and Adaptive Radiotherapy: A State-of-the-Art Approach in the Management of Glioma,” *Front. Med.*, vol. 6, no. June, 2019.

[198] W. Tinganelli *et al.*, “Kill-painting of hypoxic tumours in charged particle therapy.,” *Sci Rep.*, vol. 5, p. 17016, 2015.

[199] V. Rusch *et al.*, “Factors determining outcome after surgical resection of T3 and T4 lung cancers of the superior sulcus.,” *J Thorac Cardiovasc Surg*, vol. 119, p. 1147—53, 2000.

[200] M. Tamura, M. A. Hoda, and W. Klepetko, “Current treatment paradigms of superior sulcus tumours,” *Eur. J. Cardio-thoracic Surg.*, vol. 36, no. 4, pp. 747–753, 2009.

[201] R. Komaki *et al.*, “Outcome predictors for 143 patients with superior sulcus tumors treated by multimodality approach at the University of Texas MD Anderson Cancer Center.,” *Int J Radiat Oncol Biol Phys*, vol. 48, p. 347—54, 2000.

[202] J. Y. Chang *et al.*, “Consensus Guidelines for Implementing Pencil-Beam Scanning Proton Therapy for Thoracic Malignancies on Behalf of the PTCOG Thoracic and Lymphoma Subcommittee,” *International Journal of Radiation Oncology Biology Physics*, vol. 99, no. 1. pp. 41–50, 2017.

[203] D. R. Gomez and J. Y. Chang, “Accelerated dose escalation with proton beam therapy for non-small cell lung cancer,” *J. Thorac. Dis.*, vol. 6, no. 4, pp. 348–355, 2014.

[204] Y. Li, L. Kardar, X. Li, and E. Al., “On the interplay effects with proton scanning beams in stage III lung cancer.,” *Med Phys*, vol. 41, p. 021721, 2014.

[205] A. Lomax, “Intensity modulated proton therapy and its sensitivity to treatment uncertainties 1: the potential effects of calculational uncertainties.,” *Phys. Med. Biol.*, vol. 53, no. 4, pp. 1027–1042, 2008.

[206] M. Kang *et al.*, “A study of the beam-specific interplay effect in proton pencil beam scanning delivery in lung cancer,” *Acta Oncol. (Madr).*, vol. 56, no. 4, pp. 531–540, 2017.

[207] F. Kong, L. Quint, M. Machtay, and J. Bradley, “Radiation Therapy Oncology Group.” [Online]. Available: http://www.rtog.org/CoreLab/ContouringAtlases/LungAtlas.aspx.

[208] Y. Kang *et al.*, “4D Proton treatment planning strategy for mobile lung tumors.,” *Int. J. Radiat. Oncol. Biol. Phys.*, vol. 67, no. 3, pp. 906–914, 2007.

[209] W. A. Woodward and R. A. Amos, “Proton Radiation Biology Considerations for Radiation Oncologists,” *Int. J. Radiat. Oncol. Biol. Phys.*, vol. 95, no. 1, pp. 59–61, 2016.

[210] X. Zhang *et al.*, “Robust optimization in lung treatment plans accounting for geometric uncertainty,” no. December 2017, pp. 19–26, 2018.

[211] Z. Li, “Toward robust proton therapy planning and delivery,” *Transl. Cancer Res.*, vol. 16, no. 3, pp. 1–16, 2012.

[212] M. Moyers, D. Miller, and D. Bush, “Methodologies and tools for proton beam design for lung tumours.,” *Int J Radiat Oncol Biol Phys*, vol. 49, pp. 1429–1438, 2001.

[213] J. Chang *et al.*, “Consensus Statement on Proton Therapy in Early-Stage and Locally

Advanced Non-Small Cell Lung Cancer.," *Int J Radiat Oncol Biol Phys.*, vol. 95, no. 1, pp. 505–16, 2016.

[214] C. Nantavithya *et al.*, "Phase 2 Study of Stereotactic Body Radiation Therapy and Stereotactic Body Proton Therapy for High-Risk, Medically Inoperable, Early-Stage Non-Small Cell Lung Cancer," *Int. J. Radiat. Oncol. Biol. Phys.*, vol. 101, no. 3, pp. 558–563, 2018.

[215] J. Y. Chang *et al.*, "Long-term outcome of phase I/II prospective study of dose-escalated proton therapy for early-stage non-small cell lung cancer," *Radiother. Oncol.*, vol. 122, no. 2, pp. 274–280, 2017.

[216] H. E. Bainbridge, M. J. Menten, M. F. Fast, S. Nill, U. Oelfke, and F. McDonald, "Treating locally advanced lung cancer with a 1.5 T MR-Linac – Effects of the magnetic field and irradiation geometry on conventionally fractionated and isotoxic dose-escalated radiotherapy," *Radiother. Oncol.*, vol. 125, no. 2, pp. 280–285, 2017.

[217] D. B. Sneag *et al.*, "Prospective Respiratory Triggering Improves High-Resolution Brachial Plexus MRI Quality," *J. Magn. Reson. Imaging*, vol. 49, pp. 1723–1729, 2019.

[218] C. Paganelli, G. Meschini, S. Molinelli, C. Nazionale, M. Riboldi, and G. Baroni, "' Patient-specific validation of deformable image registration in radiation therapy : Overview and caveats ,'" *Med. Phys.*, vol. 45, no. 10, pp. 908–922, 2018.

[219] K. K. Brock, T. R. Mcnutt, and M. L. Kessler, "Use of image registration and fusion algorithms and techniques in radiotherapy : Report of the AAPM Radiation Therapy Committee Task Group No . 132," *Med. Phys.*, vol. 44, no. 7, pp. 43–76, 2017.

[220] C. Grassberger *et al.*, "Motion Interplay as a Function of Patient Parameters and Spot Size in Spot Scanning Proton Therapy for Lung Cancer," *Int J Radiat Oncol Biol Phys*, vol. 86, no. 2, pp. 380–386, 2013.

[221] C. Bert and E. Rietzel, "4D treatment planning for scanned ion beams.," *Radiat. Oncol.*, vol. 2, no. 1, p. 24, 2007.

[222] A.-C. C. Knopf, D. Boye, A. Lomax, and S. Mori, "Adequate margin definition for scanned particle therapy in the incidence of intrafractional motion," *Phys. Med. Biol.*, vol. 58, no. 17, pp. 6079–6094, 2013.

[223] Y. Li *et al.*, "On the interplay effects with proton scanning beams in stage III lung cancer.," *Med. Phys.*, vol. 41, no. 2, p. 021721, 2014.

[224] A. Schätti, M. Zakova, D. Meer, and a J. Lomax, "Experimental verification of motion mitigation of discrete proton spot scanning by re-scanning.," *Phys. Med. Biol.*, vol. 58, no. 23, pp. 8555–8572, 2013.

[225] F. Albertini, E. B. Hug, and A. J. Lomax, “Is it necessary to plan with safety margins for actively scanned proton therapy?,” *Phys. Med. Biol. Phys. Med. Biol*, vol. 56, no. 56, pp. 4399–4399, 2011.

[226] A. Fredriksson, A. Forsgren, and B. Hårdemark, “Minimax optimization for handling range and setup uncertainties in proton therapy,” *Med. Phys.*, vol. 38, no. 3, pp. 1672–1684, 2011.

[227] R. Bokrantz and A. Fredriksson, “Scenario-based radiation therapy margins for patient setup, organ motion, and particle range uncertainty,” *Phys. Med. Biol.*, vol. 62, no. 4, pp. 1342–1357, 2017.

[228] A. Fredriksson, A. Forsgren, and B. Hårdemark, “Maximizing the probability of satisfying the planning criteria in radiation therapy under setup uncertainty,” *Med. Phys.*, vol. 42, no. 7, pp. 3992–3999, 2015.

[229] A. Fredriksson and R. Bokrantz, “The scenario-based generalization of radiation therapy margins,” *Phys. Med. Biol.*, vol. 61, no. 5, pp. 2067–2082, 2016.

[230] ICRU, “ICRU REPORT 78: Prescribing, Recording, and Reporting Proton-Beam Therapy,” *J. ICRU*, vol. 7, no. 2, 2007.

[231] J. Seco, H. Panahandeh, K. Westover, J. Adams, and H. Willers, “Treatment of non-small cell lung cancer patients with proton beam-based stereotactic body radiotherapy: Dosimetric comparison with photon plans highlights importance of range uncertainty.,” *Int J Radiat Oncol Biol Phys.*, vol. 83, no. 354–61, 2012.

[232] B. Hoppe, S. Huh, S. Flampouri, R. Nichols, K. Oliver, and C. Morris, “Double-scattered proton-based stereotactic body radiotherapy for stage I lung cancer: A dosimetric comparison with photon-based stereotactic body radiotherapy.,” *Radiother Oncol.*, vol. 97, pp. 425–30, 2010.

[233] M. Engelsman, E. Rietzel, and H. M. Kooy, “Four-dimensional proton treatment planning for lung tumors,” *Int. J. Radiat. Oncol. Biol. Phys.*, vol. 64, no. 5, pp. 1589–1595, 2006.

[234] M. Engelsman and H. M. Kooy, “Target volume dose considerations in proton beam treatment planning for lung tumors,” *Med Phys*, vol. 32, no. 12, pp. 3549–3557, 2005.

[235] C. K. Speirs *et al.*, “Heart Dose Is an Independent Dosimetric Predictor of Overall Survival in Locally Advanced Non–Small Cell Lung Cancer,” *J. Thorac. Oncol.*, vol. 12, no. 2, 2017.

[236] A. Fogliata, G. Nicolini, E. Vanetti, A. Clivio, P. Winkler, and L. Cozzi, “The impact of photon dose calculation algorithms on expected dose distributions in lungs under different respiratory phases.,” *Phys Med Biol.*, vol. 53, pp. 2375–90., 2008.

[237] C. Grassberger, J. Daartz, S. Dowdell, T. Ruggieri, G. Sharp, and H. Paganetti, “Quantification of Proton Dose Calculation Accuracy in the Lung,” *Int J Radiat Oncol Biol Phys*, vol. 89, no. 2, pp. 424–430, 2014.

[238] A. N. Schreuder, D. S. Bridges, L. Rigsby, M. Blakey, J. Samantha, and G. H. John, “Validation of the RayStation Monte Carlo dose calculation algorithm using a realistic lung phantom,” no. October, pp. 127–137, 2019.

[239] J. Y. Chang *et al.*, “Significant reduction of normal tissue dose by proton radiotherapy compared with three-dimensional conformal or intensity-modulated radiation therapy in Stage I or Stage III non-small-cell lung cancer,” *Int. J. Radiat. Oncol. Biol. Phys.*, vol. 65, no. 4, pp. 1087–1096, 2006.

[240] E. T. Vitti and J. L. Parsons, “The radiobiological effects of proton beam therapy: Impact on DNA damage and repair,” *Cancers (Basel).*, vol. 11, no. 7, pp. 1–15, 2019.

[241] K. H. Vousden and X. Lu, “Live or let die: the cell’s response to p53,” *Nat. Rev. Cancer*, vol. 2, pp. 594–604, 2002.

[242] A. O. Fontana *et al.*, “Differential DNA repair pathway choice in cancer cells after proton- and photon-irradiation,” *Radiother. Oncol.*, vol. 116, no. 3, pp. 374–380, 2015.

[243] K. M. Prise, G. Schettino, M. Folkard, and K. D. Held, “New insights on cell death from radiation exposure,” *Lancet Oncol.*, vol. 6, pp. 520–28, 2005.

[244] A. Dasgupta, M. Nomura, R. Shuck, and J. Yustein, “Cancer’s Achilles’ Heel: Apoptosis and Necroptosis to the Rescue,” *Int. J. Mol. Sci.*, vol. 18, no. 1, pp. 1–20, 2016.

[245] S. Schleicher, L. Moretti, V. Varki, and B. Lu, “Progress in the unraveling of the endoplasmic reticulum stress/autophagy pathway and cancer: implications for future therapeutic approaches.,” *Drug Resist Updat.*, vol. 13, no. 3, pp. 79–86., 2010.

[246] O. Surova and B. Zhivotovsky, “Various modes of cell death induced by DNA damage,” *Oncogene*, vol. 32, no. 33, pp. 3789–3797, 2013.

[247] Z. Jin and W. El-Deiry, “Overview of cell death signaling pathways,” *Cancer Biol Ther.*, vol. 4, no. 2, pp. 139–63, 2005.

[248] A. E. Sayan *et al.*, “p73 and caspase-cleaved p73 fragments localize to mitochondria and augment TRAIL-induced apoptosis,” *Oncogene*, vol. 27, no. 31, pp. 4363–4372, 2008.

[249] H. Li *et al.*, “Cytochrome c release and apoptosis induced by mitochondrial targeting of nuclear orphan receptor TR3 [see comments] [comment],” *Science (80-.).*, vol. 289, no. 5482, pp. 1159–1164, 2000.

[250] H. Niida, S. Tsuge, Y. Katsuno, A. Konishi, N. Takeda, and M. Nakanishi, “Depletion of Chk1 leads to premature activation of Cdc2-cyclin B and mitotic catastrophe,” *J. Biol. Chem.*, vol. 280, no. 47, pp. 39246–39252, 2005.

[251] M. Castedo *et al.*, “The cell cycle checkpoint kinase Chk2 is a negative regulator of mitotic catastrophe,” *Oncogene*, vol. 23, no. 25, pp. 4353–4361, 2004.

[252] J. B. Mitchell, R. Choudhuri, K. Fabre, A. L. Sowers, S. D. Zabludoff, and J. A. Cook, “NIH Public Access,” *Cancer*, vol. 16, no. 7, pp. 2076–2084, 2011.

[253] Z. Cai *et al.*, “Plasma membrane translocation of trimerized MLKL protein is required for TNF-induced necroptosis,” *Nat. Cell Biol.*, vol. 16, no. 1, pp. 55–65, 2014.

[254] D. Kobayashi *et al.*, “Mitotic catastrophe is a putative mechanism underlying the weak correlation between sensitivity to carbon ions and cisplatin,” *Sci. Rep.*, vol. 7, no. November 2015, pp. 1–8, 2017.

[255] P. Rajendran *et al.*, “Autophagy and senescence: A new insight in selected human diseases,” *J. Cell. Physiol.*, vol. 234, no. 12, pp. 21485–21492, 2019.

[256] D. Eriksson and T. Stigbrand, “Radiation-induced cell death mechanisms,” *Tumor Biol.*, vol. 31, no. 4, pp. 363–372, 2010.

[257] J.-P. Coppé, P.-Y. Desprez, A. Krtolica, and J. Campisi, “The Senescence-Associated Secretory Phenotype: The Dark Side of Tumor Suppression,” *Annu Rev Pathol*, vol. 5, pp. 99–118, 2010.

[258] H. Rayess, M. B. Wang, and E. S. Srivatsan, “Cellular senescence and tumor suppressor gene p16,” *Int J Cancer*, vol. 130, no. 8, pp. 1715–1725, 2012.

[259] C. Deng, P. Zhang, J. Harper, S. Elledge, and P. Leder, “Mice lacking p21CIP1/WAF1 undergo normal development, but are defective in G1 checkpoint control,” *Cell*, vol. 82, pp. 675–684, 1995.

[260] J. Brugaloras, C. Chandrasekaran, J. Gordon, D. Beach, T. Jacks, and G. Hannon, “Radiation-induced cell cycle arrest compromised by p21 deficiency.,” *Nature*, vol. 377, pp. 552–557, 1995.

[261] L. I. Huschtscha, J. D. Moore, J. R. Noble, H. G. Campbell, A. W. Royds, Janice A. Braithwaite, and R. R. Reddel, “Normal human mammary epithelial cells proliferate rapidly in the presence of elevated levels of the tumor suppressors p53 and p21WAF1/CIP1,” *J. Cell Sci.*, vol. 122, pp. 2989–2995, 2009.

[262] D. Polsky, A. Z. Young, K. J. Busam, and R. M. Alani, “The transcriptional repressor of p16/Ink4a, Id1, is up-regulated in early melanomas,” *Cancer Res.*, vol. 61, no. 16, pp. 6008–6011, 2001.

[263] R. M. Alani, A. Z. Young, and C. B. Shifflett, “Id1 regulation of cellular senescence through transcriptional repression of p16/Ink4a,” *Proc. Natl. Acad. Sci. U. S. A.*, vol. 98, no. 14, pp. 7812–7816, 2001.

[264] M. Serrano, G. J. Hannon, and D. Beach, “inhibition of cyclin D / CDK4,” *Nature*, vol. 366, no. 6456, pp. 704–707, 1993.

[265] D. Parry, S. Bates, D. J. Mann, and G. Peters, “Lack of cyclin D-Cdk complexes in Rb-negative cells correlates with high levels of p16INK4/MTS1 tumour suppressor gene product.,” *EMBO J.*, vol. 14, no. 3, pp. 503–511, 1995.

[266] C. J. Sherr and F. McCormick, “The RB and p53 pathways in cancer,” *Cancer Cell*, vol. 2, no. 2, pp. 103–112, 2002.

[267] K. Yamakoshi *et al.*, “Real-time in vivo imaging of p16Ink4a reveals cross talk with p53.,” *J Cell Biol.*, vol. 186, no. 393–407, 2009.

[268] M. Wang *et al.*, “EGF Receptor Inhibition Radiosensitizes NSCLC Cells By Inducing Senescence In Cells Sustaining DNA Double-Strand Breaks,” *Cancer Res*, vol. 71, no. 19, pp. 621–6269, 2011.

[269] R. Mirzayans, B. Andrais, A. Scott, M. Paterson, and M. David, “Single cell analysis of p16INK4a and p21WAF1 expression suggets distinct mehcanisms of senescence in normal human and Li-Fraumeni Syndrome Firboblasts,” *J. Cell. Physiol.*, vol. 223, pp. 57–67, 2010.

[270] W. Leong, J. Chau, and B. Li, “p53 Deficiency leads to compensatory up-regulation of p16INK4a.,” *Mol Cancer Res.*, vol. 7, pp. 354–60, 2009.

[271] K. FJ, “RB and cyclin dependent kinase pathways: defining a distinction between RB and p16 loss in lung cancer.,” *Oncogene*, vol. 21, pp. 6908–14, 2002.

[272] Y. Sekido, K. Fong, and J. Minna, “Molecular genetics of lung cancer.,” *Annu Rev Med*, vol. 54, pp. 73–87, 2003.

[273] J. W. Shay and W. E. Pereira-Smith, O.M. Wright, “A role for both RB and p53 inthe regulation of human cellular senescence.,” *Exp. Cell Res.*, vol. 196, pp. 33–39, 1991.

[274] M. Fumagalli, F. Rossiello, and C. Mondello, “Stable Cellular Senescence Is Associated with Persistent DDR Activation,” *PLoS One*, vol. 9, no. 10, pp. 44–46, 2014.

[275] M. Narita *et al.*, “Rb-mediated heterochromatin formation andsilencing of E2 F target genes during cellular senescence.,” *Cell*, vol. 113, pp. 703–716, 2003.

[276] J. Campisi, “Senescent cells, tumor suppression, and organismal aging: goodcitizens, bad neighbors.,” *Cell*, vol. 120, pp. 513–522, 2005.

[277] L. García-Prat *et al.*, “Autophagy maintains stemness by preventing senescence.,” *Nature*, vol. 529, pp. 37–42, 2016.

[278] B. Schnabl, C. A. Purbeck, Y. H. Choi, C. . Hagedorn, and D. Brenner, “Replicative senescence of activated human hepatic stellate cells is accompanied by apronounced inflammatory but less fibrogenic phenotype.,” *Hepatology*, vol. 37, pp. 653–664, 2003.

[279] L. A. Maciel-Barón *et al.*, “Senescence associated secretory phenotype profile from primary lung mice fibroblasts depends on the senescence induction stimuli.,” *Age*, vol. 38, p. 26, 2016.

[280] F. Debacq-Chainiaux, J. D. Erusalimsky, J. Campisi, and O. Toussaint, “Protocols to detect senescence-associated beta-galactosidase (SA-βgal) activity, a biomarker of senescent cells in culture and in vivo,” *Nat. Protoc.*, vol. 4, no. 12, pp. 1798–1806, 2009.

[281] N. C. Yang and M. L. Hu, “The limitations and validities of senescence associated-beta-galactosidase activity as an aging marker for human foreskin fibroblast Hs68 cells.,” *Exp. Gerontol.*, vol. 40, pp. 813–819, 2005.

[282] J. D. Amaral, J. M. Xavier, C. J. Steer, and C. M. Rodrigues, “The role of p53 in apoptosis.,” *Discov. Med.*, vol. 9, pp. 145–152, 2010.

[283] A. Sharma, K. Singh, and A. Almasan, “Histone H2AX phosphorylation: a markerfor DNA damage.,” *Methods Mol. Biol.*, vol. 920, pp. 613–626, 2012.

[284] M. Matjusaitis, G. Chin, E. A. Sarnoski, and A. Stolzing, “Biomarkers to identify and isolate senescent cells,” *Ageing Research Reviews*. 2016.

[285] C. Janko *et al.*, *Necrosis. Mthods and Protocols. Part I: Analysis of Necrosis In Vitro*. .

[286] M. Sachet, Y. Y. Liang, and R. Oehler, “The immune response to secondary necrotic cells,” *Apoptosis*, vol. 22, no. 10, pp. 1189–1204, 2017.

[287] P. Olive, G. Frazer, and J. Banath, “Radiation-induced apoptosis measured in TK6 human B lymphoblast cells using the comet assay.,” *Radiat Res*, vol. 136, pp. 130–136, 1993.

[288] P. Olive, C. Vikse, and S. Vanderbyl, “Increase in the fraction of necrotic, not apoptotic, cells in SiHa xenograft tumors shortly after irradiation. Radiother Oncol,” vol. 50, pp. 113–119, 1999.

[289] A. Lekshmi, S. N. Varadarajan, S. S. Lupitha, D. Indira, and K. A. Mathew, “ARTICLE A quantitative real-time approach for discriminating apoptosis and necrosis,” *Nat. Publ. Gr.*, no. September 2016, pp. 1–10, 2017.

[290] L. B. Kleiman, A. M. Krebs, S. Y. Kim, T. S. Hong, and K. M. Haigis, “Comparative analysis of radiosensitizers for K-RAS mutant rectal cancers,” *PLoS One*, vol. 8, no. 12, pp. 1–12, 2013.

[291] et al. Rello-Varona S, Kepp O, Vitale I, Michaud M, Senovilla L, Jemaa M, “An automated fluorescence videomicroscopy assay for the detection of mitotic catastrophe.,” *Cell Death Dis*, vol. 1, no. e25, 2010.

[292] K. G. Vitale I, Galluzzi L, Castedo M, “Mitotic catastrophe: a mechanism for avoiding genomic instability.,” *Biol, Nat Rev Mol Cell*, vol. 12, no. 6, pp. 385–92, 2011.

[293] P. Vandenabeele, L. Galluzzi, T. Vanden Berghe, and G. Kroemer, “Molecular mechanisms of necroptosis: An ordered cellular explosion,” *Nat. Rev. Mol. Cell Biol.*, vol. 11, no. 10, pp. 700–714, 2010.

[294] H.-H. Wang *et al.*, “Ablative Hypofractionated Radiation Therapy Enhances Non-Small Cell Lung Cancer Cell Killing via Preferential Stimulation of Necroptosis In Vitro and In Vivo,” *Int. J. Radiat. Oncol.*, vol. 101, no. 1, pp. 49–62, 2018.

[295] A. Degterev, J. Hitomi, and et al. Germscheid, M, “Identification of RIP1 kinase as a specific cellular target of necrostatins.,” *Nat Chem Biol*, vol. 4, pp. 313–321, 2008.

[296] D. Zhang, J. Shoa, and et al Lin, J, “RIP3, an energy metabolism regulator that switches TNF- induced cell death from apoptosis to necrosis,” *Science (80-.).*, vol. 325, pp. 332–336, 2009.

[297] X. Wu, Z. Yang, and et al. Wang, XK, “Distinct roles of RIP1-RIP3 hetero- and RIP3-RIP3 homo-interaction in mediating necroptosis.,” *Cell Death Differ*, vol. 21, pp. 1709–1720, 2014.

[298] P. Geserick, J. Wang, and et al. Schilling, R, “Absence of RIPK3 predicts necroptosis resistance in malignant melanoma.,” *Cell Death Dis*, vol. 6, p. e1884, 2015.

[299] D. Ofengeim and J. Yuan, “Regulation of RIP1 kinase signalling at the crossroads of inflammation and cell death.,” *Nat. Rev. Mol. Cell Biol.*, vol. 14, pp. 727-736., 2013.

[300] J. Seo *et al.*, “CHIP controls necroptosis through ubiquitylation- and lysosome-dependent degradation of RIPK3.,” *Nat. Cell Biol.*, vol. 18, pp. 291–302, 2016.

[301] L. Duprez, N. Takahashi, F. Van Hauwermeiren, B. Vandendriessche, V. Goossens, and B. T. Vanden, “RIP kinase-dependent necrosis drives lethal systemic inflammatory response syndrome.,” *Immunity*, vol. 35, pp. 908-918., 2011.

[302] C. Yang *et al.*, “Regulation of RIP3 by the transcription factor Sp1 and the epigenetic regulator UHRF1 modulates cancer cell necroptosis,” *Cell Death Dis.*, vol. 8, no. 10, p. e3084, 2017.

[303] Z. Y. Yuan *et al.*, “Stereotactic Body Radiation Oncology Exert Anti-Tumor Effect via RIP3-Dependent Necroptosis in Non-Small Cell Lung Cancer Cells,” *Int. J. Radiat. Oncol.*, vol. 93, no. 3, p. E533, 2015.

[304] D. Chen, J. Yu, and L. Zhang, “Necroptosis: An alternative cell death program defending against cancer,” *Biochim. Biophys. Acta - Rev. Cancer*, vol. 1865, no. 2, pp. 228–236, 2016.

[305] T. Vanden Berghe *et al.*, “Determination of apoptotic and necrotic cell death in vitro and in vivo,” *Methods*, vol. 61, no. 2, pp. 117–129, 2013.

[306] I. Jorgensen, M. Rayamajhi, and E. A. Miao, “Programmed cell death as a defence against infection GSDMD forms a pore in membranes,” vol. 17, no. 3, pp. 151–164, 2018.

[307] B. Levine and G. Kroemer, “Biological Functions of Autophagy Genes: A Disease Perspective,” *Cell*, vol. 176, no. 1–2, pp. 11–42, 2019.

[308] C. et al. Behrends, “Network organization of the human autophagy system.,” *Nature*, vol. 466, pp. 68–76, 2010.

[309] R. Huang and W. Liu, “Identifying an essential role of nuclear LC3 for autophagy,” *Autophagy*, vol. 11, no. 5, pp. 852–853, 2015.

[310] E. Kim, J. Jeong, S. Bae, S. Kang, C. Kim, and Y. Lim, “mTOR inhibitors radiosensitize PTEN-deficient non-small-cell lung cancer cells harboring an EGFR activatingmutation by inducing autophagy.,” *J Cell Biochem*, vol. 114, pp. 1248–56, 2013.

[311] Y. Li *et al.*, “Rapamycin-induced autophagy sensitizes A549 cells to radiation associated with DNA damage repair inhibition,” *Thorac. Cancer*, vol. 7, no. 4, pp. 379–386, 2016.

[312] G. Cheng, D. Kong, and X. et al. Hou, “The tumor suppressor, p53, contributes to radiosensitivity of lung cancer cells by regulating autophagy and apoptosis. Cancer Biother Radiopharm,” vol. 28, pp. 153–9, 2013.

[313] E. L. H. Leung *et al.*, “Inhibition of KRAS-dependent lung cancer cell growth by deltarasin: Blockage of autophagy increases its cytotoxicity article,” *Cell Death Dis.*, vol. 9, no. 2, 2018.

[314] T. Sharif *et al.*, “Autophagic homeostasis is required for the pluripotency of cancer stem cells,” *Autophagy*, vol. 13, no. 2, pp. 264–284, 2017.

[315] R. J. Carter, C. M. Nickson, J. M. Thompson, A. Kacperek, M. A. Hill, and J. L. Parsons, “Complex DNA Damage Induced by High Linear Energy Transfer Alpha-Particles and Protons Triggers a Specific Cellular DNA Damage Response,” *Radiat.*

Oncol. Biol., vol. 100, no. 3, pp. 776–784, 2018.

[316] N. A. P. Franken, H. M. Rodermond, J. Stap, J. Haveman, and C. van Bree, "Clonogenic assay of cells in vitro," *Nat. Protoc.*, vol. 1, no. 5, pp. 2315–2319, 2006.

[317] H. Vakifahmetoglu, M. Olsson, and B. Zhivotovsky, "Death through a tragedy: Mitotic catastrophe," *Cell Death Differ.*, vol. 15, no. 7, pp. 1153–1162, 2008.

[318] B. G. Wouters, *Cell death after irradiation: how, when and why cells die. Basic Clinical Radiobiology.*, 4th ed. London: Hodder Education., 2009.

[319] J. Mikuła-Pietrasik, A. Niklas, P. Uruski, A. Tykarski, and K. Książek, "Mechanisms and significance of therapy-induced and spontaneous senescence of cancer cells," *Cell. Mol. Life Sci.*, vol. 77, no. 2, pp. 213–229, 2020.

[320] X. He *et al.*, "MiR-34a modulates ionizing radiation-induced senescence in lung cancer cells," *Oncotarget*, vol. 8, no. 41, pp. 69797–69807, 2017.

[321] V. Probin, Y. Wang, A. Bai, and D. Zhou, "Busulfan selectively induces cellular senescence but not apoptosis in WI38 fibroblasts via a p53-independent but extracellular signal-regulated kinase-p38 mitogen- activated protein kinase-dependent mechanism.," *J Pharmacol Exp Ther*, vol. 319, pp. 551 – 560, 2006.

[322] L. Girard, S. Zochbauer-Muller, A. K. Virmani, A. F. Gazdar, and J. D. Minna, "Genome-wide allelotyping of lung cancer identifies new regions of allelic loss, differences between small cell lung cancer and non-small cell lung cancer, and loci clustering," *Cancer Res.*, vol. 60, no. 17, pp. 4894–4906, 2000.

[323] M. Grigorova, R. C. Lyman, C. Caldas, and P. A. W. Edwards, "Chromosome abnormalities in 10 lung cancer cell lines of the NCI-H series analyzed with spectral karyotyping," *Cancer Genet. Cytogenet.*, vol. 162, no. 1, pp. 1–9, 2005.

[324] T. Isaka, A. Nestor, T. Takada, and D. Allison, "Chromosomal variations within aneuploid cancer lines.," *J Histochem Cytochem.*, vol. 51, no. 10, pp. 1343–53, 2003.

[325] F. Ianzini, R. Cherubini, and M. A. Mackey, "Mitotic catastrophe induced by exposure of V79 Chinese hamster cells to low-energy protons," *Int. J. Radiat. Biol.*, vol. 75, no. 6, pp. 717–723, 1999.

[326] S. Jeay *et al.*, "A distinct p53 target gene set predicts for response to the selective p53- HDM2 inhibitor NVP-CGM097," *Elife*, vol. 4, no. MAY, pp. 1–23, 2015.

[327] B. DJWJ., "Constraints on energy deposition and target size of multiply damaged sites associated with DNA double-strand breaks.," *Int J Radiat Biol.*, vol. 61, pp. 737–48., 1992.

[328] A. Asaithamby, B. Hu, and D. J. Chen, "Unrepaired clustered DNA lesions induce

chromosome breakage in human cells.," *Proc. Natl. Acad. Sci. U. S. A.*, vol. 108, no. 20, pp. 8293–8, 2011.

[329] A. Asaithamby and D. J. Chen, "Mechanism of cluster DNA damage repair in response to high- atomic number and energy particles radiation," *Mutat Res*, vol. 711, no. 1–2, pp. 87–99, 2011.

[330] L. R. Gomes, C. F. M. Menck, and G. S. Leandro, "Autophagy roles in the modulation of DNA repair pathways," *Int. J. Mol. Sci.*, vol. 18, no. 11, 2017.

[331] E. Gollapalle *et al.*, "Detection of oxidative clustered DNA lesions in X-irradiated mouse skin tissues and human MCF-7 breast cancer cells.," *Radiat Res.*, vol. 167, pp. 207–216, 2007.

[332] Y. Sun, Y. Zheng, C. Wang, and Y. Liu, "Glutathione depletion induces ferroptosis, autophagy, and premature cell senescence in retinal pigment epithelial cells.," *Cell Death Dis.*, vol. 9, no. 7, p. 753, 2018.

[333] M. Tan, E. Parkinson, L. Yap, and I. Paterson, "Relationship between autophagy, activation and senescence in normal and cancer-associated human oral fibroblasts.," *AACR, AM*, vol. 458, 2018.

[334] C. Kang *et al.*, "The DNA damage response induces inflammation and senescence by inhibiting autophagy of GATA4," *Science (80-.).*, vol. 349, p. 6255, 2015.

[335] L. Gao *et al.*, "Lung cancer deficient in the tumor suppressor GATA4 is sensitive to TGFBR1 inhibition," *Nat. Commun.*, vol. 10, no. 1, pp. 1–15, 2019.

[336] M. Guo *et al.*, "Hypermethylation of the GATA genes in lung cancer," *Clin. Cancer Res.*, vol. 10, no. 23, pp. 7917–7924, 2004.

[337] W. K. De Jong, G. F. Verpooten, H. Kramer, J. Louwagie, and H. J. M. Groen, "Promoter methylation primarily occurs in tumor cells of patients with non-small cell lung cancer," *Anticancer Res.*, vol. 29, no. 1, pp. 363–369, 2009.

[338] K. J. Mackenzie *et al.*, "cGAS surveillance of micronuclei links genome instability to innate immunity," *Nature*, vol. 548, no. 7668, pp. 461–465, 2017.

[339] L. Sun, J. Wu, F. Du, X. Chen, and Z. Chen, "Cyclic GMP-AMP synthase is a cytosolic DNA sensor that activates the type I interferon pathway.," *Science (80-.).*, vol. 339, pp. 786–791, 2013.

[340] J. Wu and E. Al., "Cyclic GMP-AMP is an endogenous second messenger in innate immune signaling by cytosolic DNA.," *Science (80-.).*, vol. 339, pp. 826–830, 2013.

[341] S. Kitajima *et al.*, "Suppression of STING associated with lkb1 loss in KRAS-driven lung cancer," *Cancer Discov.*, vol. 9, no. 1, pp. 34–45, 2019.

[342] H. Yang, H. Wang, U. Ren, Q. Chen, and Z. J. Chena, “CGAS is essential for cellular senescence,” *Proc. Natl. Acad. Sci. U. S. A.*, vol. 114, no. 23, pp. E4612–E4620, 2017.

[343] S. Girdhani, C. Lamont, P. Hahnfeldt, A. Abdollahi, and L. Hlatky, “Proton irradiation suppresses angiogenic genes and impairs cell invasion and tumor growth.,” *Radiat Res*, vol. 178, pp. 33–45, 2012.

[344] C. Di Pietro *et al.*, “Cellular and molecular effects of protons: Apoptosis induction and potential implications for cancer therapy,” *Apoptosis*, vol. 11, no. 1, pp. 57–66, 2006.

[345] S. Kedracka-Krok *et al.*, “Proteomic analysis of proton beam irradiated human melanoma cells.,” *PLoS One*, vol. 9, p. e84621, 2014.

[346] J. Unkelbach, P. Botas, D. Giantsoudi, B. Gorissen, and H. Paganetti, “Reoptimization of intensity- modulated proton therapy plans based on linear energy transfer,” *Int J Radiat Oncol Biol Phys*, vol. 96, no. 5, pp. 1097–1106, 2016.

[347] J. L. Kirkland and T. Tchkonia, “Cellular Senescence: A Translational Perspective,” *EBioMedicine*, vol. 21, pp. 21–28, 2017.

[348] P. P. Shah *et al.*, “Lamin B1 depletion in senescent cells triggers large-scale changes in gene expression and the chromatin landscape,” *Genes Dev.*, vol. 27, no. 16, pp. 1787–1799, 2013.

[349] P. Chantal *et al.*, “Personalized In Vitro and In Vivo Cancer Models to Guide Precision Medicine,” *Cancer Discov*, vol. 7, no. 5, pp. 462–477, 2017.

[350] F. Pampaloni, E. G. Reynaud, and E. H. K. Stelzer, “The third dimension bridges the gap between cell culture and live tissue,” *Nat. Rev. Mol. Cell Biol.*, vol. 8, no. october, pp. 839–845, 2007.

[351] G. Gamerith *et al.*, “3D-cultivation of NSCLC cell lines induce gene expression alterations of key cancer-associated pathways and mimic in-vivo conditions,” *Oncotarget*, vol. 8, no. 68, pp. 112647–112661, 2017.

[352] K. Simon *et al.*, “Metabolic response of lung cancer cells to radiation in a paper-based 3D cell culture system.,” *Biomaterials.*, vol. 95, pp. 47–59., 2016.

[353] Z. Xu *et al.*, “Application of a microfluidic chip-based 3D co-culture to test drug sensitivity for individualized treatment of lung cancer.,” *Biomaterials.*, vol. 34, pp. 4109–4117, 2013.

[354] C. Jensen and Y. Teng, “Is It Time to Start Transitioning From 2D to 3D Cell Culture?,” *Front. Mol. Biosci.*, vol. 7, no. March, pp. 1–15, 2020.

[355] Public Health England, “PHE cancer data sets , linkage and availability (v1 . 1),” no.

June 2017, pp. 1–10.

[356] S. Morganti, P. Tarantino, E. Ferraro, P. D'Amico, B. Duso, and G. Curigliano, "Next Generation Sequencing (NGS): A Revolutionary Technology in Pharmacogenomics and Personalized Medicine in Cancer.," *Adv Exp Med Biol.*, vol. 1168, pp. 9-30., 2019.

[357] S. Y. Nishio and S. I. Usami, "The Clinical Next-Generation Sequencing Database: A Tool for the Unified Management of Clinical Information and Genetic Variants to Accelerate Variant Pathogenicity Classification," *Hum. Mutat.*, vol. 38, no. 3, pp. 252–259, 2017.

[358] C. S. Mayo *et al.*, "The big data effort in radiation oncology: Data mining or data farming?," *Adv. Radiat. Oncol.*, vol. 1, no. 4, pp. 260–271, 2016.

[359] T. M. Deist *et al.*, "Distributed learning on 20 000+ lung cancer patients – The Personal Health Train," *Radiother. Oncol.*, vol. 144, pp. 189–200, 2020.

[360] J. A. Langendijk, P. Lambin, D. De Ruysscher, J. Widder, M. Bos, and M. Verheij, "Selection of patients for radiotherapy with protons aiming at reduction of side effects : The model-based approach," *Radiother. Oncol.*, vol. 107, no. 3, pp. 267–273, 2013.

[361] J. Scherman *et al.*, "Incorporating NTCP into randomized trials of proton versus photon therapy," *Int. J. Part. Ther.*, vol. 5, no. 3, pp. 24–32, 2019.

Appendices

Appendix 1. Lung Cancer Staging (AJCC 7th Ed).

Appendix 2. ICD-10 codes indicating primary site lung malignancies.

Appendix 3. ICD-10 codes indicating secondary site malignancies or complications from recurrent/ progressive/ metastatic disease.

Appendix 4a. Table of OPCS codes identified for primary presentation and investigation.

Appendix 4b. Table of OPCS and ICD10 codes identifying primary management.

Appendix 5a. Table of OPCS codes identified for recurrent, progressive or metastatic disease presentation and investigation.

Appendix 5b. Table of OPCS codes identifying secondary management.

Appendix 5: ECOG/ WHO Performance Status.

Appendix 6: Published papers:

A methodology to extract outcomes from routine healthcare data for patients with locally advanced non-small cell lung cancer. Wong, SL., Ricketts, K., Royle, G., Williams, M. and Mendes, R. *BMC Health Services Research.* 2018. **18**:278.

Retrospective planning study of patients with superior sulcus tumours comparing pencil beam scanning protons to volumetric modulated arc therapy. Wong, SL., Alshaikhi, J., Grimes, H., Amos, RA., Poynter, A., Rompokos, V., Gulliford, S., Royle, G., Liao, Z., Sharma, RA., Mendes, R. *Clin Oncol*, 2020. DOI 10.1016/j.clon.2020.07.016

Appendix 7: Radiotherapy for Non-small cell lung cancer (non- SABR). University College London Hospital Radiotherapy Department Work Instruction.

Appendix 8: Manuscript in progress for submission to the International Journal of Radiation Oncology Biology Physics: **Critical research gaps and recommendations to inform research prioritisation for improved outcomes in lung cancer using proton radiotherapy.** *Cobben, D., ***Wong, SL**, Aznar, M., Dempsey, C., Faivre-Finn, C., Hiley, C., Lines, D., Mohindra, P., Taylor, M., Teoh, S., Salem, A. (**Joint 1st authors*).

Appendix 1. Lung Cancer Staging (AJCC 7th Ed)

TNM definitions	
Tis	Carcinoma in situ
T1	Tumour ≤3cm, surrounded by lung or visceral pleura, without bronchoscopic evidence of invasion more proximal that the lobar bronchus
T2	Tumour more than 3cm but 7cm or less or tumour with any of the following features: involves main bronchus, 2cm or more distal to the carina, invades visceral pleura; associated with atelectasis or obstructive pneumonitis that extends to the hilar region but does not involve the entire lung
T3	Tumour more than 7cm or one that directly invades any of the following: parietal pleura, chest wall (including superior sulcus tumours), diaphragm, phrenic nerve, mediastinal pleural, parietal pericardium; or tumour in the main bronchus less than 2cm distal to the carina but without involvement of the carina; or associated atelectasis or obstructive pneumonitis of the entire lung or separate tumour nodules(s) in the same lobe.
T4	Tumour of an size that invades any of the following: mediastinum, heart, great vessels, trachea, recurrent laryngeal nerve, oesophagus, vertebral body, carina, separate tumour nodules (s) in a different ipsilateral lobe
N0	**No regional lymph node metastases**
N1	Metastasis in ipsilateral peribronchial and/or ipsilateral hilar lymph nodes and intrapulmonary nodes, including involvement by direct extension
N2	Metastasis in ipsilateral mediastinal and/or subcarinal lymph node(s)
N3	Metastasis in contralateral mediastinal, contralateral hilar, ipsilateral or contralateral scalene, or supraclavicular lymph node(s)
M0	No distant metastasis
M1a	Separate tumour nodules(s) in a contralateral lobe, tumour with pleural nodules or malignant pleural (or pericardial) effusion
M1b	**Distant metastasis (in extrathoracic organs)**
Stage	
IA	T1a-1bN0M0
IB	T2aN0M0
IIA	T1a-T2aN1M0 T2bN0M0
IIB	T2bN1M0 T3N0M0
IIIA	T3N1M0 T1a-3N2M0 T4N0M0
IIIB	T4N2M0 T1a-4N3M0
IV	Any T, any N, M1a-b

Appendix 2. ICD-10 codes indicating primary site lung malignancies

ICD-10 codes indicating primary site lung malignancy	
C34	Malignant neoplasm of bronchus or lung
C34.0	Main bronchus, Carina, Hilum of lung
C34.1	Upper lobe, bronchus or lung
C34.2	Middle lobe, bronchus or lung
C34.3	Lower lobe, bronchus or lung
C34.8	Overlapping lesion of bronchus and lung
C34.9	Malignant neoplasm of bronchus or lung, unspecified
C38	Malignant neoplasm of heart, mediastinum and pleura
C38.3	Malignant neoplasm of mediastinum, part unspecified
C38.4	Pleura
C38.8	Overlapping lesion of heart, mediastinum and pleura
C77.1	*Secondary & unspecified malignant neoplasm of intrathoracic lymph nodes
Additional indicator ICD-10 codes	
R91	§Abnormal findings on diagnostic imaging of lung

*This code is included in the primary presentation list of codes as patients with locally advanced NSCLC often have mediastinal lymph node disease. §This code is used to denote "coin lesions not otherwise specified" and "lung mass not otherwise specified" and whilst such findings cannot confirm diagnosis, they are highly suggestive of lung malignancy and this is often the first indication to clinicians that a patient may have a lung malignancy.

Appendix 3. ICD-10 codes indicating secondary site malignancies or complications from recurrent/ progressive/ metastatic disease

C77.0	Secondary & unspecified malignant neoplasm of lymph nodes of head, face & neck
C77.1	Secondary & unspecified malignant neoplasm of intrathoracic lymph nodes
C77.2	Secondary & unspecified malignant neoplasm of intra-abdominal lymph nodes
C77.3	Secondary & unspecified malignant neoplasm of axillary and upper limb lymph nodes
C77.4	Secondary & unspecified malignant neoplasm of inguinal and lower limb lymph nodes
C77.5	Secondary & unspecified malignant neoplasm of intrapelvic lymph nodes
C77.8	Secondary & unspecified malignant neoplasm of lymph nodes of multiple regions
C78.0	Secondary malignant neoplasm of lung
C78.1	Secondary malignant neoplasm of mediastinum
C78.2	Secondary malignant neoplasm of pleura; Malignant pleural effusion NOS
C78.3	secondary malignant neoplasm of other and unspecified respiratory organs
C78.6	Secondary malignant neoplasm of retroperitoneum & peritoneum
C79.0	Secondary malignant neoplasm of kidney & renal pelvis
C79.2	Secondary malignant neoplasm of skin
C79.3	Secondary malignant neoplasm of brain & cerebral meninges
C79.5	Secondary Malignant Neoplasm Of Bone And Bone Marrow
C79.7	Secondary malignant neoplasm of adrenal gland
C79.8	Secondary malignant neoplasm of other specified sites
C79.9	Secondary malignant neoplasm, unspecified site; Carcinomatosis (secondary); Disseminated (secondary): cancer NOS, malignancy NOS; Generalized (secondary):cancer NOS, malignancy NOS; Multiple secondary cancer NOS
ICD-10 codes indicating complications from disease	
R91	§Abnormal findings on diagnostic imaging of lung
M50.1	Radiculopathy-Cervical
G54.0	Brachial plexus disorders
G55.0	Nerve root and plexus compressions in neoplastic disease
G95.2	Cord compression, unspecified
G83.4	Cauda equina syndrome

NOC (not otherwise classified). §This code is used to denote “coin lesions not otherwise specified” and “lung mass not otherwise specified” and whilst such findings cannot confirm diagnosis, they are highly suggestive of lung malignancy and this is often the first indication to clinicians that a patient may have a lung malignancy.

Appendix 4a. Table of OPCS codes identified for primary presentation & investigation.

Biopsy OPCS Codes	
E59.1	Needle biopsy of lesion of lung
E59.3	Biopsy of lesion of lung NEC
T09.2	Open biopsy of lesion of pleura
T12.1	Drainage of lesion of pleura NEC
T12.3	Aspiration of pleural cavity
T87.4	Excision or biopsy of mediastinal lymph node
Y20.4	Fine needle aspiration NOC
Y21.1	Brush cytology of organ NOC
X55.1	Biopsy of lesion of unspecified organ
Other Diagnostic Procedure OPCS Codes	
E49.2	†Diagnostic fibreoptic endoscopic examination of lower respiratory tract and lavage of lesion of lower respiratory tract
E63.2	†Endobronchial ultrasound examination of mediastinum
E63.9	Unspecified diagnostic endoscopic examination of mediastinum
Y53.2	Approach to organ under ultrasonic control
Y74.4	Thoracoscopic video-assisted approach to thoracic cavity
Diagnostic Imaging OPCS Codes	
U36.2	Positron emission tomography with computed tomography NEC
U26.1	Glomerular filtration rate testing
U05.1	Computed tomography of head
U21.2 AND Y98.3 AND Z92.4	Computed tomography NEC -Radiology of three body areas (or 20-40 minutes)- Chest NEC
U21.2 AND Y98.3 AND Z92.6	Computed tomography NEC -Radiology of three body areas (or 20-40 minutes)- Abdomen NEC
U21.2 AND Y98.3 AND Z75.9	Computed tomography NEC -Radiology of three body areas (or 20-40 minutes)- Bone of pelvis NEC

NEC (not elsewhere classified).NOC (not otherwise classified). §Band numbers relating to the chemotherapy are assigned for costing purposes and do not help identify tumour type or origin, nor if the treatment is radical or palliative.

Appendix 4b. Table of OPCS and ICD10 codes identifying primary management.

Radiotherapy OPCS Codes	
X65.4	Delivery of a fraction of external beam radiotherapy NEC
Y92.1	Technical support for preparation for radiotherapy
X67.1	Preparation for intensity modulated radiation therapy
X67.7	Preparation for complex conformal radiotherapy
Y91.1	Megavoltage treatment for complex radiotherapy
Y91.4	Megavoltage treatment for adaptive radiotherapy
Chemotherapy OPCS Codes	
Z51.1	Chemotherapy session for neoplasm
X70.3	§Procurement of drugs for chemotherapy for neoplasm for regimens in Band 3
X72.1	Delivery of complex chemotherapy for neoplasm including prolonged infusional treatment at first attendance
X71.5	§Procurement of drugs for chemotherapy for neoplasm for regimens in Band 10
X71.1	§Procurement of drugs for chemotherapy for neoplasm for regimens in Band 6
X70.5	§Procurement of drugs for chemotherapy for neoplasm for regimens in Band 5
Interventional OPCS Codes	
L76.9	Unspecified endovascular placement of stent
L79.3	Insertion of stent into vena cava NEC
T10.2	Endoscopic pleurodesis using talc

NEC (not elsewhere classified).NOC (not otherwise classified). §Band numbers relating to the chemotherapy are assigned for costing purposes and do not help identify tumour type or origin, nor if the treatment is radical or palliative.

Appendix 5a. Table of OPCS codes identified for recurrent, progressive or metastatic disease presentation and investigation

Diagnostic Procedure OPCS Codes	
E63.2	Endobronchial ultrasound examination of mediastinum
T87.4	Excision or biopsy of mediastinal lymph node
Y20.4	Fine needle aspiration NOC
Y53.2	Approach to organ under ultrasonic control
E59.1	Needle biopsy of lesion of lung
E63.9	Unspecified diagnostic endoscopic examination of mediastinum
T87.4	Excision or biopsy of mediastinal lymph node
E59.3	Biopsy of lesion of lung NEC
Y21.1	Brush cytology of organ NOC
E49.2	Diagnostic fibreoptic endoscopic examination of lower respiratory tract and lavage of lesion of lower respiratory tract
T12.3	Aspiration of pleural cavity
T09.2	Open biopsy of lesion of pleura
Y21.1	Brush cytology of organ NOC
T12.1	Drainage of lesion of pleura NEC
Y74.4	Thoracoscopic video-assisted approach to thoracic cavity
X55.1	Biopsy of lesion of unspecified organ
Diagnostic Imaging OPCS Codes	
U36.2	Positron emission tomography with computed tomography NEC
U26.1	Glomerular filtration rate testing
U21.1 AND Z06.1	Magnetic resonance imaging NEC- Cervical spinal cord
U21.1 AND Z06.2	Magnetic resonance imaging NEC- Thoracic spinal cord
U21.1 AND Z99.2	Magnetic resonance imaging NEC- Intervertebral disc of thoracic spine
U21.1 AND Z06.3	Magnetic resonance imaging NEC- Lumbar spinal cord
U05.1	Computed tomography of head
U14.1	Nuclear bone scan of whole body
U21.2 AND Y98.3 AND Z92.4	Computed tomography NEC -Radiology of three body areas (or 20-40 minutes)- Chest NEC
U21.2 AND Y98.3 AND Z92.6	Computed tomography NEC -Radiology of three body areas (or 20-40 minutes)- Abdomen NEC
U21.2 AND Y98.3 AND Z75.9	Computed tomography NEC -Radiology of three body areas (or 20-40 minutes)- Bone of pelvis NEC

NEC (not elsewhere classified). NOC (not otherwise classified). §Band numbers relating to the chemotherapy are assigned for costing purposes and do not help identify tumour type or origin, nor if the treatment is radical or palliative. *Whilst “Preparation for intensity modulated radiation therapy” implies complex radiotherapy that is usually delivered in the radical setting, it is also used to code for SABR (stereotactic ablative radiotherapy), which can be a used for

oligometastatic (single or few systemic metastases that are amenable to surgery or ablative therapy) disease.

Appendix 5b. Table of OPCS codes identifying secondary management.

Radiotherapy OPCS Codes	
X65.4	Delivery of a fraction of external beam radiotherapy NEC
X67.5	Preparation for simple radiotherapy with imaging and simple calculation
Y91.2	Megavoltage treatment for simple radiotherapy
X67.1	Preparation for intensity modulated radiation therapy *
E59.5	Percutaneous radiofrequency ablation of lesion of lung
Chemotherapy OPCS Codes	
Z51.1	Chemotherapy session for neoplasm
X70.3	§Procurement of drugs for chemotherapy for neoplasm for regimens in Band 3
X72.1	Delivery of complex chemotherapy for neoplasm including prolonged infusional treatment at first attendance
X71.5	§Procurement of drugs for chemotherapy for neoplasm for regimens in Band 10
X73.1	Delivery of exclusively oral chemotherapy for neoplasm
X71.1	§Procurement of drugs for chemotherapy for neoplasm for regimens in Band 6
Interventional OPC Codes	
L79.3	Insertion of stent into vena cava NEC
L76.9	Unspecified endovascular placement of stent
T10.2	Endoscopic pleurodesis using talc

NEC (not elsewhere classified).*Whilst “Preparation for intensity modulated radiation therapy” implies complex radiotherapy that is usually delivered in the radical setting, it is also used to code for SABR (stereotactic ablative radiotherapy), which can be a used for oligometastatic (single or few systemic metastases that are amenable to surgery or ablative therapy) disease. §Band numbers relating to the chemotherapy are assigned for costing purposes and do not help identify tumour type or origin, nor if the treatment is radical or palliative.

Appendix 5: ECOG/ WHO Performance Status [54]

Score	
0	Fully active, able to carry on all pre-disease performance without restriction
1	Restricted in physically strenuous activity, but ambulatory and able to carry out work of a light and sedentary nature
2	Ambulatory and capable of all self-care but unable to carry out any work activities. Up and about more than 50% of waking hours
3	Capable of only limited self-care, confined to bed or chair more than 50% of waking hours
4	Completely disabled. Cannot carry on any self-care. Totally confined to bed or chair
5	Dead

ECOG/ WHO Performance status is a graded score reflecting patients’ fitness. It is used by clinicians to guide decisions on patients’ suitability for intensive radical treatment and their prognosis. Patients with PS 0-1 are considered fit for radical treatment. There may be exceptional cases where patients with PS2 are offered a radical dose of radiotherapy alone but this is not standard practice and should be done with caution. It would not be appropriate to offer radical treatment to patients with a PS of 3-4 and best supportive care is the mainstay treatment for those patients[61].

Appendix 6: Full published papers